Order Number 9408478

A multi-region computer model for predicting nuclear excursions in aqueous homogeneous solution assemblies

Kimpland, Robert Herbert, Ph.D.

The University of Arizona, 1993

U·M·I
300 N. Zeeb Rd.
Ann Arbor, MI 48106

A MULTI-REGION COMPUTER MODEL FOR PREDICTING NUCLEAR EXCURSIONS IN AQUEOUS HOMOGENEOUS SOLUTION ASSEMBLIES

by

Robert Herbert Kimpland

A Dissertation Submitted to the Faculty of the

DEPARTMENT OF NUCLEAR AND ENERGY ENGINEERING

In Partial Fulfillment of the Requirements
For the Degree of

DOCTOR OF PHILOSOPHY
WITH A MAJOR IN NUCLEAR ENGINEERING

In the Graduate College

THE UNIVERSITY OF ARIZONA

1 9 9 3

THE UNIVERSITY OF ARIZONA
GRADUATE COLLEGE

As members of the Final Examination Committee, we certify that we have read the dissertation prepared by Robert Herbert Kimpland entitled A Multi-region Computer Model for Predicting Nuclear Excursions in Aqueous Homogeneous Solution Assemblies

and recommend that it be accepted as fulfilling the dissertation requirement for the Degree of Doctor of Philosophy - Engineering

David L. Hetrick David L Hetrick	8/6/93 Date
Phillip A. Secker, Jr.	8/6/93 Date
William L. Filippone BY John G. Wil	8/6/93 Date
	Date
	Date

Final approval and acceptance of this dissertation is contingent upon the candidate's submission of the final copy of the dissertation to the Graduate College.

I hereby certify that I have read this dissertation prepared under my direction and recommend that it be accepted as fulfilling the dissertation requirement.

David L. Hetrick David L. Hetrick — 8/9/93
Dissertation Director — Date

STATEMENT BY AUTHOR

This dissertation has been submitted in partial fulfillment of requirements for an advanced degree at The University of Arizona and is deposited in the University Library to be made available to borrowers under rules of the Library.

Brief quotations from this dissertation are allowable without special permission, provided that accurate acknowledgement of source is made. Requests for permission for extended quotation from or reproduction of this manuscript in whole or in part may be granted by the head of the major department or the Dean of the Graduate College when in his or her judgement the proposed use of the material is in the interests of scholarship. In all other instances, however, permission must be obtained from the author.

SIGNED: Robert Kirkland

ACKNOWLEDGEMENTS

I would like to thank my advisor and mentor, Dr. David L. Hetrick, for his guidance during the course of this work. Also, my thanks to the faculty and staff of the Department of Nuclear and Energy Engineering for their help and advice.

Most of all, I would like to thank my parents for their support and encouragement. My academic "journey" has been a long one, but they were always there for me every step of the way.

To my parents

TABLE OF CONTENTS

TABLE OF CONTENTS-*Continued*

LIST OF TABLES

LIST OF ILLUSTRATIONS

LIST OF ILLUSTRATIONS-*Continued*

LIST OF ILLUSTRATIONS-*Continued*

LIST OF ILLUSTRATIONS-*Continued*

LIST OF ILLUSTRATIONS-*Continued*

ABSTRACT

Fissile materials in the form of aqueous homogeneous solutions are used during the chemical processing of nuclear fuel. In this form there exists the possibility of an accidental criticality of the solution. To determine the consequences of such accidents, computer models have been developed to simulate nuclear excursions.

A one-region model and a multi-region model have been developed to simulate both power and pressure pulses. These models include a new radiolytic gas production model that tracks the number of radiolytic gas bubbles produced during an excursion. Also, an equation of state, which accounts for the production of inertial pressure due to a "lag" in thermal expansion and the creation of radiolytic gas bubbles, has been developed for both models. The multi-region model can account for the spatial distribution of the nuclear energy deposited in the solution and both axial and radial acceleration of the fuel material caused by the production of inertial pressure.

Predicted power and pressure pulses have been compared with experimental data from the KEWB, CRAC, and SILENE experiments. The

computer models have been very successful in predicting the magnitude of both power and pressure pulses. Also, the multi-region model has provided new information on the spatial distribution of solution parameters during an excursion.

CHAPTER 1

INTRODUCTION

1.1 Historical Background

The reprocessing of nuclear fuel usually involves the process of chemical separation. The fuel, which is usually in oxide form (e.g. UO_2), is first dissolved with some type of acid, such as nitric, sulfuric, or hydrofluoric acid. This results in the fuel being transformed into a homogeneous aqueous solution. In this form there may be a higher probability of an accidental criticality of the solution, especially when being transported through pipes or stored in vessels.

From 1958 to 1970, there were seven accidental supercritical excursions in U.S. processing plants. These accidents have been summarized by Paxton (1975). All these accidents occurred with homogeneous aqueous fissile solutions of either uranium or plutonium. Initial pulse yields ranged from 10^{15} to $6x10^{17}$ fissions. Radiation exposures from these accidents ranged from negligible to 10000 rads and resulted in

two fatalities, one at the Los Alamos Scientific Laboratory and one at United Nuclear Corporation's Wood River Junction plant.

Although every effort is made to avoid criticality accidents, the risk of such accidents is never totally eliminated. It is therefore necessary to reproduce and analyze hypothetical accidents through experiments with research reactors and theoretical models. The goal of this work is a better understanding of solution criticality, excursion dynamics, and shutdown mechanisms. It should be noted that any future accident will probably be the result of a situation not previously considered in accident studies. It is therefore of major importance to try to determine the basic physical mechanisms of such accidents.

1.2 Review of Previous Work

The British, the French, the Soviets, and the Americans have all conducted theoretical and experimental work in the area of fissile aqueous solution criticality safety. The result of this research has been the generation of experimental data from research reactors and the development of theoretical models which attempt to simulate excursion dynamics. A

survey of this work and its importance to the work being presented in this report is included here.

The Kinetic Experiment on Water Boiler (KEWB) program was conducted in the late 1950's and early 1960's to study the safety and dynamics of homogeneous solution reactors using highly enriched uranium sulphate. This program produced a wealth of valuable data, such as the peak power and the peak pressure of various transients, which were used to develop mathematical simulations of such transients (Dunenfeld and Stitt, 1963). One of the most important findings of the KEWB program was on the phenomenon of fission track nucleation of radiolytic gas bubbles (Spiegler et al, 1962). The formation of radiolytic gas and its contribution to inertial pressure is very important in short-period power excursions.

In November 1969, the French Commissariat à L'Énergie Atomique began the Consequences Radiologiques d'un Accident de Criticité (CRAC) program, which investigated excursions in homogeneous solutions. This program used highly enriched uranyl nitrate solutions with which forty excursions with various uranium concentrations were observed. The CRAC experiments provided important data on aqueous solution assemblies over a wide range of core dimensions and uranium concentrations (Lécorché and

Seale, 1973). Another important finding of these experiments was the possibility of multiple pulses occurring during an accident, caused by the solution returning to a supercritical configuration after the initial burst.

The SILENE reactor program, conducted by the French Commissariat à L'Énergie Atomique, involves excursions in a solution of highly enriched uranyl nitrate. The SILENE reactor has been very successful in the area of safety analysis. It can be operated in a "pulse" mode, where the power excursion is very fast (a few ms), or it can be operated in a "free evolution" mode, where power excursions are allowed to evolve freely in order to simulate an accident. An important result of the SILENE experiments was the confirmation of two shutdown mechanisms, namely an increase in the temperature of the fissile material and the formation of radiolytic gas bubbles (Barbry, 1983). The program also produced important data, such as peak power and peak pressure for various transients.

The Solution High Energy Burst Assembly (SHEBA) constructed at the Los Alamos National Laboratory in 1980, was used to evaluate criticality alarm detectors and calibrate personnel dosimetry instrumentation. This low enrichment uranium fluoride solution reactor is intended to become a solution burst machine in the future, with the goal of studying

radiolytic gas formation and thermal expansion as shutdown mechanisms (Malenfant et al, 1980).

Along with the experimental results from research reactors, mathematical simulations have been developed to model excursions in fissile solution reactors. During the KEWB program, a model simulating the KEWB experiments was developed. This model included a nonlinear shutdown mechanism that assumed the dissolved gas concentration was a linear function of the energy released and the nucleation rate of bubbles was proportional to the power. See Dunenfeld et al (1962) and Hetrick (1971). Dunenfeld and Stitt (1963) added an energy threshold model to the KEWB model, which allowed them to match pressure data to the power data. However, they first had to assume exponential time functions for the inertial pressure.

The United Kingdom Atomic Energy Authority (UKAEA) has developed a computer code (CRITEX) to simulate a sudden excursion in fissile solutions (Bickley et al, 1987). CRITEX computes the growth and movement of a gas void as it migrates toward the solution surface. This model predicts the power oscillations observed in the CRAC experiments, but the simulation of transient pressure was not included. The UKAEA has

also developed another computer code (CHAMPAGNE), which calculates the expansion of a gas bubble in a fissile liquid solution super-saturated with radiolytic gas (Mather, 1988). In this code, a bubble is nucleated at a small radius and expands subject to surface tension, inertia, and viscous forces.

The Soviets have also developed a mathematical simulation of fissile solution reactors (Sizov, 1985). This model incorporates some of the theoretical results from the KEWB program with Soviet kinetics and hydrodynamics equations. The Soviets have also developed "radiolytic boiling" equations, which describe the behavior of a group of gas bubbles produced on fission fragment tracks during the course of a pulse. Also, the number of bubbles produced per fission and their size has been investigated with this model.

A new method in solution excursion simulations has been developed at the University of Arizona. A complete equation of state for a liquid containing bubbles of radiolytic gas has been derived by Hetrick (1987). The nuclear fission dynamics and the reactivity feedback are coupled with equations of state, energy, and momentum. This method, derived from quasi-static thermodynamic theory, has been successful in computing the

maximum power and pressure for a number of excursions of various sizes, which were observed in the KEWB, CRAC, and SILENE experiments. Two additions to this model were proposed by Pribyl (1989). The first was the concept of momentum dissipation, which added an additional term to the fluid acceleration equation in order to dissipate some of the kinetic energy of the fluid as it expands. The second addition was a bubble growth model, which accounted for changes in bubble radius and its effect on physical properties. Another modification to the model was proposed by Smith (1989). This modification involved the idea of multiple regions, which could better simulate the spatial distribution of energy and acceleration. These additions to the original model, as implemented, did not significantly improve the model's ability to predict pressure pulses. However, they helped provide the foundation upon which the work in this report was begun.

This report presents new developments made to the simulation model developed at the University of Arizona. A radiolytic gas production model, which includes dynamic bubble equations that track the number of bubbles during a pulse, has been added. The equation of state has been modified to provide a better account of the relationship between radiolytic gas bubbles

and inertial pressure. Also, the model has been expanded into a two-dimensional multiple region model. The predictive capability of the model is then compared with experimental data from research reactors, such as KEWB, CRAC, and SILENE.

CHAPTER 2

RADIOLYTIC GAS

2.1 Fission Track Nucleation Phenomena

The water used as moderator or coolant in an aqueous solution reactor may become sufficiently superheated or gas supersaturated for radiation nucleation of vapor or gas bubbles to occur during high power operation. Under these conditions the large flux of ionizing particles, especially fission fragments, will produce large numbers of bubbles. This process begins with fission fragments slowing down in the liquid. In scattering collisions with the liquid, the fission fragments can cause dissociation of the liquid into various products, such as hydrogen and oxygen in aqueous solutions. Also, while moving through the liquid, the fission fragments create a "thermal spike," which is a region of high temperature along the fission track (Norman and Spiegler, 1963; Seitz, 1957). The "thermal spike" expands rapidly and breaks up into separate regions of mixed water vapor and radiolytic gas. These vapor-gas

microbubbles can act as nucleation centers for very large bubbles when the liquid is superheated or gas supersaturated. A gas bubble will then shrink or grow by diffusion, depending on whether the solution is over saturated or undersaturated.

2.2 Radiolytic Gas Production Model

The amount of radiolytic gas in the form of gas bubbles and the rate at which these bubbles appear in a liquid solution are of major importance when calculating inertial pressure during a nuclear power pulse. Also, the void fraction, f (total volume of gas divided by total solution volume) is required in order to calculate solution properties. To track these quantities as a function of time, a dynamic gas model has been developed. This model assumes that the dominant nucleation process is radiation nucleation along fission tracks, and neglects other nucleation sites such as small particles in the liquid solution and the surface of the reactor vessel. Also, it is assumed that the radiolytic gas of an aqueous solution is a mixture of hydrogen and oxygen.

The total amount of dissolved gas produced during a pulse, x_E, expressed as a mass fraction (total mass of gas divided by the total mass of the solution), is given by

$$x_E = GE(t)/M \tag{2-1}$$

where

G = the dissociation rate in mass of hydrogen and oxygen per unit energy

$E(t)$ = nuclear energy of pulse

M = total mass of solution.

When the dissolved gas concentration reaches a threshold concentration x_T, the solution is dynamically saturated and any additional gas produced can be used to form large gas bubbles. The excess concentration x is given by

$$x = \begin{cases} 0, & x_E < x_T \\ x_E - x_T, & x_E > x_T \end{cases} \tag{2-2}$$

where the threshold concentration x_T is approximately 10^{-4} kg of radiolytic gas per kg of water solution for fast transients. The excess gas concentration x is also the total amount of radiolytic gas that will eventually come out of solution after a pulse.

The amount of gas in the form of bubbles is dependent on the fission rate, the dissolved gas concentration, and the solution pressure. A power excursion can be separated into three stages, each with its own bubble formation mechanism.

The first stage extends from the start of the excursion to the point of threshold concentration. During this stage, the liquid solution is dynamically undersaturated with dissolved radiolytic gas. Only microbubbles formed along the fission tracks are present. Surface tension collapses these bubbles quickly, forcing gaseous products such as hydrogen and oxygen into solution. Previous studies have concluded that microbubbles are nucleated at a fixed radius of 5×10^{-8} m independent of temperature, liquid pressure, surface tension, dissolved gas concentration, and uranium concentration (Spiegler et al, 1962). A microbubble is formed by each fission fragment. A dynamic model of this may be written as

$$\frac{dN_1}{dt} = 2 \times n_f(t) - \frac{N_1(t)}{L_1} \qquad (2\text{-}3)$$

where

N_1 = number of microbubbles

$n_f(t)$ = fission rate

L_1 = microbubble lifetime (10 microseconds).

These bubbles are very small ($5.2 \times 10^{-22\ m^{-3}}$), and their effect on inertial pressure is negligible. However, they constitute enough void volume to produce an increase in isothermal compressibility. The total volume of these bubbles is given by

$$V_{bl} = N_1 v_{bl} \tag{2-4}$$

where

V_{bl} = total volume of microbubbles

v_{bl} = volume of each microbubble.

The void fraction for this stage is given by

$$f = \frac{V_{bl}}{V_0} \tag{2-5}$$

where V_0 is the initial solution volume.

The second stage is from the point of threshold concentration to the point of peak pressure. During this stage, the dissolved gas concentration is large enough to support the formation and expansion of large gas bubbles. These larger bubbles are formed at microbubble sites along the fission track. Dissolved gas diffuses into the microbubbles causing them to

expand rapidly. Recent work on radiolytic gas bubble growth suggests that these bubbles expand extremely rapidly to a size of approximately $5x10^{-13}$ m^3 within 10^{-5} seconds (Mather, 1988). This expansion time is extremely short when compared with the duration of fast pulses. It is therefore assumed in this model that large gas bubbles appear fully grown. A dynamic model of large gas bubbles is given by

$$\frac{dN_2}{dt} = \frac{F_2 x(t) n_f(t)}{P(t)} - \frac{N_2(t)}{L_2} \qquad (2\text{-}6)$$

where

N_2 = number of large bubbles

$x(t)$ = excess gas concentration

$P(t)$ = solution pressure

L_2 = large bubble lifetime (50 microseconds)

F_2 = empirical constant.

This model reflects some basic physical mechanisms that are believed to be important in the formation of radiolytic gas bubbles. First, since the number of microbubbles is directly proportional to the fission rate, the number of large gas bubbles is also directly proportional to fission rate. Secondly, the rate at which large gas bubbles are formed is directly

proportional to the excess concentration of dissolved gas. More dissolved gas means that more of the potential microbubble sites can form large bubbles. And finally, the rate at which large bubbles are formed is inversely proportional to solution pressure. As pressure increases, it becomes more difficult for bubbles to expand. The dynamic pressure increase eventually causes the collapse of the large bubbles.

The empirical constant F_2, which was determined to be on the order of 10^{-4} from transient data, reflects the fact that large bubbles form at only a fraction of the potential nucleation sites. As described later, calculations made with this model have shown that bubbles formed during this stage use only about one tenth of the total excess dissolved gas available.

The total volume of gas appearing in the form of bubbles during this stage, is given by

$$V_g = v_{b1} N_1 + v_{b2} N_2 \tag{2-7}$$

where v_{b2} is the volume of a large gas bubble. Note also, that the rate at which this void appears is given by

$$\frac{dV_g}{dt} = v_{b1}\frac{dN_1}{dt} + v_{b2}\frac{dN_2}{dt}. \tag{2-8}$$

The void fraction for this stage is given by

$$f = \frac{V_g}{V_0}. \tag{2-9}$$

The final stage occurs immediately after peak pressure. As a result of the sudden relief in pressure, the excess dissolved gas comes out of solution rapidly. It is believed that this process is similar in nature to violent cavitation. To compute the additional increase in the void fraction for this region, the excess concentration x, which is now the mass fraction of gas in the solution, is combined with the ideal gas law and the equation of state for a bubble. The ideal gas law may be written as

$$v_g = \frac{R_g T}{P_i} \tag{2-10}$$

where

v_g = specific volume of gas

R_g = gas constant for radiolytic gas

T = temperature of gas

P_i = internal pressure of gas bubble.

The equation of state for a gas bubble is given by

$$P_i = P + \frac{2\sigma}{r_b} \tag{2-11}$$

where σ is the surface tension and r_b is the bubble radius. If we take

$$V = V_l + V_{g'}$$

and

$$v = (1-x)v_l + xv_g,$$

then a void-quality relation can be written as follows

$$\Delta f = \frac{V_{g'}}{V} = x\frac{v_g}{v} \tag{2-12}$$

where $V_{g'}$ is the excess dissolved gas coming out of solution. If we substitute equations (2-10) and (2-11) into equation (2-12), we obtain

$$\Delta f = \frac{xR_gT}{(P + \frac{2\sigma}{r_b})(1-x)v_l + xR_gT}. \tag{2-13}$$

However, a modification to this model has been made to obtain

$$\Delta f = \frac{x R_g T}{(P + \frac{2\sigma}{r_b})(1-x)v_l + x R_g T}\left(1 - \frac{P(t)}{P_{\max}}\right). \qquad (2\text{-}14)$$

This modification accounts for the fact that not all the dissolved gas comes out of solution at once. Observations of this model have shown that a linear function of pressure provides the best fit with transient data.

During a pulse, the void fraction, as a function of time, can be written as

$$f(t) = \begin{cases} \dfrac{v_{b1}N_1(t) + v_{b2}N_2(t)}{V_0} & t < t_p \\ \dfrac{v_{b1}N_1(t) + v_{b2}N_2(t)}{V_0} + \Delta f & t > t_p \end{cases} \qquad (2\text{-}15)$$

where t_p is the time at which peak pressure occurs.

Once the liquid solution has reached saturation, the reactor behaves like a gas bubble chamber. This gas production model was developed to simulate this situation. Also, a dynamic bubble production model is vital to the calculation of inertial pressure, which will be presented next.

CHAPTER 3

ONE-REGION MODEL

The following is a brief summary of the physical events that occur during a large power burst in typical homogeneous aqueous solution assemblies.

After a large reactivity insertion, the reactor responds with an exponential power burst. This burst causes a rapid increase in the temperature of the fuel solution. Some inertial pressure may be created by a "lag" in thermal expansion. Fission fragments cause radiolysis of the water, which produces dissolved gas. Once the threshold concentration of dissolved gas is reached, large gas bubbles are formed and additional inertial pressure is created. The inertial pressure causes the fuel solution to be accelerated rapidly. This acceleration causes an expansion of the fuel solution volume. This volume expansion, along with an increase in the temperature of the fuel material, compensates for the initial reactivity insertion and cause a self-shutdown of the pulse.

To analyze these excursions, a mathematical model, which describes the relevant physical mechanisms, is used. The starting point is a one-region, lumped parameter model. This is a very simple model, which does not take into account any spatial variations in temperature or pressure. However, this model was used to develop the gas production model presented in chapter 2, and to determine which physical mechanisms are the most important during an excursion.

3.1 Inertial Pressure

Two mechanisms are responsible for the formation of inertial pressure in aqueous solutions. The first is a "lag" in thermal expansion during an exponential power burst. This effect may occur in any fuel-bearing material. The rate at which the temperature of the fuel material increases is so large that the volume of the material cannot expand fast enough to relieve the pressure produced. The second mechanism by which inertial pressure is produced is radiolytic gas formation. On the microscopic level, a gas bubble expands rapidly or explosively causing a pressure wave in the liquid surrounding it. The pressure at the bubble wall is given by

$$P = \frac{3}{2}\rho_l \left(\frac{dr_b}{dt}\right)^2$$

where ρ_l is the liquid density and r_b is the bubble radius (Norman and Spiegler, 1963). This expression is for the pressure at the wall of a uniformly expanding sphere in an incompressible liquid. On the macroscopic level however, the sum of these pressure waves results in inertial pressure. The radiolytic gas bubbles form and expand so rapidly that the overall volume of the liquid solution cannot grow fast enough to accommodate the displacement of liquid by gas bubbles. This results in a transient compression of the liquid solution and enhancement of inertial pressure.

A differential equation of state for a solution containing radiolytic gas bubbles has been derived by Hetrick (1987) from quasi-static thermodynamic theory. The quasi-static differential representation for liquid pressure is found by assuming that the liquid pressure is a function of the liquid solution temperature and volume only. If we take $P=P(T,V_l)$, then

$$\frac{dP}{dt} = \left(\frac{\partial P}{\partial T}\right)_{V_l} \frac{dT}{dt} + \left(\frac{\partial P}{\partial V_l}\right)_T \frac{dV_l}{dt}. \qquad (3\text{-}1)$$

The isobaric compressibility is defined as

$$\beta_0 = \frac{1}{V_l}\left(\frac{\partial V_l}{\partial T}\right)_p . \tag{3-2}$$

The isothermal compressibility is defined as

$$\kappa_0 = -\frac{1}{V_l}\left(\frac{\partial V_l}{\partial P}\right)_T . \tag{3-3}$$

Equations (3-2) and (3-3) may be used to obtain

$$\left(\frac{\partial P}{\partial T}\right)_{V_l} = -\frac{\left(\frac{\partial V_l}{\partial T}\right)_P}{\left(\frac{\partial V_l}{\partial P}\right)_T} = \frac{\beta_0}{\kappa_0} \tag{3-4}$$

and

$$\left(\frac{\partial P}{\partial V_l}\right)_T = -\frac{1}{\kappa_0 V_l} . \tag{3-5}$$

substituting equations (3-4) and (3-5) into (3-1) gives

$$\frac{dP}{dt} = \frac{\beta_0}{\kappa_0}\frac{dT}{dt} - \frac{1}{\kappa_0 V_l}\frac{dV_l}{dt} . \tag{3-6}$$

Equation (3-6) is the equation of state for the liquid solution; However, the presence of radiolytic gas bubbles distributed throughout the solution

significantly alters the physical properties of the liquid solution. Values for the isobaric and isothermal compressibility are needed for a liquid containing various volumes of gas bubbles. For the purpose of computing these values it is assumed that the total volume of the solution is the sum of the liquid volume and the gas bubble volume, $V=V_g+V_l$. Equations (3-2) and (3-3) may then be replaced by

$$\beta = \frac{1}{V}\left(\frac{\partial V}{\partial T}\right)_P = \frac{1}{V}\left(\frac{\partial V_l}{\partial T}\right)_P + \frac{1}{V}\left(\frac{\partial V_g}{\partial T}\right)_P \tag{3-7}$$

and

$$\kappa = -\frac{1}{V}\left(\frac{\partial V}{\partial P}\right)_T = -\frac{1}{V}\left(\frac{\partial V_l}{\partial P}\right)_T - \frac{1}{V}\left(\frac{\partial V_g}{\partial P}\right)_T . \tag{3-8}$$

Equations (3-7) and (3-8) may be rearranged to give the following expressions

$$\beta = \frac{V_l}{V}\frac{1}{V_l}\left(\frac{\partial V_l}{\partial T}\right)_P + \frac{V_g}{V}\frac{1}{V_g}\left(\frac{\partial V_g}{\partial T}\right)_P \tag{3-9}$$

and

$$\kappa = -\frac{V_l}{V}\frac{1}{V_l}\left(\frac{\partial V_l}{\partial P}\right)_T - \frac{V_g}{V}\frac{1}{V_g}\left(\frac{\partial V_g}{\partial P}\right)_T. \qquad (3\text{-}10)$$

By using the void fraction f, given by equation (2-15), and substituting equations (3-2) and (3-3) into (3-9) and (3-10), we obtain

$$\beta = (1-f)\beta_0 + \frac{f}{V_g}\left(\frac{\partial V_g}{\partial T}\right)_P \qquad (3\text{-}11)$$

and

$$\kappa = (1-f)\kappa_0 - \frac{f}{V_g}\left(\frac{\partial V_g}{\partial P}\right)_T. \qquad (3\text{-}12)$$

To compute the partial derivatives in equations (3-11) and (3-12) it is assumed that each bubble is in mechanical equilibrium, which is given by equation (2-11). It is also assumed that the ideal gas law holds for the gas inside each bubble. In the gas production model presented in chapter 2, it was assumed that all the large bubbles were of uniform size. This means an increase in the gas volume is an increase in the number of bubbles. It is also assumed that the gas bubbles are in thermal equilibrium with the surrounding liquid. The ideal gas law may be rewritten as

$$P_i = \frac{mR_gT}{V_g} \tag{3-13}$$

where P_i is the internal gas pressure of the bubble and m is the mass of gas in all the bubbles. The total volume of gas in the system is equal to the volume of a single bubble times the total number of bubbles. This may be written as

$$V_g = N\frac{4}{3}\pi r_b^3 \tag{3-14}$$

where N is the total number of bubbles. Substituting equation (3-13) and equation (3-14) into equation (2-11) gives

$$PV_g = mR_gT - 2\sigma\left(\frac{4}{3}\pi N\right)^{1/3} V_g^{2/3}. \tag{3-15}$$

Differentiation of equation (3-15) gives

$$PdV_g + V_g dP = mR_g dT - \frac{4}{3}\sigma\left(\frac{4}{3}\pi N\right)^{1/3} V_g^{-1/3} dV_g. \tag{3-16}$$

Rearrangement of equation (3-16) gives

$$\left(P + \frac{4\sigma}{3r_b}\right)\frac{dV_g}{V_g} + dP = \left(P + \frac{2\sigma}{r_b}\right)\frac{dT}{T}. \tag{3-17}$$

In a constant temperature process (dT=0), equation (3-17) becomes

$$\frac{1}{V_g}\left(\frac{\partial V_g}{\partial P}\right)_T = \frac{-1}{P + \dfrac{4\sigma}{3r_b}}. \tag{3-18}$$

In a constant pressure process (dP=0), equation (3-17) becomes

$$\frac{1}{V_g}\left(\frac{\partial V_g}{\partial T}\right)_P = \left(\frac{1}{T}\right)\frac{P + \dfrac{2\sigma}{r_b}}{P + \dfrac{4\sigma}{3r_b}}. \tag{3-19}$$

Substituting equations (3-18) and (3-19) into equations (3-11) and (3-12), the isobaric and isothermal compressibility become

$$\beta = (1-f)\beta_0 + \left(\frac{f}{T}\right)\frac{P + \dfrac{2\sigma}{r_b}}{P + \dfrac{4\sigma}{3r_b}} \tag{3-20}$$

and

$$\kappa = (1-f)\kappa_0 + \frac{f}{P + \dfrac{4\sigma}{3r_b}}. \tag{3-21}$$

It should be noted that the isothermal compressibility of a bubble liquid mixture is strongly dependent on bubble radius, void fraction and liquid pressure. Large gas bubbles, nucleated later in the second stage after

threshold, will expand in a medium whose isothermal compressibility has increased significantly. These later gas bubbles will produce less system pressure than bubbles formed earlier in the stage. It is for this reason that the isothermal compressibility is the most important physical property in the equation of state.

An equation for the change in liquid solution volume as a function of time may be written as

$$\frac{dV_l}{dt} = \left(\frac{dV_l}{dt}\right)_{acceleration} + \left(\frac{dV_l}{dt}\right)_{gas\ compression} . \qquad (3\text{-}22)$$

The second term on the right hand side of equation (3-22) is due to radiolytic gas. The effect of radiolytic gas bubbles forming and expanding in the liquid solution is to decrease the liquid volume and compress the liquid. The rate at which the liquid solution volume is compressed is directly proportional to the rate at which gas bubble volume appears. An expression for the rate at which radiolytic gas bubble volume appears is given by equation (2-8). Substituting equation (2-8) into (3-22) gives

$$\frac{dV_l}{dt} = \left(\frac{dV_l}{dt}\right)_{acceleration} - \left(v_{b1}\frac{dN_1}{dt} + v_{b2}\frac{dN_2}{dt}\right). \qquad (3\text{-}23)$$

The first term on the right hand side of equation (3-23) is the acceleration of the liquid solution produced by the inertial pressure. This term will be presented later in this chapter.

3.2 The Energy Equation

In order to use the equation of state, an expression for the temperature change in the liquid solution is required. The energy equation from quasi-static thermodynamic theory and the first law of thermodynamics has been used to develop a temperature equation. First, the internal energy, which is a function of the nuclear energy generated and the mechanical work done by the fluid, is differentiated to obtain the following expression

$$\frac{dU}{dt} = \left(\frac{\partial U}{\partial V_l}\right)_T \frac{dV_l}{dt} + \left(\frac{\partial U}{\partial T}\right)_{V_l} \frac{dT}{dt}. \qquad (3\text{-}24)$$

The first law of thermodynamics for this system may be written as

$$\frac{dU}{dt} = \frac{dE}{dt} - P\frac{dV_l}{dt} \tag{3-25}$$

where E is the thermal energy deposited in the system by nuclear fission. By using the definition of specific heat

$$C_v = \left(\frac{\partial U}{\partial T}\right)_V \tag{3-26}$$

and combining equations (3-24) and (3-25), we obtain

$$\frac{dT}{dt} = \frac{1}{C_v}\left\{\frac{dE}{dt} - \left[P + \left(\frac{\partial U}{\partial V_l}\right)_T\right]\frac{dV_l}{dt}\right\}. \tag{3-27}$$

Equation (3-27) may be rewritten as

$$\frac{dT}{dt} = \frac{1}{C_v}\left[\frac{dE}{dt} - T\left(\frac{\partial P}{\partial T}\right)_{V_l}\frac{dV_l}{dt}\right]. \tag{3-28}$$

See Reynolds and Perkins (1977). Substituting equation (3-4) into equation (3-28) gives

$$\frac{dT}{dt} = \frac{1}{C_v}\left[\frac{dE}{dt} - \frac{\beta}{\kappa}T\frac{dV_l}{dt}\right]. \tag{3-29}$$

Equation (3-29) is the energy equation for the one-region model.

3.3 Momentum Equation

As the inertial pressure increases, the liquid solution is accelerated rapidly upward into the void above the core. This acceleration increases the volume of the liquid, which in turn relieves the inertial pressure and brings the burst to an end. An expression for the acceleration may be given by

$$\rho \frac{du}{dt} = -\nabla P \tag{3-30}$$

where u is the velocity of the expanding solution volume. For simplicity the pressure gradient has been approximated by

$$-\nabla P = \frac{P - P_0}{h} \tag{3-31}$$

where

P = solution pressure

P_0 = pressure of void above core

h = height of core.

By using $\rho = M/V_l$ and $V_l = Ah$, where A is the cross-sectional area of the core, we can rewrite equation (3-30) as

$$\frac{d^2V_l}{dt^2} = \frac{A^2(P-P_0)}{M}. \qquad (3\text{-}32)$$

Equation (3-32) is quite artificial, particularly in a lumped parameter model. However, this formulation of acceleration forces the equation of state to predict the pressure at the bottom of the core, which is where the maximum pressure occurs. This approach differs from earlier formulations of acceleration, which used the equation of state to predict an average system pressure and assumed a pressure distribution with the maximum pressure twice the average (Hetrick, 1987). Since the earlier model predicted average pressure, it is believed that it may underestimate the amount of radiolytic gas produced.

3.4 Reactor Kinetics

The power generated by this system is strictly due to the fissile material in the liquid solution. The point reactor kinetics model is used to describe the power, and from this the total energy deposited in the solution can be computed. A step input of reactivity is used to start the model's power excursion. The KEWB and SILENE experiments were initiated with step inputs, but the CRAC experiments used a slow ramp insertion of

reactivity. However, the fast CRAC experiments were performed without external sources, so they were effectively initiated with random reactivity step. The power excursions are limited by reactivity feedbacks. These feedbacks include expansion of the solution volume and temperature increase of the fuel material.

The point reactor kinetics equations may be written as follows

$$\frac{dn}{dt} = \frac{\rho - \beta}{\ell} n(t) + \sum_{i=1}^{6} \lambda_i c_i \qquad (3\text{-}33)$$

and

$$\frac{dc_i}{dt} = \frac{\beta_i}{\ell} n(t) - \lambda_i c_i, \quad i = 1,6 \qquad (3\text{-}34)$$

where

n = the neutron power

c_i = the precursor latent power

ρ = the reactivity

β = the delayed neutron fraction

ℓ = the neutron generation time

λ_i = the decay constant for the specific precursor.

For this system, the six group precursor model has been used. The reactivity, which includes the step input and the reactivity feedback, may be written as

$$\rho = \rho_0 - \beta \phi (V - V_0) \tag{3-35}$$

where

ρ_0 = the step input reactivity

ϕ = the volume feedback reactivity coefficient

V = the solution volume

V_0 = the initial solution volume.

For the one-region model, the feedback effects of temperature and expansion have been combined into one volumetric feedback coefficient. Also, the neutron temperature coefficient, which is less important for high concentration uranium solutions, has been neglected.

The amount of energy deposited in the fuel solution may be obtained from

$$E(t) = \int_0^t n(\tau)\, d\tau\,. \tag{3-36}$$

By differentiating equation (3-36) we obtain

$$\frac{dE}{dt} = n(t). \tag{3-37}$$

Equations (3-36) and (3-37) complete the one-region model. The one-region model has been used to simulate various experiments, such as KEWB, CRAC, and SILENE. The results of these simulations are presented next in Chapter 4.

CHAPTER 4

ONE-REGION MODEL RESULTS

The one-region model has been implemented in a computer code and used to simulate excursions in aqueous homogeneous solution assemblies. These computations were performed on a 386 PC, using DESIRE, an interactive dynamic system simulation software package (Korn, 1989). Power and pressure data from the KEWB, CRAC, and SILENE experiments were used as a benchmark for the model. Predicted power and pressure traces produced by the one-region model are compared with actual power and pressure traces from the KEWB, CRAC, and SILENE experiments. In addition, the one-region model has been used to simulate hypothetical excursions in the SHEBA reactor.

4.1 KEWB

The KEWB experiments used both a spherical and a cylindrical core configuration. The spherical core had a graphite reflector surrounding it.

The cylindrical core also used a graphite reflector in two series of experiments, but in the last series of experiments, KEWB-5, the core was unreflected. The one-region model has been used to simulate excursions in the KEWB-5 core, because it is an unreflected cylindrical solution assembly like CRAC and SILENE.

The KEWB-5 core had a diameter of 12 in. and an overall length of 36 in.. The walls of the vessel were 0.25 in. thick and made of stainless steel. A tube with an inner diameter of 1.99 in. passed horizontally through the cylinder 6 in. from the bottom of the vessel. This tube held a poison rod used to initiate power pulses. There were also four 1 in. tubes containing normal control rods passing through the vessel parallel to the vertical axis of the cylinder. The vessel also had 110 feet of water-filled cooling coils passing through it. These cooling coils had an outer diameter of 0.25 in.. In the KEWB-5 core, the uranyl sulfate fuel concentration was 203 gU^{235} per liter and the solution volume was 24 liters.

In the KEWB experiments, a pulse was initiated by moving the control rods to a position that would give the desired reactivity release. The poison rod would then be removed rapidly. A rapid ejection of the poison rod could approximate a step reactivity insertion.

In order to simulate the power and pressure pulses of experimental reactors, two adjustable parameters were used in the one-region model. The volumetric coefficient of reactivity, given in equation (3-35), is the parameter used to match the calculated and experimental peak power. To match the calculated peak pressure with the experimental data, the empirical constant F_2, given in equation (2-6), was adjusted. These parameters were only used to match one set of pulses from each reactor. Values for these parameters for each reactor are given in Table 4-1.

Figures 4-1 and 4-2 give a comparison between the one-region model's results for peak power and peak pressure and the KEWB-5 results (Dunenfeld and Stitt, 1963). The calculated peak power for several transients as a function of maximum inverse period has a slope of 1.7, which compares closely to the 1.9 slope of the experimental data. The maximum relative error between calculated peak power and the experimental data is approximately 25%, which occurs for the slowest transient. The calculated peak pressure for several transients as a function of maximum inverse period also compares quite well with the experimental data. The maximum relative error between calculated peak pressure and

experimental data is approximately 19%, which also occurs for the slowest transient. Results from the one-region model are given in Table 4-2.

Figures 4-3 and 4-4 show a comparison between the model's computed power and pressure traces as a function of time and the experimental power and pressure traces for the KEWB-5 experiment #3041. The computed power trace matches the experiment quite well and has the same characteristic features as the experiment. The power decreases much more rapidly than it rises. However, the one-region model undershoots the delayed neutron tail. The computed pressure pulse also shows the main characteristics of the experimental trace. The pressure rises slowly at the beginning of the pulse due to the "lag" in thermal expansion. The pressure then rises sharply once the dissolved gas concentration reaches threshold, and large gas bubbles are formed. After peak pressure, the pressure decreases much more slowly than it rose. However, the one-region model's predicted pressure pulse is not broad enough. The pressure relief after the peak occurs much more rapidly than it should. Also, the initial rise in computed pressure is much slower than in the experimental trace. Figures 4-5 through 4-8 give the model's results for several of the KEWB-5 experiments. These transients range in size from a $2.46 pulse to a $4.227

pulse. A copy of the one-region computer model for the KEWB-5 experiments is given in Appendix A.

4.2 CRAC

Two series of experiments were run in the CRAC program. The first used a 300 mm diameter cylindrical core, and the second used an 800 mm diameter cylindrical core. The one-region model was used to simulate a set of fast transients in the first series of experiments. The reactor vessel in this series was 2090 mm high and had walls that were 3 mm thick. All the transients modeled had a solution volume of approximately 18 liters and a solution height of approximately 27 cm. The solution had a fuel concentration that ranged from 188 to 203 gU^{235}/liter.

To initiate a power pulse the fuel solution was injected into the cylinder at a constant rate. This produced a ramp increase in reactivity. After a supercritical volume of solution had been pumped into the cylinder, the power would increase until fuel material temperature and radiolytic gas shut the pulse down.

Figures 4-9 and 4-10 show a comparison between the one-region model's calculated peak power and pressure and experimental values for several different transients (Lécorché and Seale, 1973). The calculated peak power as a function of maximum inverse period has a slope of 1.8, which compares closely to the 1.9 slope of the experimental data. The maximum relative error between calculated and experimental peak power is 13%, which occurs for the slowest transient. Table 4-3 gives the one-region model's predicted peak power and pressure for several CRAC experiments.

Figures 4-11 and 4-12 show a comparison between the model's predicted power and pressure traces and the experimental traces for CRAC experiment #08 (Barbry, 1973). The model's predicted power and pressure traces have the same important characteristics as the experimental traces, as described above. However, as in the case of the KEWB model the predicted power trace undershoots the delayed neutron tail. Also, the predicted pressure trace is not as broad as the experimental pressure trace. Figure 4-13 shows the model's predicted power and pressure traces for the CRAC experiment #20.4, which is a much slower transient than experiment #08.

4.3 SILENE

The SILENE reactor vessel is a stainless steel annular cylinder with a diameter of 360 mm. A vertical channel with a diameter of 70 mm is located at the center of the vessel. This channel contains a reactivity insertion rod. The part of the vessel containing the fuel solution has a length of 1000 mm (Barbry, 1981 and 1987). All the experiments modeled had a solution volume of 37 liters. The uranyl nitrate fuel solution was enriched to 93.5% U^{235}, and the fuel concentration was 71 gU/liter.

To initiate a power pulse, the fuel solution would first be pumped into the reactor vessel. The vessel would be filled with a predetermined supercritical volume. The control rod would then be ejected rapidly causing the power to increase until feedback mechanisms shut the pulse down.

Figures 4-14 and 4-15 show a comparison between the model's peak power and pressure and the experimental results for several of the SILENE experiments (Barbry, 1975). The calculated peak power as a function of maximum inverse period has a slope of 1.8, which compares closely to a slope of 1.7 for the experimental data. The maximum relative error between the computed peak power and the experimental data is 20%, which occurs

for the slowest transient. The maximum relative error in computed peak pressure and experimental data is 29%, which also occurs for the slowest transient. Table 4-4 gives the peak power and pressure results for the one-region model.

Figures 4-16 through 4-23 give a comparison between the model's predicted power and pressure traces and the experimental traces for several of the SILENE experiments. Like KEWB and CRAC the model predicts the same important characteristics of the experimental traces, as described above. However, like KEWB and CRAC the model also undershoots the delayed neutron tail and produces pressure pulses which are not broad enough.

4.4 SHEBA

The SHEBA reactor vessel is a simple stainless steel cylindrical tank with a 6.35 mm thick wall. The vessel has an outer diameter of 520 mm and a length of 1020 mm. A vertical channel containing a control rod is located at the center of the vessel, and has an outer diameter of 31.75 mm. The uranyl fluoride fuel solution has a uranium density of 1 kg/liter, and

the uranium is only 5% enriched (Malenfant et al, 1980). The assembly being modeled here has a solution volume of 84 liters.

The reactivity of the SHEBA assembly is given by the following expression

$$\rho = \rho_0 - \beta\phi(V - V_0) - \beta\alpha_T\Delta T \qquad (4\text{-}1)$$

where

ρ = the step input reactivity

β = the delayed neutron fraction

ϕ = the volume feedback reactivity coefficient

V = the solution volume

V_0 = the initial solution volume

α_T = the temperature feedback coefficient of reactivity

ΔT = the temperature change of the solution.

Since the SHEBA assembly is only 5% enriched uranium, a temperature feedback coefficient has been added to account for Doppler feedback. Values for both the temperature and volume feedback coefficients have been calculated by Kornreich (1992 and 1993), and are given as follows

$$\alpha_T = 0.019\,\$/C \quad \phi = 2600\,\$/m^3.$$

Since SHEBA most closely resembles the SILENE reactor, the empirical constant F_2, is given a value of $5x10^{-4}$.

Figures 4-24 through 4-27 show the one-region model's predicted power and pressure traces for four hypothetical transients in the SHEBA reactor. These transients range in size from a pulse of \$2.0 to a pulse of \$5.0. As in the case of the other reactors modeled the power decreases much more rapidly after peak power than it rose. Also, the pressure increases slowly at first, then at the threshold dissolved gas concentration the pressure rises sharply. After peak pressure the pressure decreases much more slowly than it rose. Figures 4-28 and 4-29 show the model's predicted peak power and pressure for the four transients modeled. The predicted peak power as a function of maximum inverse period has a slope of 1.6. Table 4-5 gives the model's predicted peak power and pressure for the transients modeled.

Table 4-1 Empirical constant F_2 and volume feedback coefficient of reactivity ϕ for the reactors modeled.

	KEWB	CRAC	SILENE	SHEBA
F_2	1.45×10^{-4}	2.75×10^{-4}	4.7×10^{-4}	5.0×10^{-4}
ϕ ($/m^3)	10000	13500	8400	2600

Table 4-2 Predicted peak power and pressure for several of the KEWB experiments.

Experiment #	Peak Power (MW)	Peak Pressure (MPa)
3039	499	0.286
3041	713	0.430
3043	916	0.568
3014	1543	1.110
3027	1946	1.310
3016	2271	1.560
3017	2698	1.880
3018	3546	2.580

Table 4-3 Predicted peak power and pressure for several of the CRAC experiments.

Experiment #	Peak Power (MW)	Peak Pressure (MPa)
61	138	0.08
22	221	0.19
62.3	279	0.26
20.4	339	0.31
08	843	0.80

Table 4-4 Predicted peak power and pressure for several of the SILENE experiments.

Experiment #	Peak Power (MW)	Peak Pressure (MPa)
S1-11	222	0.12
S5-08	402	0.29
S1-169	419	0.31
S2-12	501	0.37
S1-16	576	0.43
S2-169	603	0.45
S4-169	623	0.47
S2-173	765	0.57

Table 4-5 Predicted peak power and pressure for several hypothetical SHEBA experiments.

Step Input Reactivity ($)	Peak Power (MW)	Peak Pressure (MPa)
2.0	869	0.34
3.0	2724	0.88
4.0	5207	1.78
5.0	8397	2.84

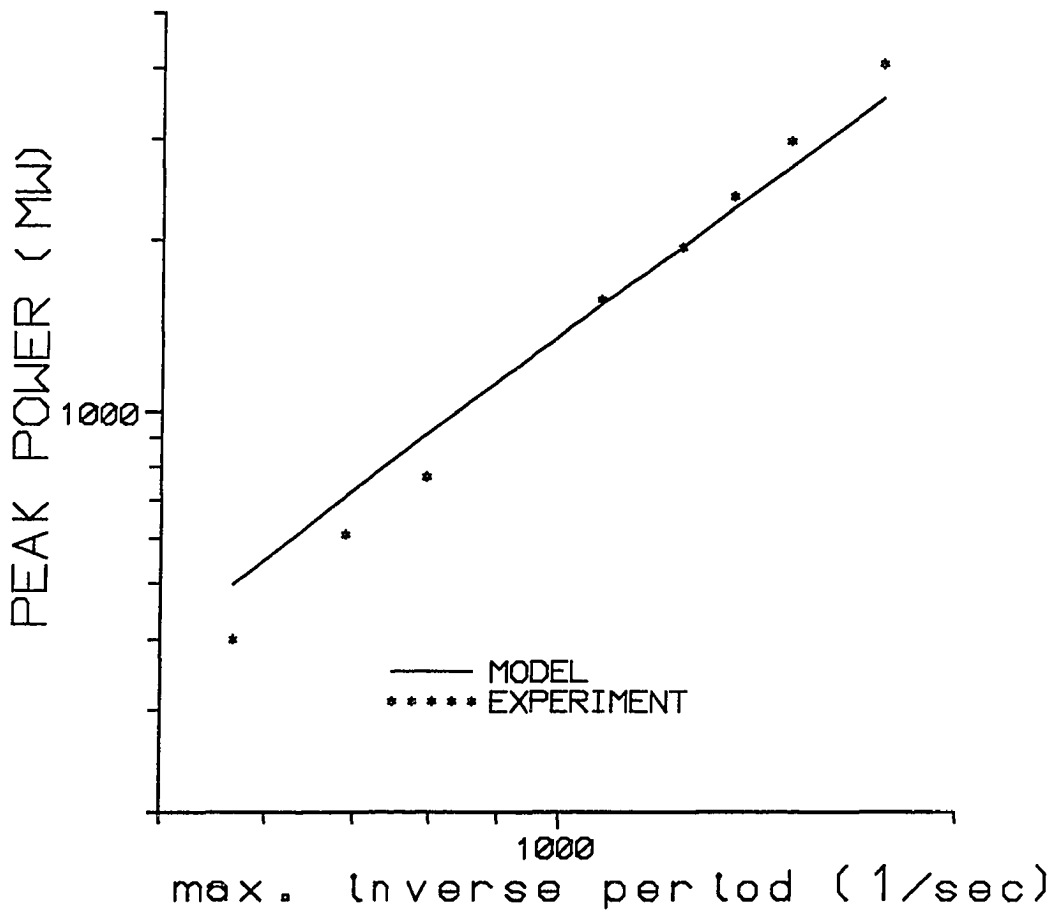

Figure 4-1 Peak power versus maximum inverse period for the KEWB-5 experiments.

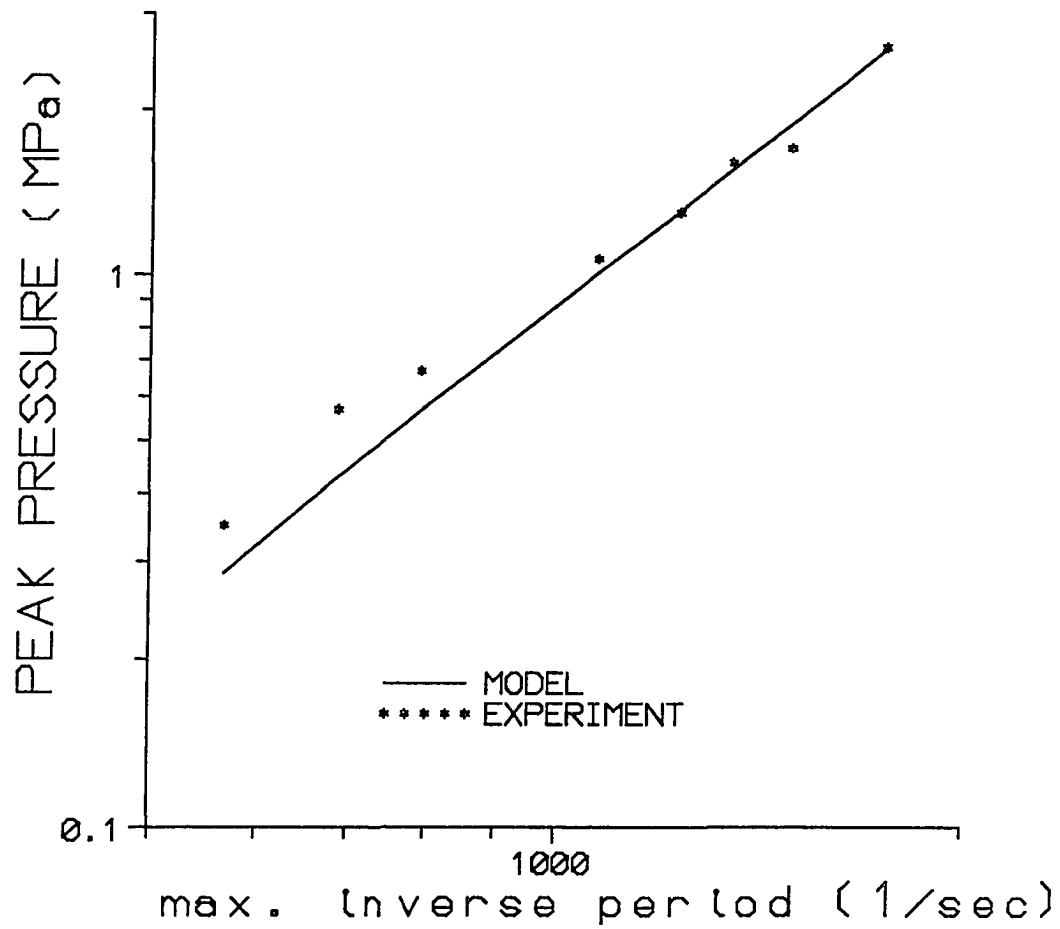

Figure 4-2 Peak pressure versus maximum inverse period for the KEWB-5 experiments.

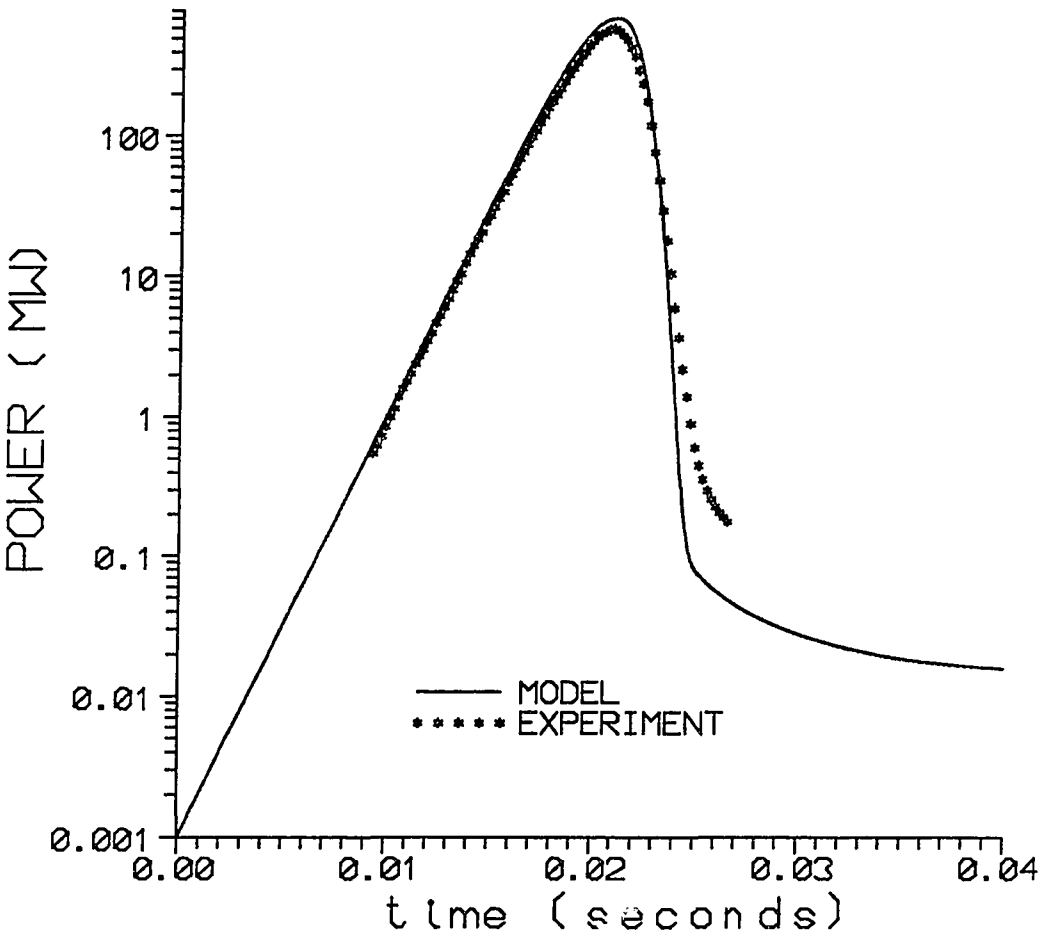

Figure 4-3 Predicted power versus time for KEWB-5 experiment #3041.

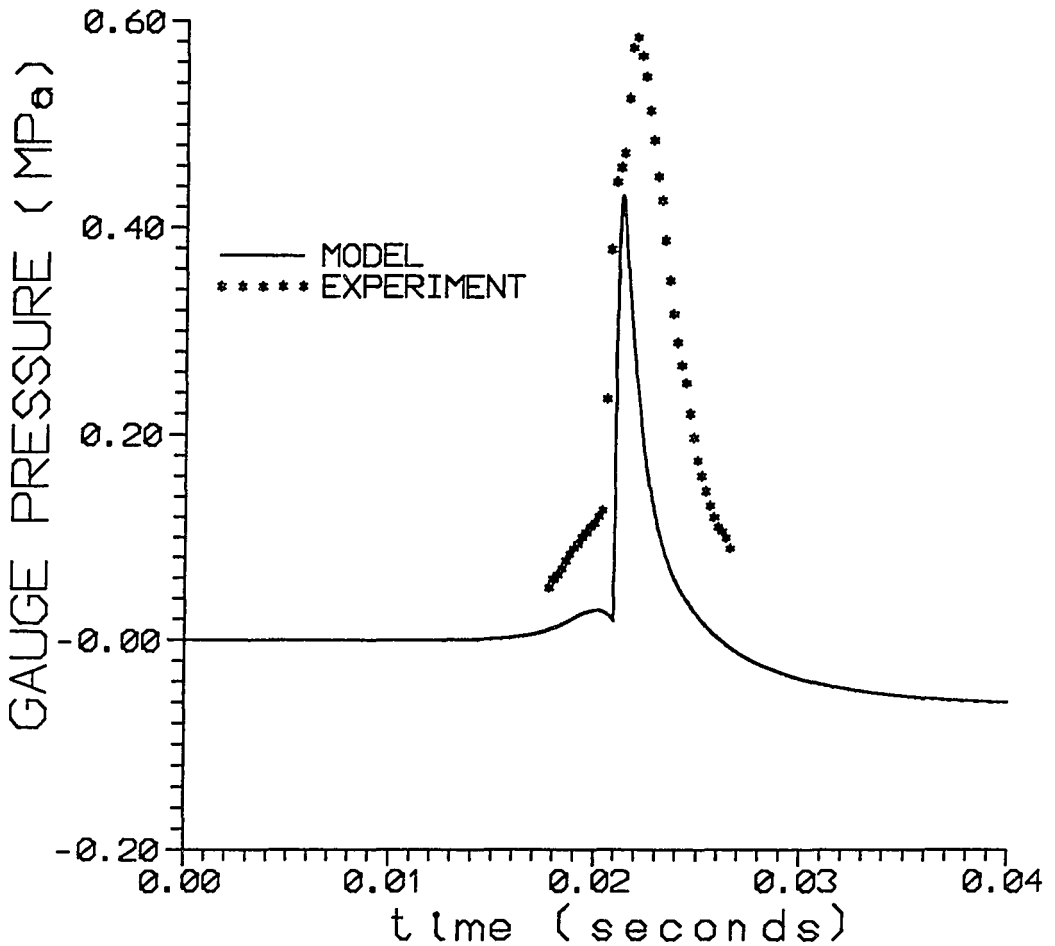

Figure 4-4 Predicted pressure versus time for KEWB-5 experiment #3041.

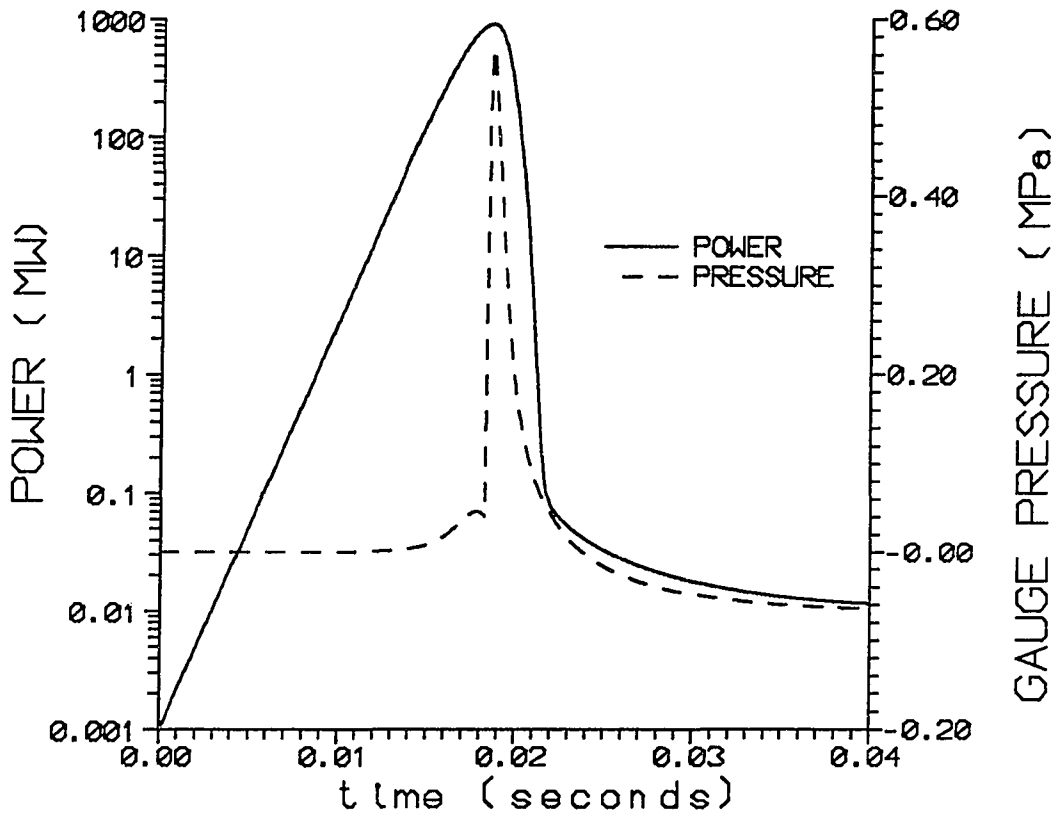

Figure 4-5 Predicted power and pressure versus time for KEWB-5 experiment #3043.

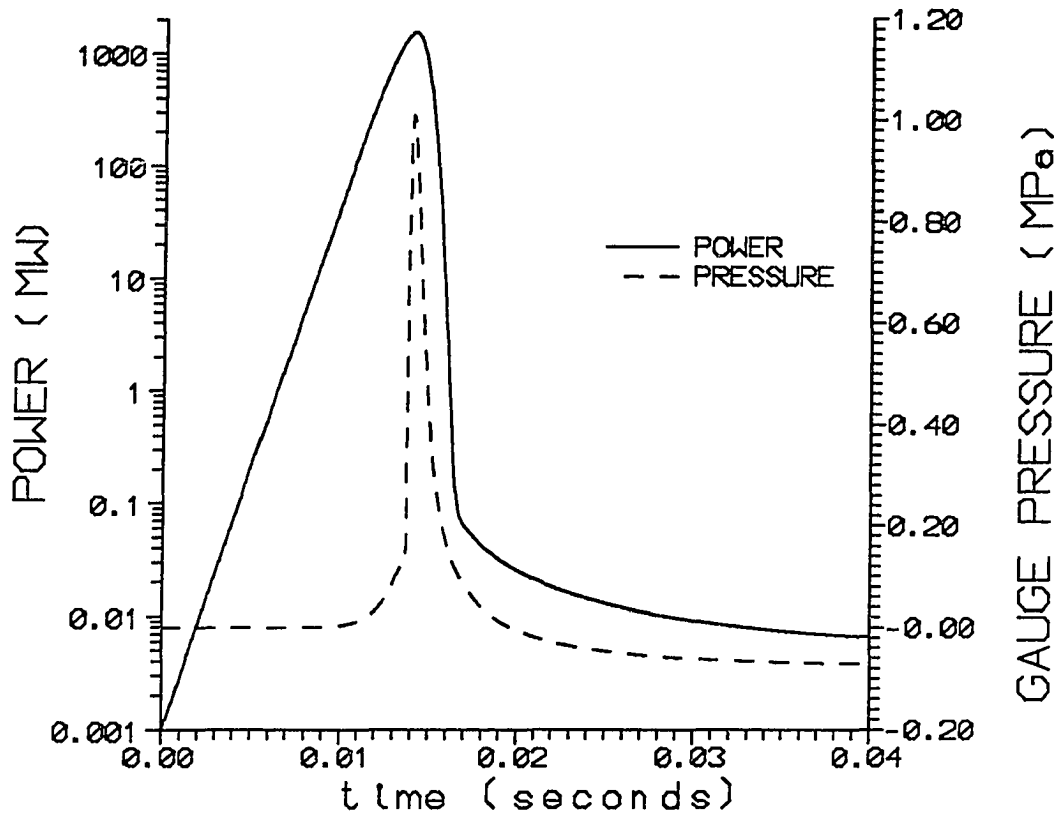

Figure 4-6 Predicted power and pressure versus time for KEWB-5 experiment #3014.

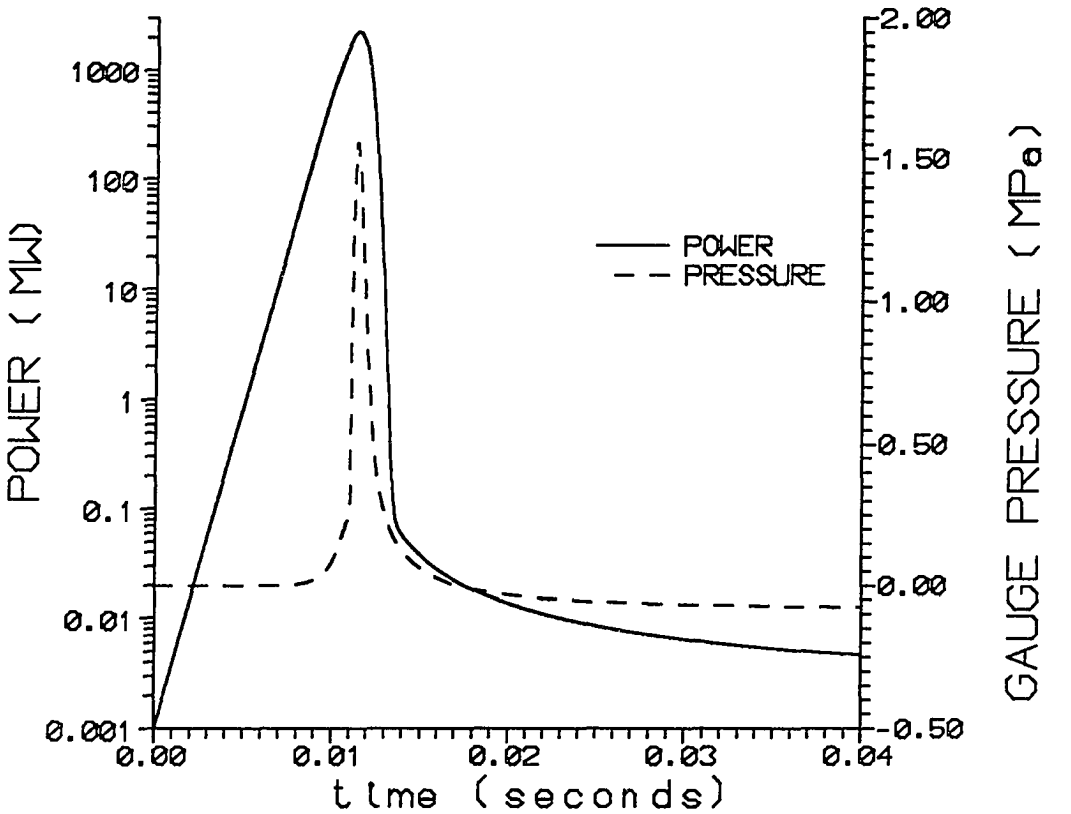

Figure 4-7 Predicted power and pressure versus time for KEWB-5 experiment #3016.

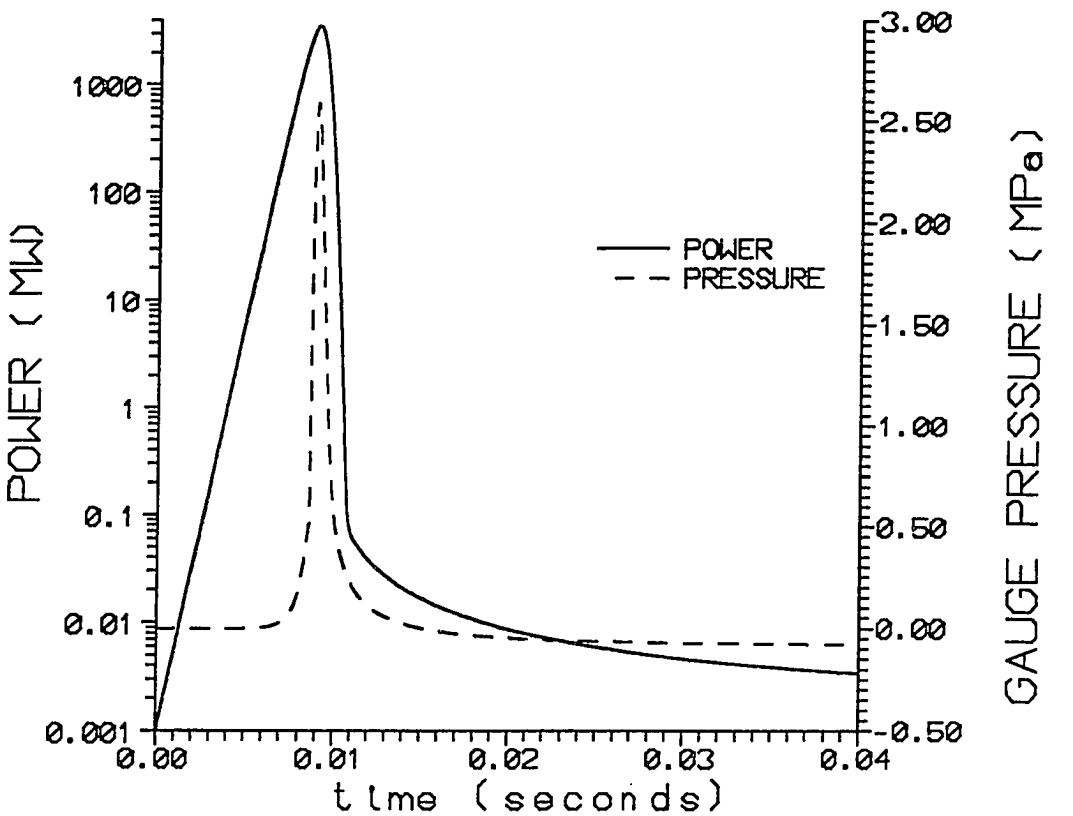

Figure 4-8 Predicted power and pressure versus time for KEWB-5 experiment #3018.

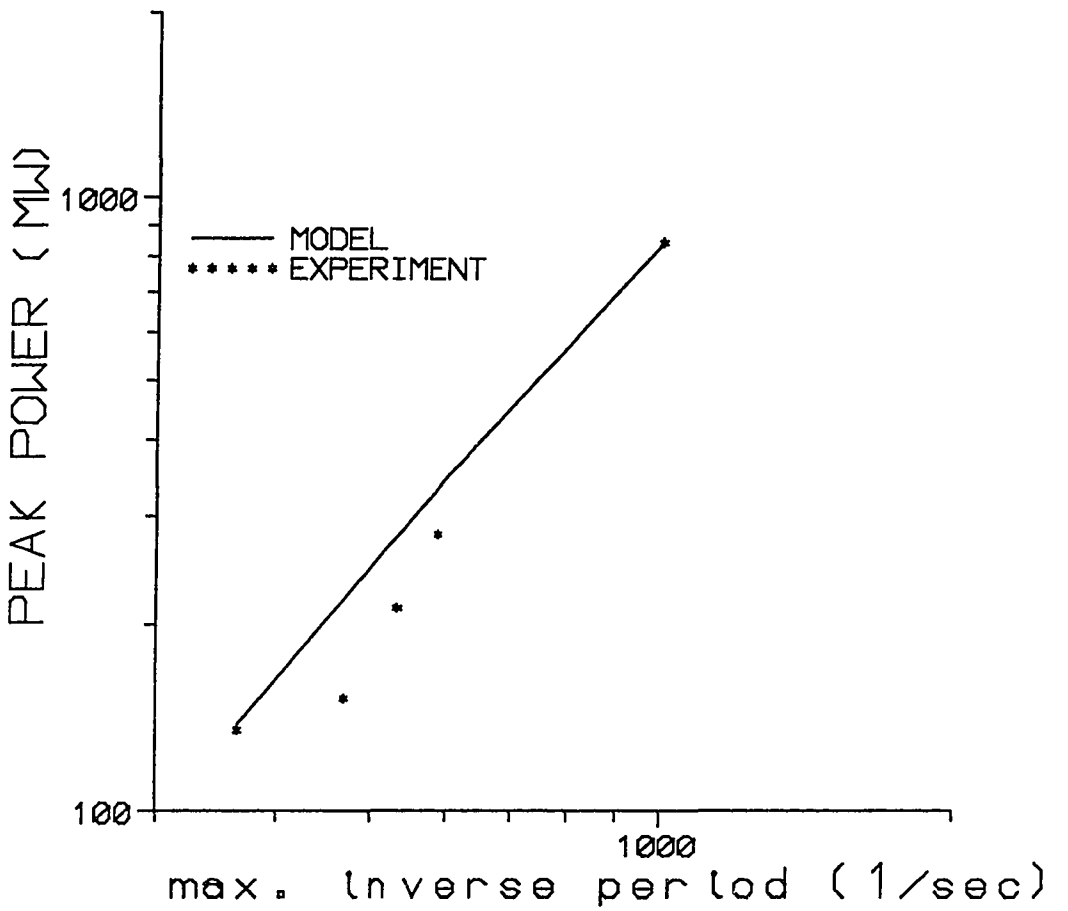

Figure 4-9 Peak power versus maximum inverse period for the CRAC experiments.

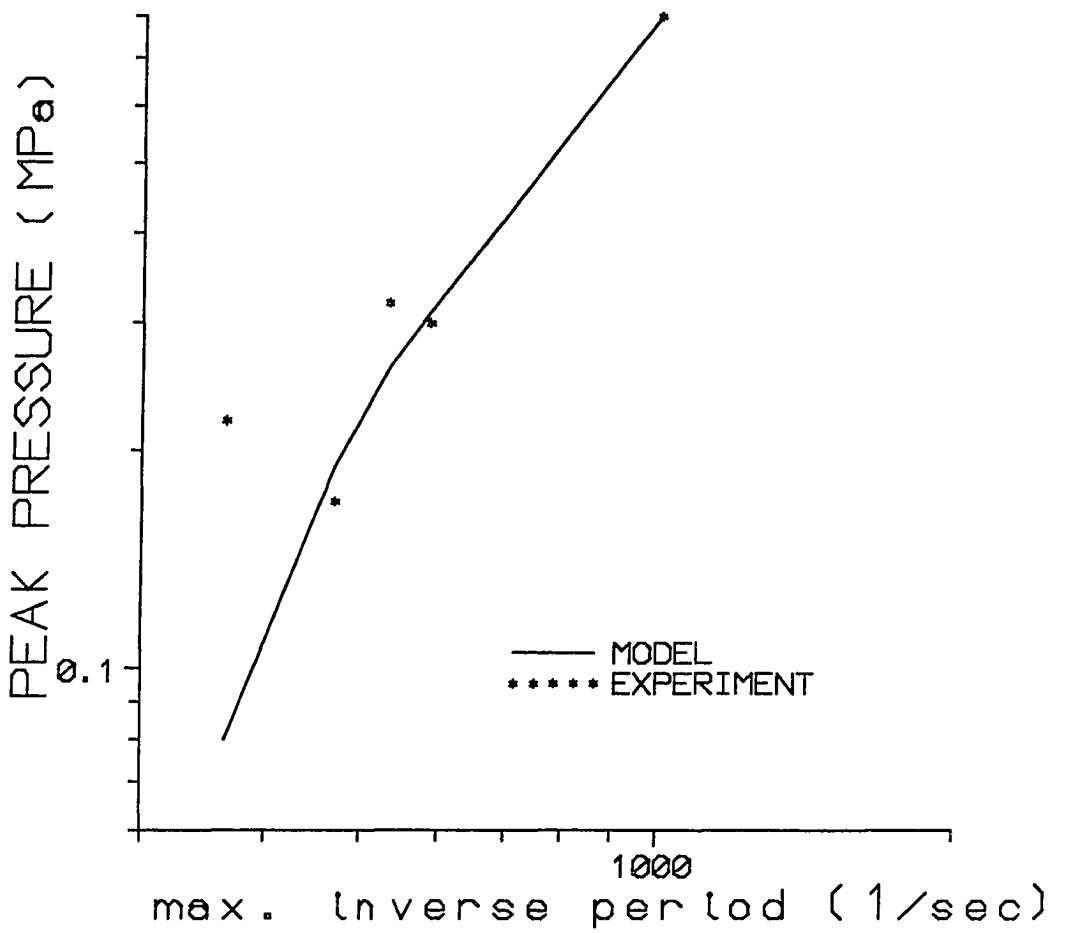

Figure 4-10 Peak pressure versus maximum inverse period for the CRAC experiments.

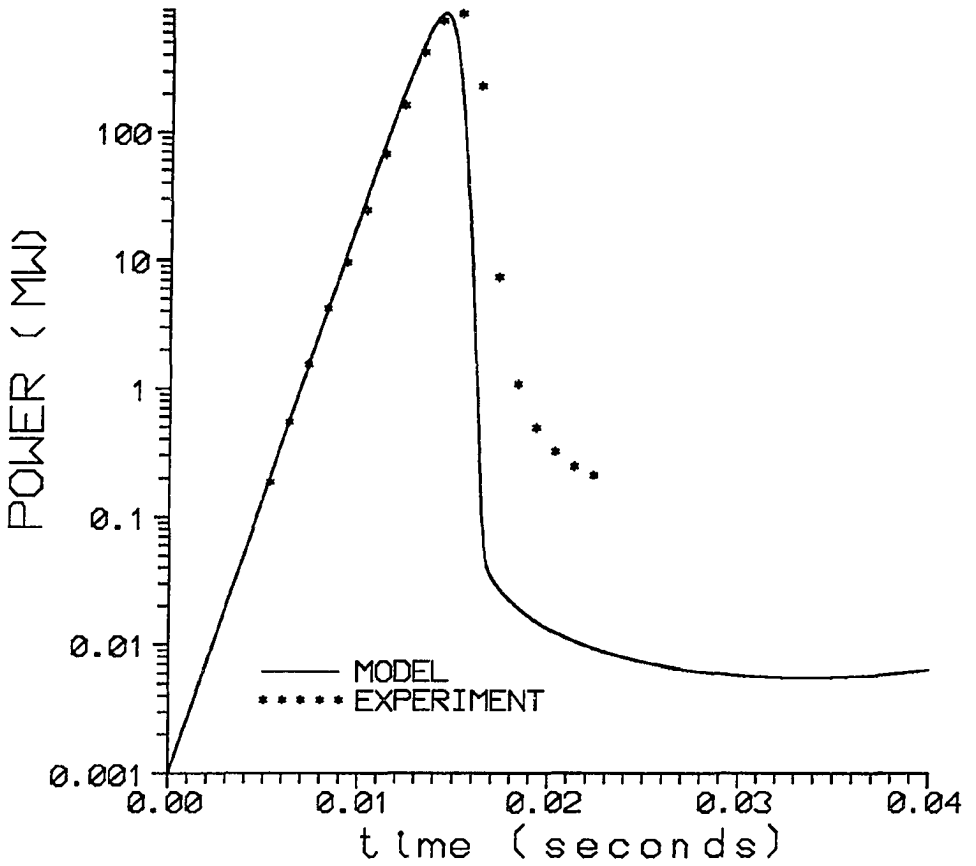

Figure 4-11 Predicted power versus time for CRAC experiment #08.

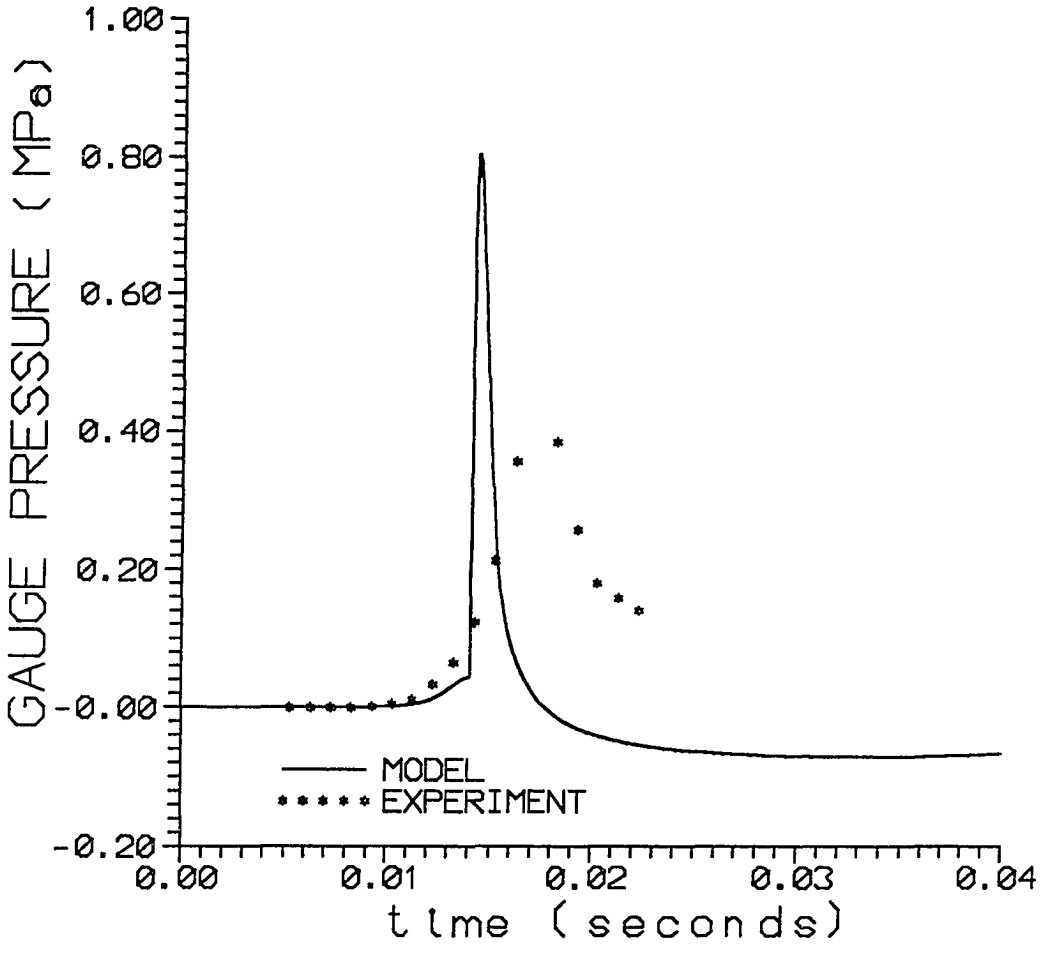

Figure 4-12 Predicted pressure versus time for CRAC experiment #08.

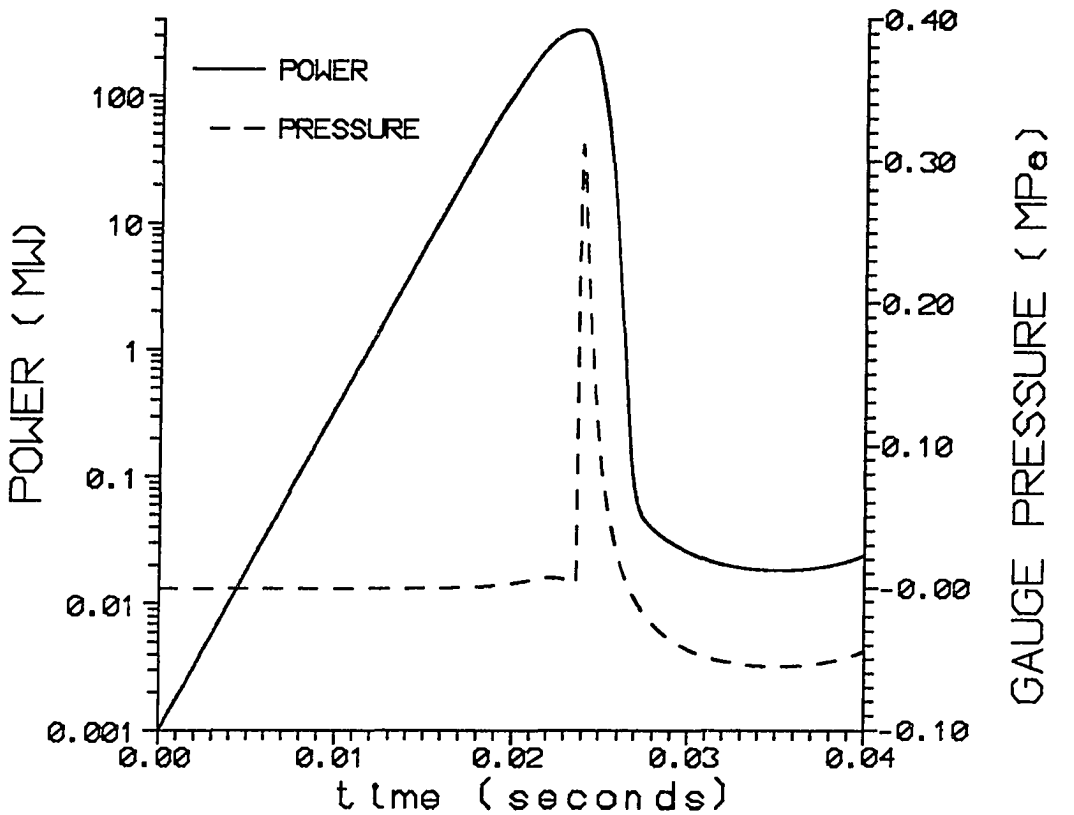

Figure 4-13 Predicted power and pressure for CRAC experiment #20.4.

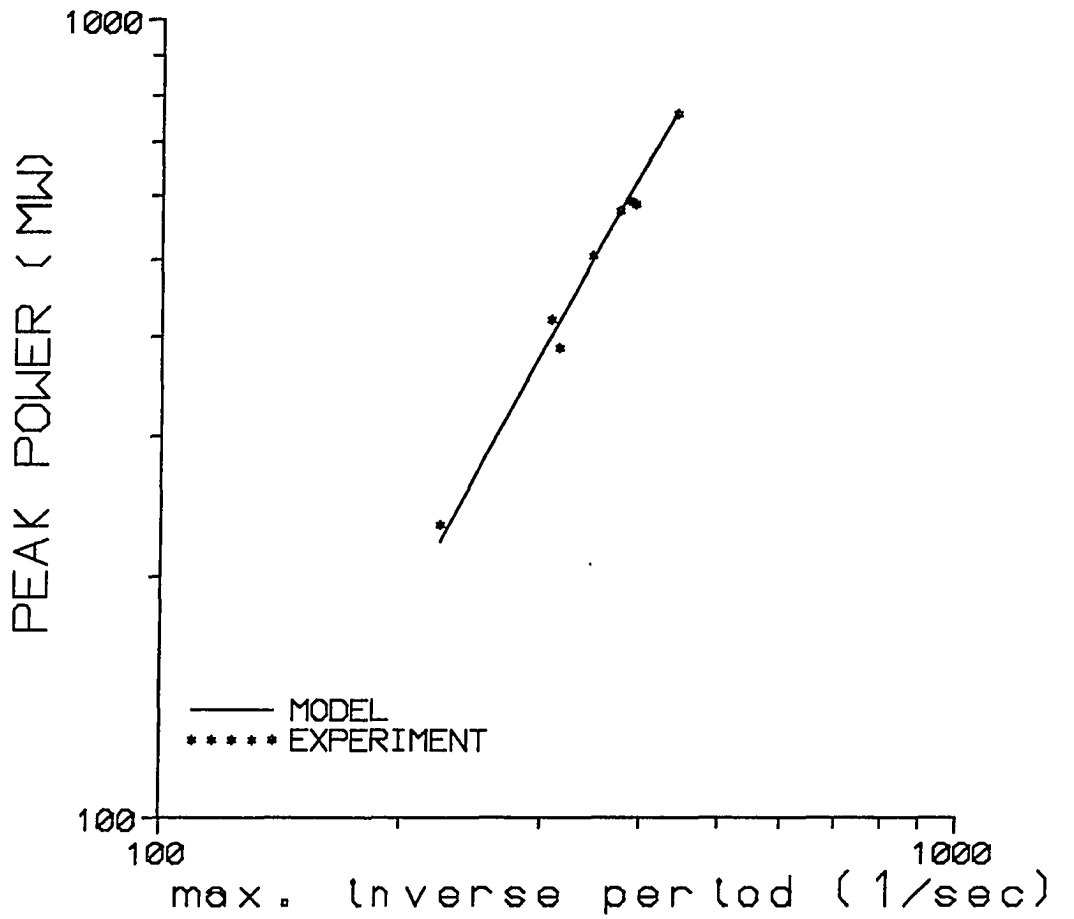

Figure 4-14 Peak power versus maximum inverse period for the SILENE experiments.

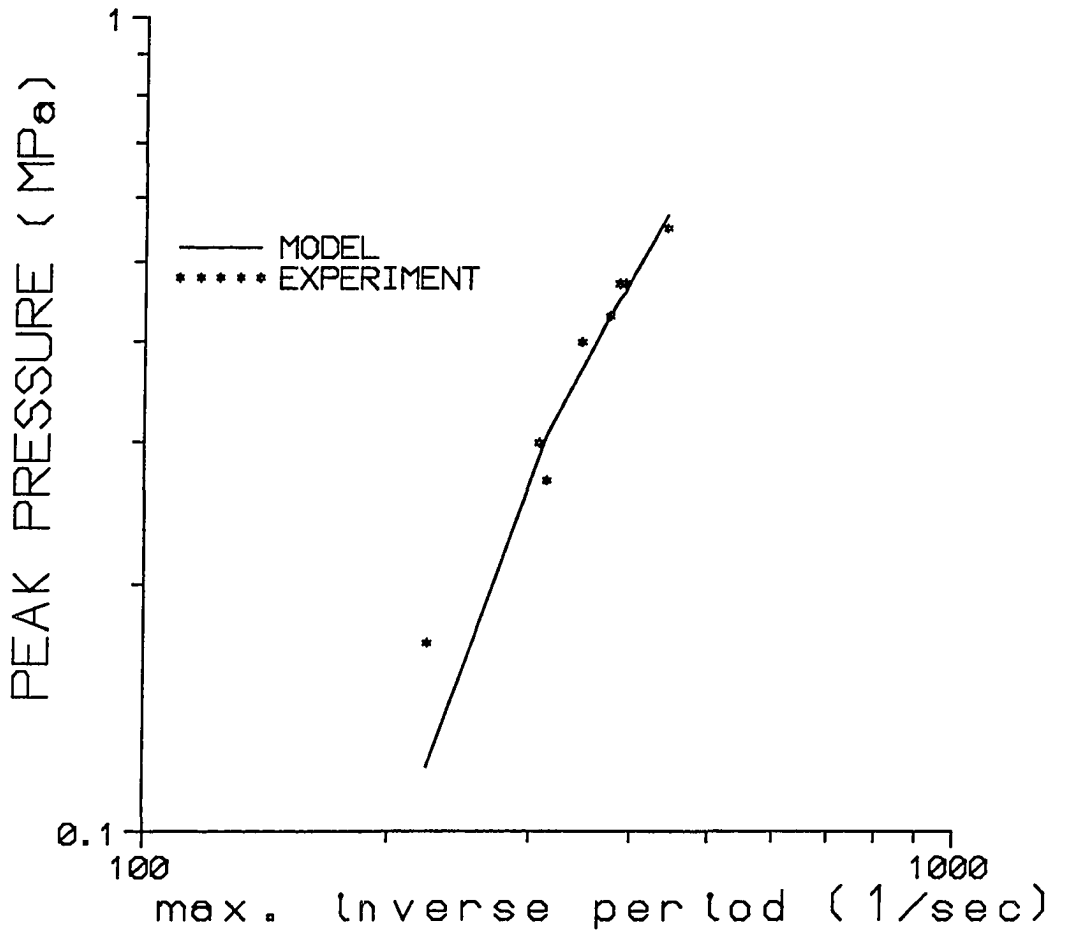

Figure 4-15 Peak pressure versus maximum inverse period for the SILENE experiments.

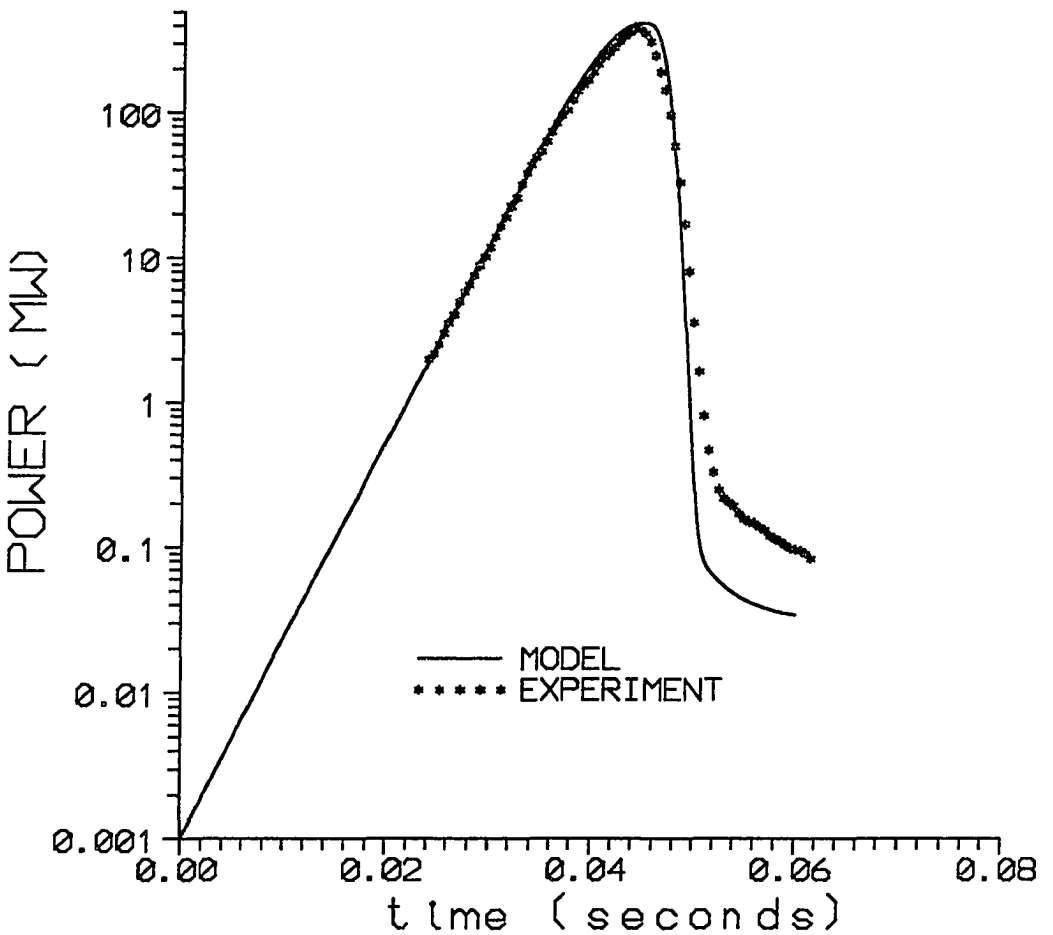

Figure 4-16 Predicted power versus time for SILENE experiment #S1-169.

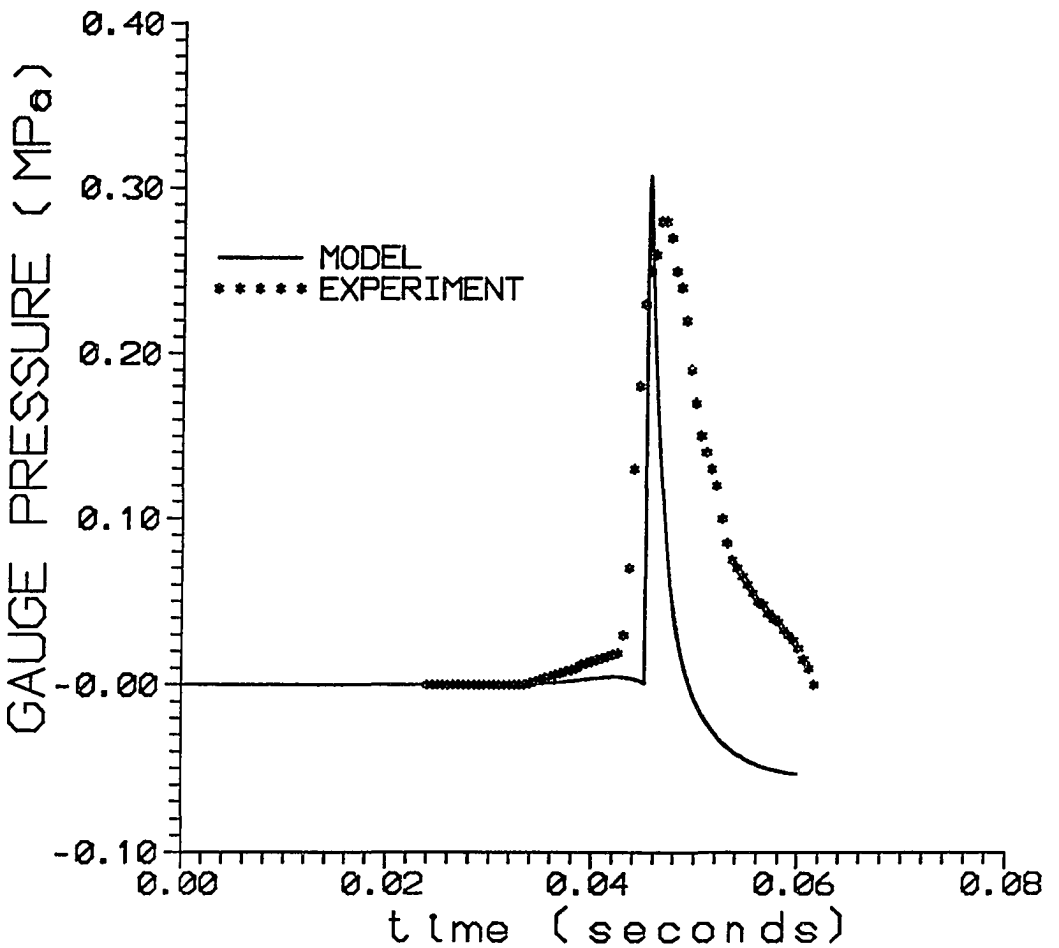

Figure 4-17 Predicted pressure versus time for SILENE experiment #S1-169.

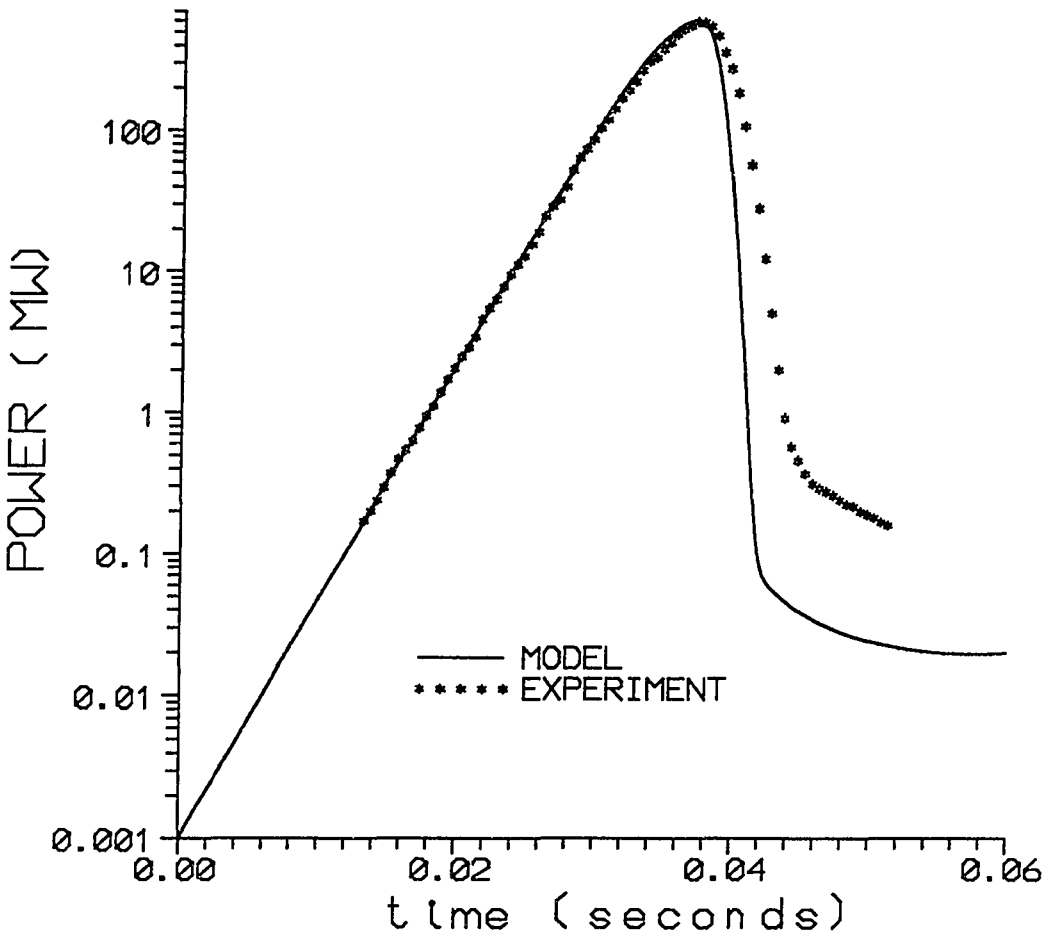

Figure 4-18 Predicted power versus time for SILENE experiment #S2-169.

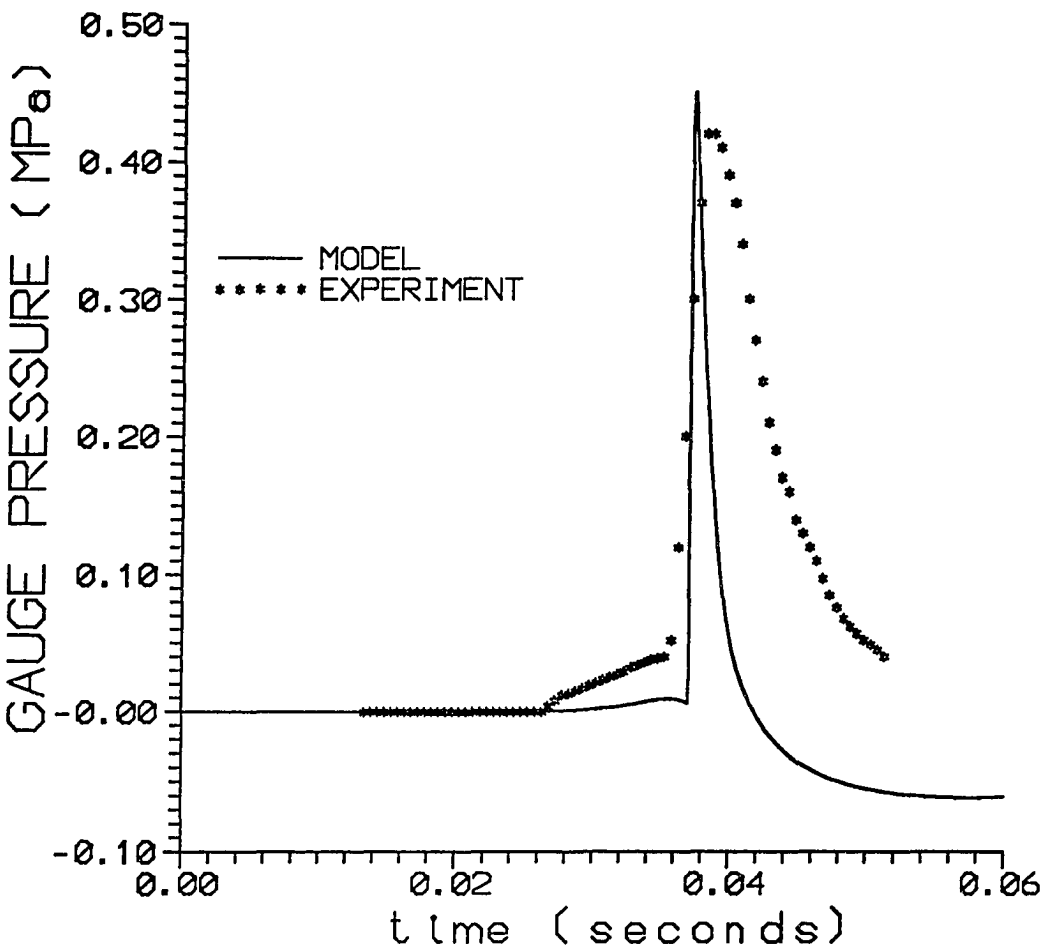

Figure 4-19 Predicted pressure versus time for SILENE experiment #S2-169.

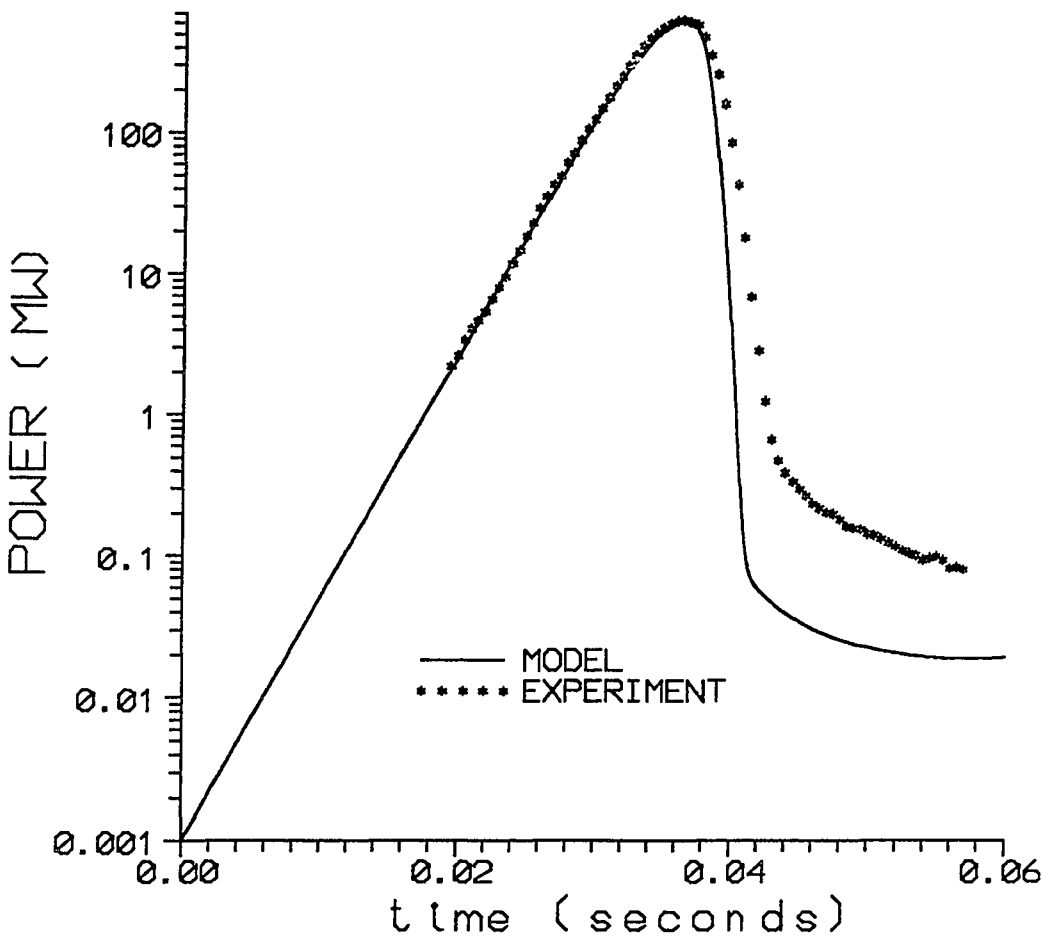

Figure 4-20 Predicted power versus time for SILENE experiment #S4-169.

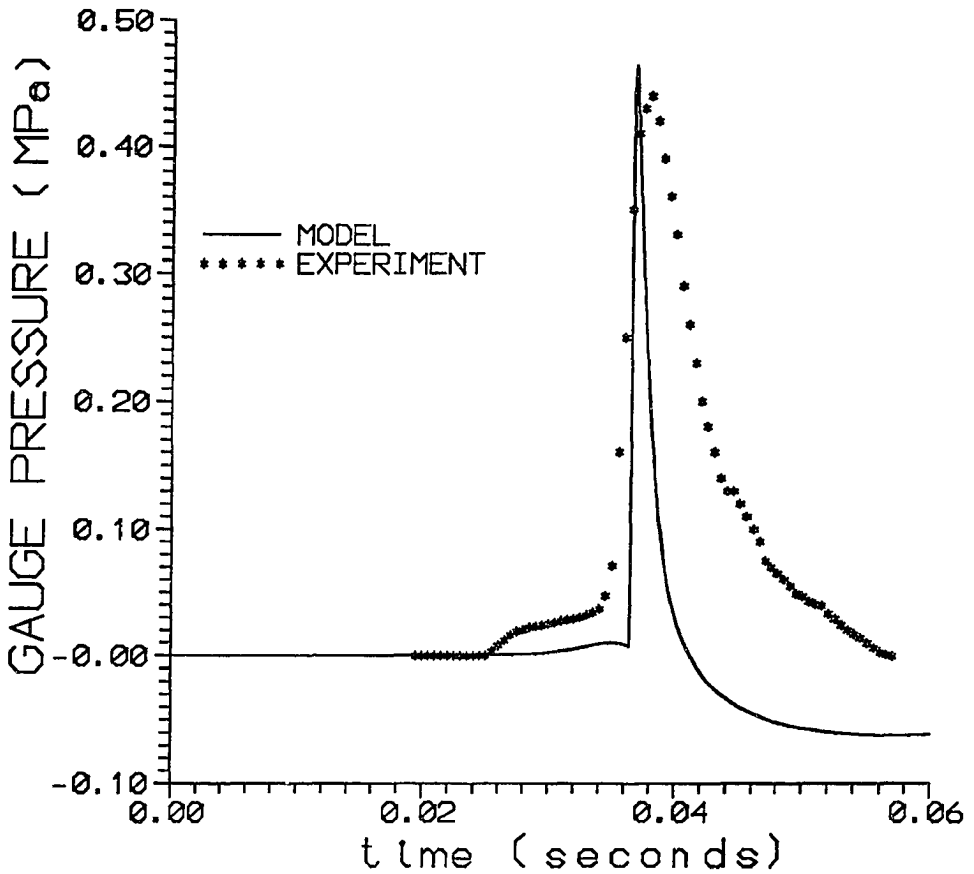

Figure 4-21 Predicted pressure versus time for SILENE experiment #S4-169.

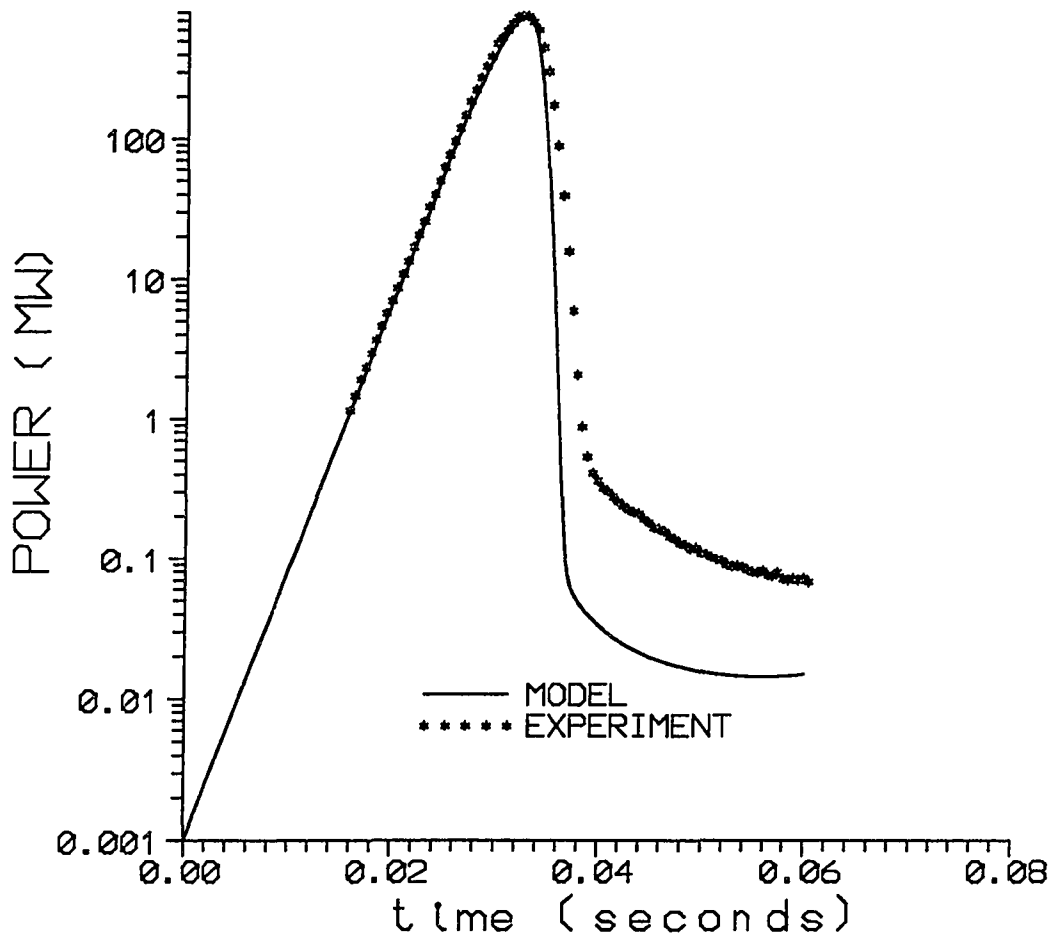

Figure 4-22 Predicted power versus time for SILENE experiment #S2-173.

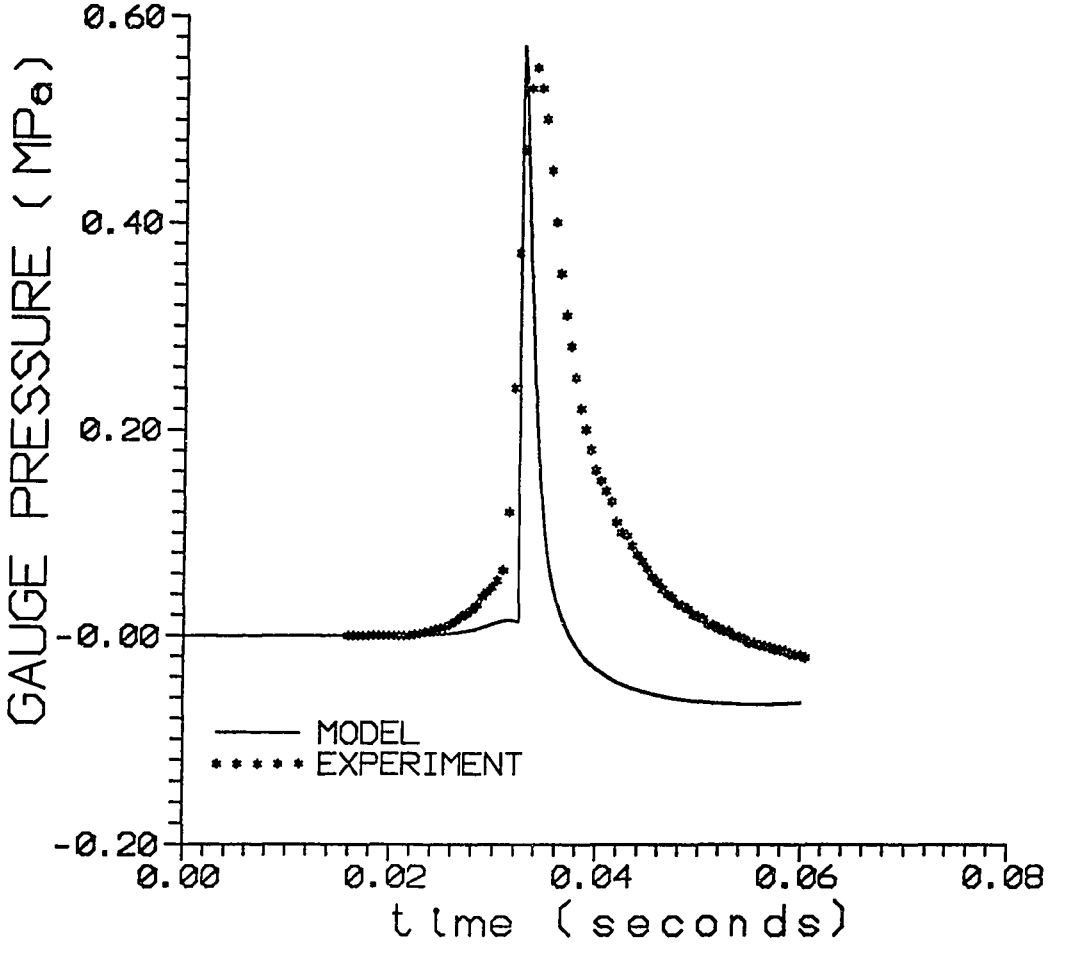

Figure 4-23 Predicted pressure versus time for SILENE experiment #S2-173.

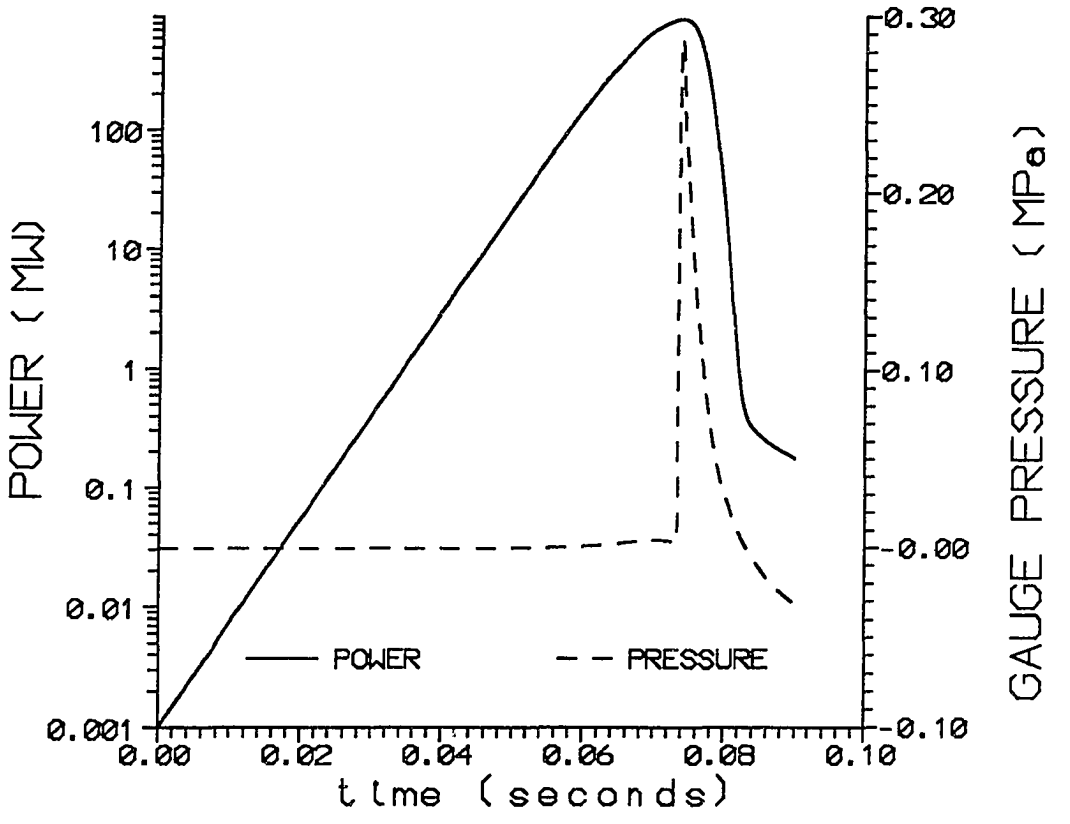

Figure 4-24 Predicted power and pressure versus time for a hypothetical $2.0 pulse in SHEBA.

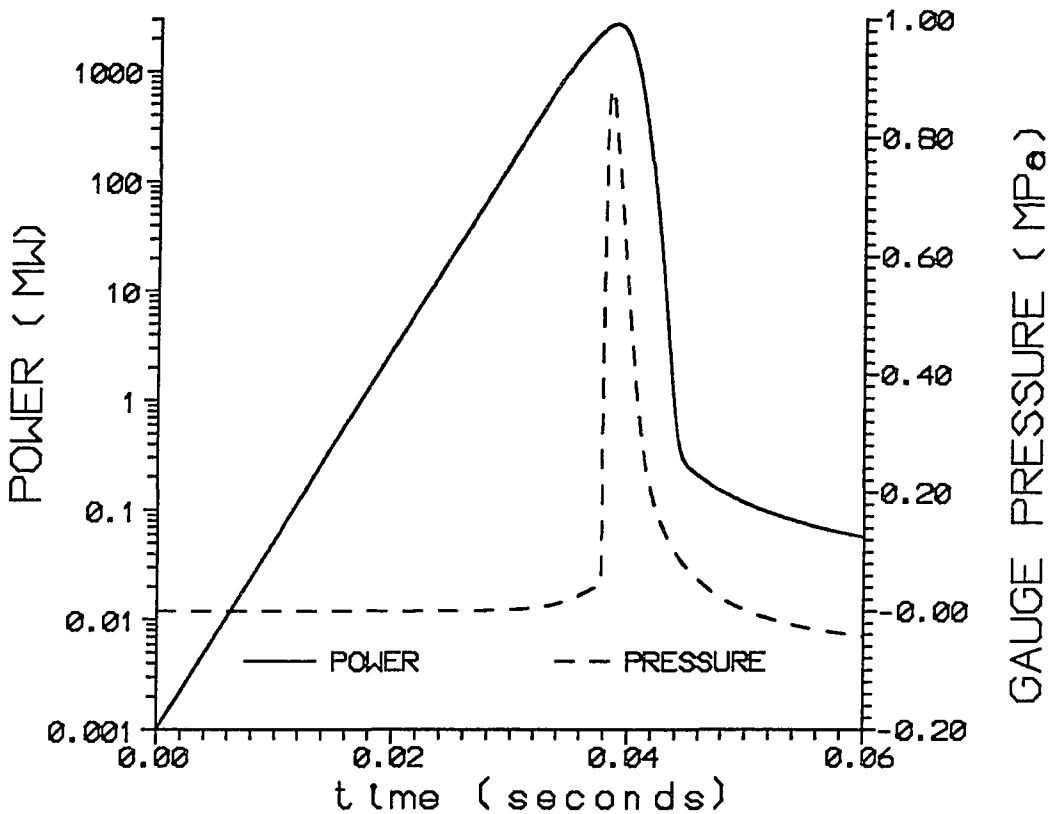

Figure 4-25 Predicted power and pressure versus time for a hypothetical $3.0 pulse in SHEBA.

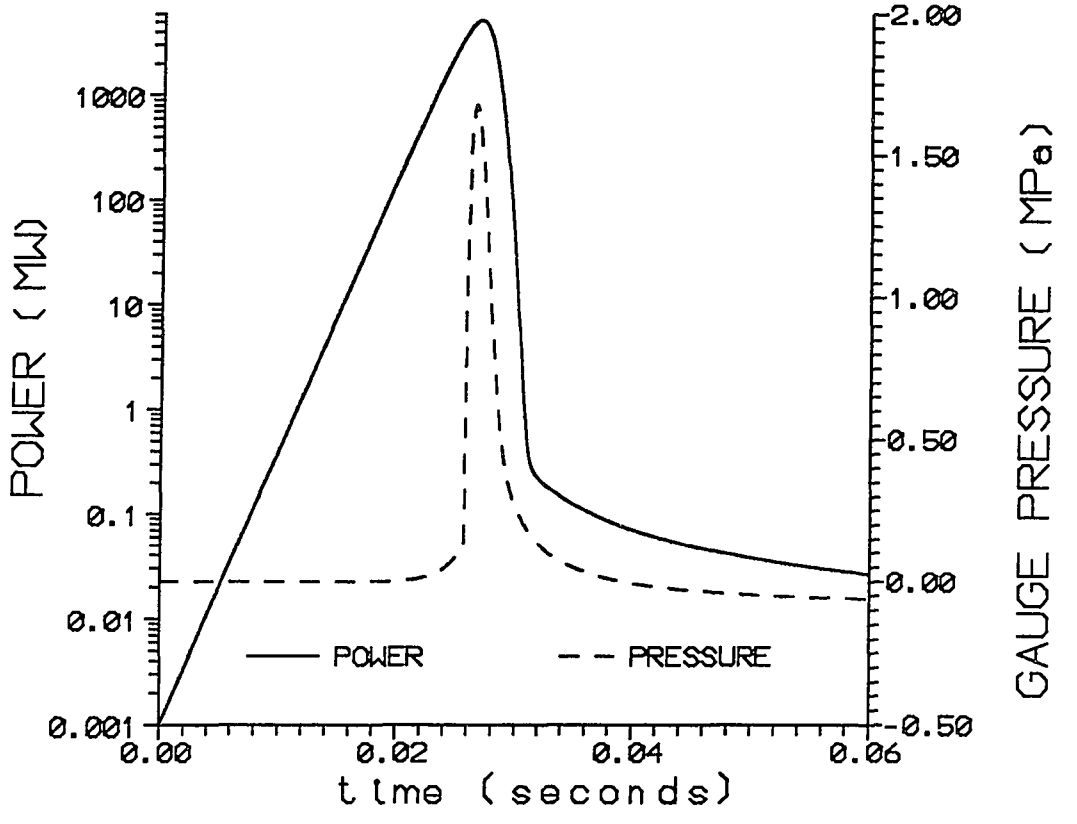

Figure 4-26 Predicted power and pressure versus time for a hypothetical $4.0 pulse in SHEBA.

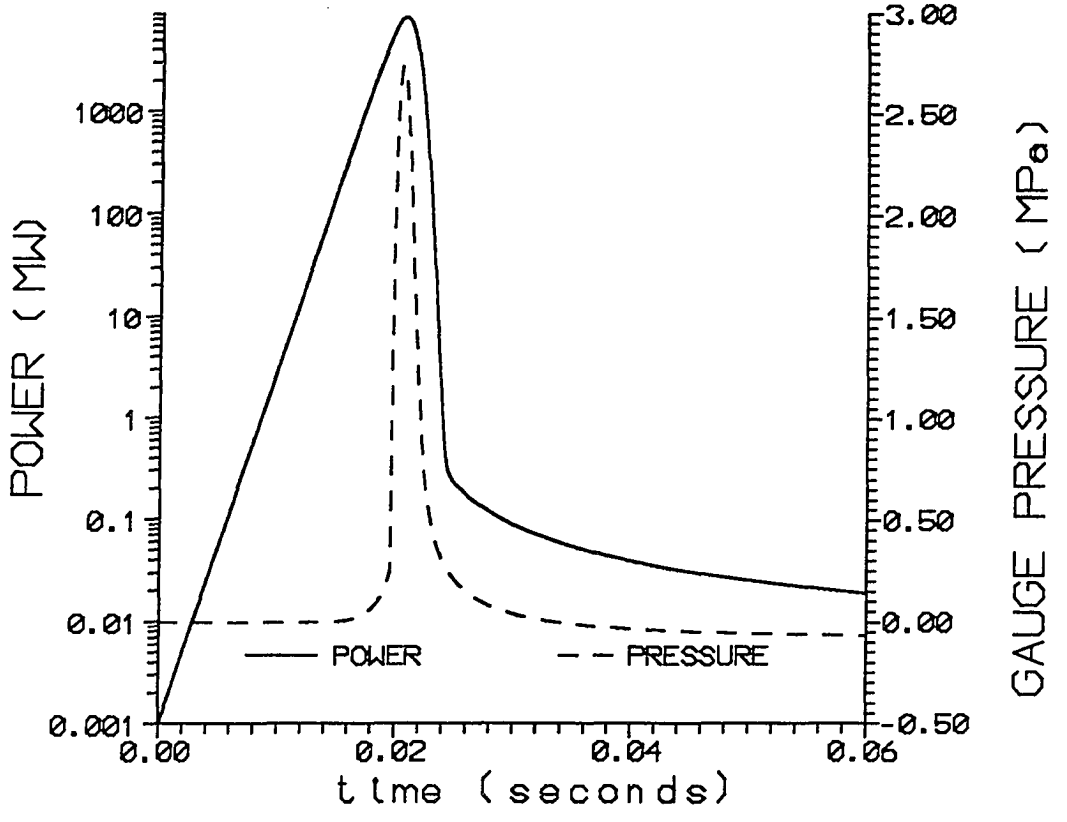

Figure 4-27 Predicted power and pressure versus time for a hypothetical $5.0 pulse in SHEBA.

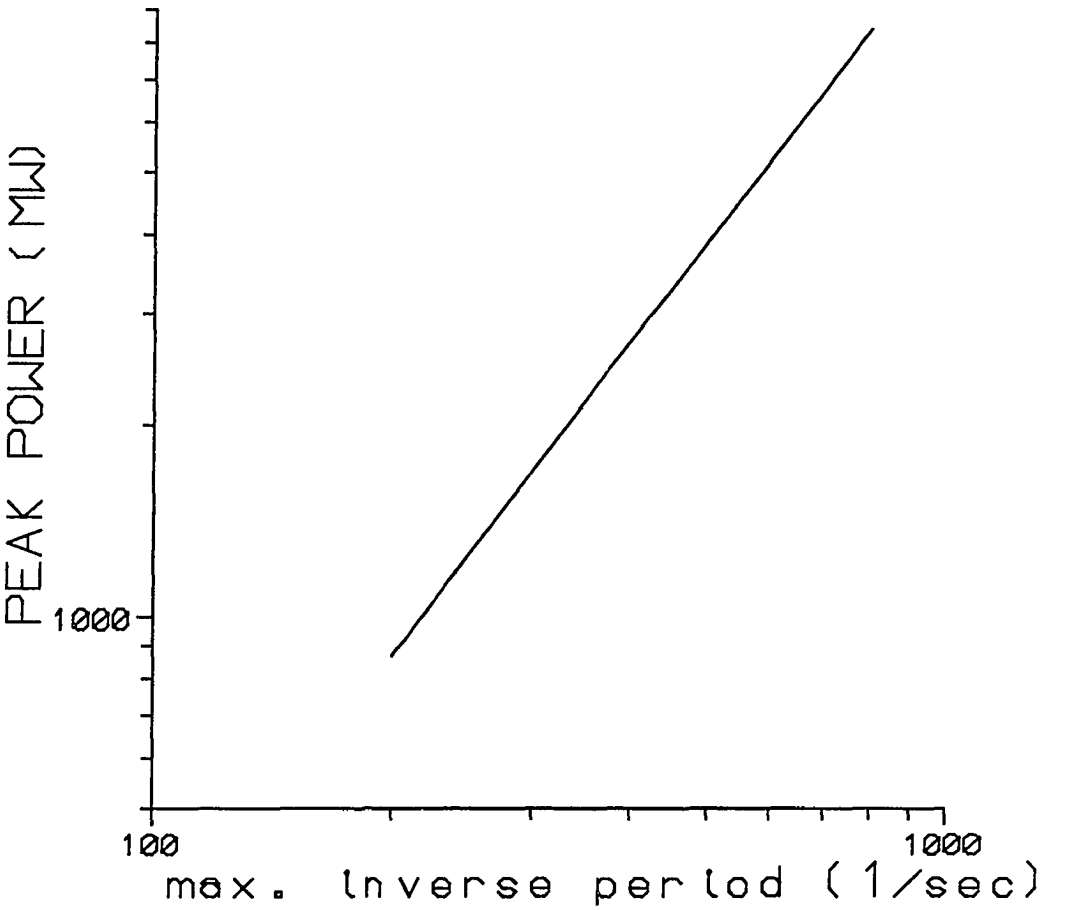

Figure 4-28 Peak power versus maximum inverse period for the hypothetical SHEBA experiments.

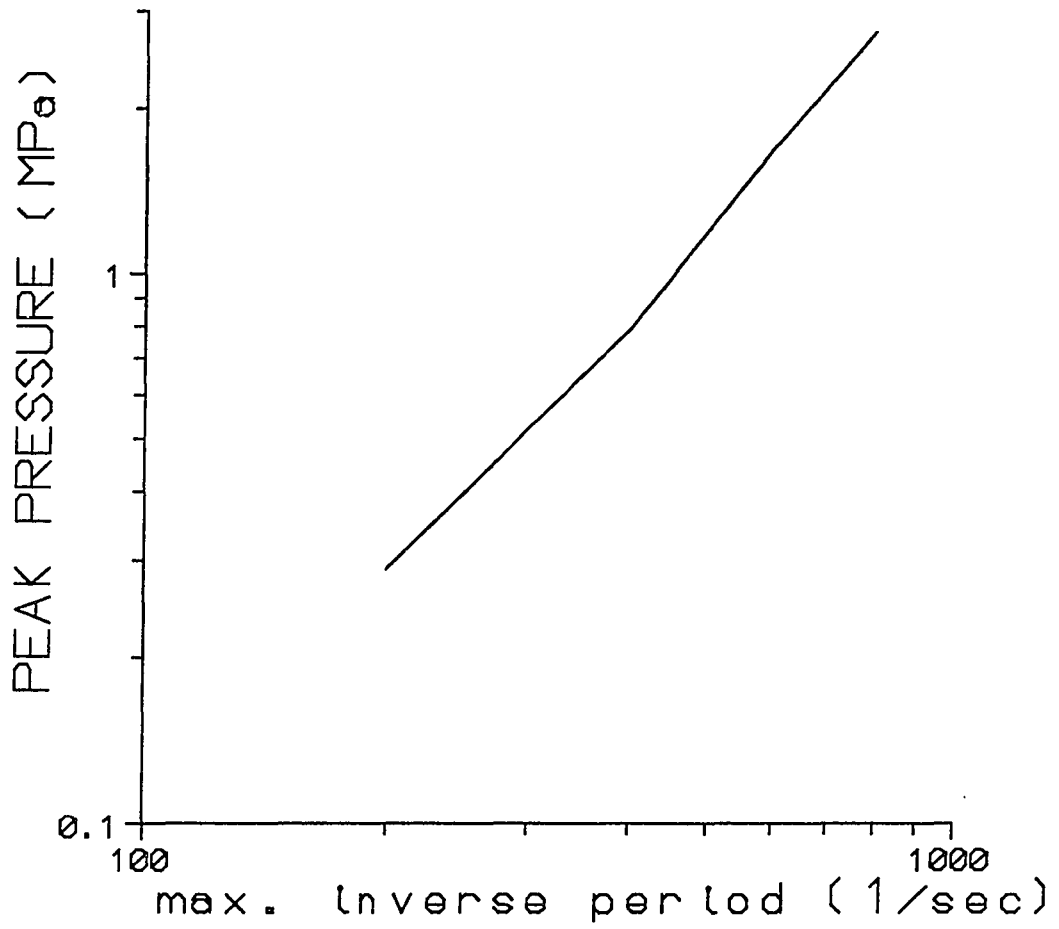

Figure 4-29 Peak pressure versus maximum inverse period for the hypothetical SHEBA experiments.

CHAPTER 5

MULTI-REGION MODEL

The one-region model presented in Chapter 3 assumed that the temperature and pressure were the same everywhere in the core. In this chapter, a multi-region model is presented which takes into account spatial variation in several parameters. A multi-region model can represent the spatial distribution of nuclear energy produced throughout the core. The model can account for the fact that the solution temperature changes more rapidly at the center of the core than it does near the outer surfaces. This is important to the calculation of inertial pressure caused by a lag in thermal expansion. A multi-region model can also model the spatial distributions of both axial and radial velocities produced during an excursion. The acceleration of the solution is also important to the calculation of inertial pressure. Expansion of the solution is the relief mechanism by which the inertial pressure is diminished. As a result of these two features, a multi-region model can predict the spatial distribution of inertial pressure.

One and two-dimensional models have been developed by choosing a set of mesh points axially and radially throughout a solution assembly. Each mesh point and its immediate neighborhood represents a region. Each region contains its own equation of state and its own energy, momentum, and continuity equations.

Both one and two-dimensional models have been developed, but only the two-dimensional model will be presented. A brief description of the one-dimensional model is given below. Important results gained from the one-dimensional model are given later in the chapter.

A one-dimensional model of a cylindrical solution assembly is created by splitting the core up into regions of equal volume along the vertical axis. This results in a stack of disc shaped regions piled one atop another. A cosine power shape is assumed along the vertical axis, and the appropriate amount of energy is deposited into each region. The equation of state and the energy equation for each region are given by equations (3-6) and (3-29). A momentum equation for each region may be given by

$$\frac{dU_i}{dt} = \frac{1}{M_i}(P_i - P_{i-1})A \qquad (5\text{-}1)$$

where

U_i = upper boundary velocity of region i

M_i = mass of region i

P_i = pressure in region i

P_{i-1} = pressure in region i-1 directly above region i

A = cross-sectional area of core perpendicular to vertical axis.

The boundary velocity of a region is caused by the pressure in that region pushing the region above it upwards like a piston being driven by an expanding gas (Kimpland, 1992; Peterson et al, 1976). An equation for the change in volume of region i may be given by

$$\frac{dV_i}{dt} = A(U_i - U_{i+1}) \tag{5-2}$$

where U_{i+1} is the upper boundary velocity of the region directly below region i. Since the upper boundary of a region is actually the lower boundary of the region directly above, the change in the volume of a region is just the change in its upper and lower boundaries.

The total volume of the system is the sum of the individual region volumes. The point reactor kinetics model along with a simple volumetric feedback similar to the one in the one-region model were used to determine the power as a function of time.

The one-dimensional model has been used to predict transients in the KEWB, CRAC, and SILENE reactors. The most important result of these calculations was that a multi-region model is much better at predicting inertial pressure relief than a one-region model. The pressure traces produced by this model were much broader than those produced by the one-region model. The inertial pressure decreased more slowly, which is more in line with the experimental data. This is due to the multi-region model's ability to account for spatial variation in the acceleration of the solution material. Since the one-dimensional model only allows expansion along the vertical axis, a two-dimensional model has been developed, which can account for radial acceleration as well.

5.1 Two-Dimensional Model

In the one-dimensional model it was possible to track the change in the volume of an individual region. Each region had a constant cross-sectional area and only the upper and lower boundaries changed. In a two-dimensional model it would be very difficult to track changes in discrete volumes both radially and axially. Therefore, the two-dimensional model

only looks at points within the solution. A region is then defined as the immediate neighborhood surrounding each point.

The quasi-static differential representation for liquid solution pressure is found by assuming that the liquid pressure is a function of the liquid solution temperature and density. If we take $P=P(T,\rho_l)$, then

$$\frac{dP}{dt}=\left(\frac{\partial P}{\partial T}\right)_{\rho_l}\frac{dT}{dt}+\left(\frac{\partial P}{\partial \rho_l}\right)_{T}\frac{d\rho_l}{dt}. \tag{5-3}$$

Noting that

$$\frac{d\rho_l}{\rho_l}=-\frac{dV_l}{V_l} \tag{5-4}$$

we obtain

$$\left(\frac{\partial P}{\partial T}\right)_{\rho_l}=-\frac{\left(\frac{\partial V_l}{\partial T}\right)_{P}}{\left(\frac{\partial V_l}{\partial P}\right)_{T}}=\frac{\beta_0}{\kappa_0} \tag{5-5}$$

and

$$\left(\frac{\partial P}{\partial \rho_l}\right)_T = \frac{1}{\kappa_0 \rho_l}. \tag{5-6}$$

Substituting equations (5-5) and (5-6) into equation (5-3) we obtain

$$\frac{dP}{dt} = \frac{\beta_0}{\kappa_0}\frac{dT}{dt} + \frac{1}{\kappa_0 \rho_l}\frac{d\rho_l}{dt}. \tag{5-7a}$$

As in the case of the one-region model, the liquid solution properties are replaced with the liquid-gas mixture properties. Equation (5-7a) then becomes

$$\frac{dP}{dt} = \frac{\beta}{\kappa}\frac{dT}{dt} + \frac{1}{\kappa \rho_l}\frac{d\rho_l}{dt}. \tag{5-7b}$$

The isobaric and isothermal compressibilities used in equation (5-7b) are defined by equations (3-20) and (3-21), which are for a liquid solution containing radiolytic gas bubbles.

The rate at which the liquid density changes with time may be written as

$$\frac{d\rho_l}{dt} = \left(\frac{d\rho_l}{dt}\right)_{acceleration} + \left(\frac{d\rho_l}{dt}\right)_{gas\ compression}. \tag{5-8}$$

The first term on the right hand side of equation (5-8) represents the density change due to acceleration of the liquid solution. An expression for the change in liquid density of each region may be obtain from the continuity equation for a cylinder. This may be written as

$$\left(\frac{d\rho_l}{dt}\right)_{acceleration} = -\rho_l\left[\frac{\partial u_z}{\partial z} + \frac{1}{r}\frac{\partial (r u_r)}{\partial r}\right] \qquad (5\text{-}9)$$

where u_z and u_r are the axial and radial velocities of the liquid solution. To obtain these velocities, a simplified version of the Navier-Stokes equations are used. In cylindrical coordinates, these equations may be written as

$$\rho_l \frac{\partial u_z}{\partial t} = -\frac{\partial P}{\partial z} \qquad (5\text{-}10)$$

and

$$\rho_l \frac{\partial u_r}{\partial t} = -\frac{\partial P}{\partial r}. \qquad (5\text{-}11)$$

The spatial acceleration terms have been neglected in these momentum equations. Although the temporal acceleration in both the axial and radial directions can be quite large, the solution pulses are very short (approximately 10 milliseconds). Thus, the resulting velocities are small,

and the spatial acceleration can be ignored. Testing of the one-dimensional model has confirmed this numerically.

The second term on the right hand side of equation (5-8) is the change in liquid density due radiolytic gas bubble compression of the liquid. As in the case of the one-region model we can use equation (2-8) along with equation (5-4) to obtain

$$\left(\frac{d\rho_l}{dt}\right)_{gas\ compression} = \frac{\rho_l}{V_0}\left(v_{b1}\frac{dN_1}{dt} + v_{b2}\frac{dN_2}{dt}\right) \qquad (5\text{-}12)$$

where V_0 is the initial solution volume. Combining equation (5-9) and equation (5-12) with equation (5-8) gives

$$\frac{d\rho_l}{dt} = \frac{\rho_l}{V_0}\left(v_{b1}\frac{dN_1}{dt} + v_{b2}\frac{dN_2}{dt}\right) - \rho_l\left(\frac{\partial u_z}{\partial z} + \frac{1}{r}\frac{\partial r u_r}{\partial r}\right). \qquad (5\text{-}13)$$

Equation (5-13) represents the total change in liquid density of a particular region.

Two important results gained in calculations made with the one-dimensional model have been used to develop an energy equation for the two-dimensional model. A ten-region model was used to compare the amount of energy used in the form of work done by the liquid (PdV) and

the amount of energy used to change the internal energy of the liquid (dU). Calculations showed that the work required only a fraction of a percent of the total energy. It is therefore assumed in the two-dimensional model that all the nuclear energy produced is used as sensible heat in the liquid solution. Calculations with the ten-region model have also shown that the heat transfer between regions due to conduction is negligible. It has also been assumed that the spatial shape of the power distribution is fixed. As a result, the energy equation for the entire liquid solution is given by

$$\rho_l C_p \frac{\partial T}{\partial t} = \frac{n(t)}{V_0} J_0(\alpha_r r)\cos(\beta_z z) \qquad (5\text{-}14)$$

where

C_p = specific heat at constant pressure

$n(t)$ = nuclear power

α_r, β_z = radial and axial buckling.

As in the case of the one-region model the nuclear power is calculated with the point reactor kinetics model.

5.2 Discretization

In order to solve the two-dimensional model equations, a discretization scheme has been used. A set of mesh points are chosen both axially and radially throughout the solution assembly. Each mesh point and its immediate neighborhood represent a region. The discretized equation of state for the two-dimensional model, equation (5-7b), may be written as

$$\frac{dP_{ij}}{dt} = \frac{\beta_{ij}}{\kappa_M}\frac{dT_{ij}}{dt} + \frac{1}{\rho_{lij}\kappa_M}\frac{d\rho_{lij}}{dt} \qquad (5\text{-}15)$$

where the indices ij represent the mesh point whose coordinates are (z_i, r_j). For this model it is assumed that i increases from the bottom of the solution assembly to the top, and j increases from the center outward. The regions along the upper surface of the solution assembly are assumed to expand thermally rather than expanding due to acceleration caused by inertial pressure. The model assumes that the upper surface of the solution assembly is open to the atmosphere. Therefore the pressure in these regions is assumed to remain at the pressure of the atmosphere above them.

The isobaric compressibility is strongly dependent of the liquid solution temperature. It is calculated individually at each mesh point using the local temperature. The isothermal compressibility is strongly dependent

on the total amount of radiolytic gas at every point in the liquid solution. A medium isothermal compressibility is calculated and used at all the mesh points. The medium isothermal compressibility is defined as

$$\kappa_M = (1-f)\kappa_0 + \frac{f}{P_{av} + \frac{4\sigma}{3r_b}} \tag{5-16}$$

where P_{av} is the average liquid solution pressure.

The total change in liquid density, equation (5-13), in discretized form may be written as

$$\frac{d\rho_{lij}}{dt} = \frac{\rho_{lij}}{V_0}\left(v_{b1}\frac{dN_1}{dt} + v_{b2}\frac{dN_2}{dt}\right) - \rho_{lij}\left[\frac{u_{zij} - u_{zi-1j}}{\Delta z} + \frac{1}{r_{ij}}\frac{r_{ij}u_{rij} - r_{ij-1}u_{rij-1}}{\Delta r}\right] \tag{5-17}$$

where Δz and Δr are the axial and radial distances between regions. The discretized momentum equations may be written as

$$\rho_{lij}\frac{du_{zij}}{dt} = -\frac{P_{i+1j} - P_{ij}}{\Delta z} \tag{5-18}$$

and

$$\rho_{lij}\frac{du_{rij}}{dt} = -\frac{P_{ij+1} - P_{ij}}{\Delta r}. \qquad (5\text{-}19)$$

The radial velocity of the regions along the outermost portions of the assembly is set to zero.

The energy equation for a particular region may be written as

$$\frac{dT_{ij}}{dt} = \frac{1}{\rho_{lij} C_p}\frac{n(t)}{V_0} J_0(\alpha_r r_j)\cos(\beta_z z_i). \qquad (5\text{-}20)$$

Physical properties such as specific heat, surface tension, and the radiolytic gas constant have been assumed to be independent of position.

A two-dimensional 45-region model (9 axial points and 5 radial points) has been developed. This model has been used to simulate various experiments, such as KEWB, CRAC, and SILENE. The results of these simulations is presented next in Chapter 6.

CHAPTER 6

MULTI-REGION MODEL RESULTS

The multi-region model has been implemented in a computer code and used to simulate excursions in aqueous homogeneous solution assemblies. These computations were performed on a 386 PC, using the DESIRE software package. Power and pressure data from the KEWB, CRAC, and SILENE experiments were used as a benchmark for the model. Predicted power and pressure traces produced by the multi-region model are compared with actual power and pressure traces from the KEWB, CRAC, and SILENE experiments. Also, the multi-region model's ability to predict the axial and radial distribution of such parameters as pressure, liquid density, and velocity are demonstrated.

In the multi-region model the reactivity of the solution assembly is given by

$$\rho = \rho_0 - \beta \alpha_T \Delta T - \beta \phi_g V_g \qquad (6\text{-}1)$$

where

ρ_0 = the step input reactivity

β = the delayed neutron fraction

α_T = the temperature feedback coefficient of reactivity

ΔT = the average solution temperature change

ϕ_g = the radiolytic gas feedback coefficient of reactivity

V_g = the radiolytic gas volume.

To match the calculated peak power with the experimental data, the temperature feedback coefficient of reactivity is used as an adjustable parameter. The radiolytic gas feedback coefficient of reactivity is used to help match the shape of predicted power traces and experimental power traces. In particular, it is used to help predict the delayed neutron tail. It should be noted that the radiolytic gas feedback coefficient of reactivity has a negligible effect on peak power, since the volume of radiolytic gas prior to peak power is quite small. As in the one-region model, the empirical constant F_2, given in equation (2-6), is used to match the calculated peak pressure with experimental data. Table 6-1 gives the values of these parameters for the KEWB, CRAC, and SILENE reactors. The multi-region model was not used to simulate hypothetical excursions in the SHEBA

reactor since it requires three adjustable parameters, and no experimental data exist for such transients.

6.1 KEWB

Figures 6-1 and 6-2 give a comparison between the multi-region model's calculated peak power and pressure and the KEWB-5 experimental data. The calculated peak power as a function of maximum inverse period for several transients has a slope of 1.85, which compares closely to the 1.9 slope of the experimental data. The maximum relative error between the calculated peak power and the experimental data is 16%, which occurs for the slowest transient. The calculated peak pressure as a function of maximum inverse period for several transients also compares quite well with the experimental data. The maximum relative error between calculated peak pressure and experimental data is approximately 12%, which also occurs for the slowest transient. Results from the multi-region model are given in Table 6-2.

Figures 6-3 and 6-4 show a comparison between the model's computed power and pressure traces as a function of time and the

experimental power and pressure traces for the KEWB-5 experiment #3041. The computed power trace matches the experiment quite well and has the same characteristic features of the experiment. The power decreases much more rapidly than it rises. Also, the multi-region model predicts the delayed neutron tail much more accurately than the one-region model. The computed pressure pulse also shows the important characteristic features of the experiment pulse. The pressure rises slowly at the beginning of the pulse due to the "lag" in thermal expansion. The pressure then rises sharply once the dissolved gas concentration reaches threshold, and large gas bubbles are formed. After peak pressure, the pressure decreases much more slowly than it rose. The multi-region model produces pressure pulses that are much broader and much closer to the actual shape of the experimental pressure traces than those produced by the one-region model. However, the multi-region model also fails to predict the initial rise in pressure due to the "lag" in thermal expansion accurately. The computed rise in pressure is much slower than that of the experimental trace. Figures 6-5 through 6-8 give the multi-region model's results for several of the KEWB-5 experiments. These transients range in size from a $2.46 pulse to a $4.227 pulse.

Figures 6-9 and 6-10 give the multi-region model's predicted axial and radial distributions of pressure at the time of peak pressure for KEWB-5 experiment #3014. The maximum pressure occurs at the bottom of the assembly and in the center region. The radial variation in pressure is quite small. The pressure decreases slowly from the center region outward until the outermost regions. The pressure rises slightly for the outermost regions, which are next to the vessel wall and cannot expand outward. Figures 6-11 and 6-12 show the model's predicted axial and radial distributions of solution velocity at the time of peak pressure in experiment #3014. The axial velocity increases from the bottom of the assembly to the top. Thus, the rate at which pressure relief occurs also increases from the bottom of the assembly to the top. The radial velocity decreases from the centermost regions outward. Figures 6-13 and 6-14 show the model's predicted axial and radial distributions of liquid solution density at the time of peak pressure for experiment #3014. These figures show that the density increases from the center of the assembly outward in all directions. The rate at which the pressure increases due to the "lag" in thermal expansion is directly proportional to the rate at which the temperature increases. This pressure increase has a maximum at the center of the assembly. It produces

a velocity field which causes the solution material to expand outward from the center in all directions. This causes the solution density to decrease in the center of the assembly and increase at the outer boundaries. These predicted axial and radial distributions are typical of all the KEWB-5 experiments modeled. They are also typical of the CRAC and SILENE experiments modeled. A copy of the multi-region computer model for the KEWB-5 experiments is given in Appendix B.

6.2 CRAC

Figures 6-15 and 6-16 show a comparison between the multi-region model's calculated peak power and pressure and experimental values for several transients. The calculated peak power as a function of maximum inverse period has a slope of approximately 2.0, which compares closely to the 1.9 slope of the experimental data. The maximum relative error between calculated and experimental peak power is 23%, which occurs for the slowest transient. Table 6-3 gives the multi-region model's calculated peak power and pressure for several of the CRAC experiments.

Figures 6-17 and 6-18 show a comparison between the model's predicted power and pressure traces and the experimental traces for CRAC experiment #08. The predicted power trace matches the experimental trace more closely than the trace produced by the one-region model. The predicted power pulse undershoots the delayed neutron tail, but the width of the predicted pulse matches that of the experimental pulse. The predicted pressure pulse also matches the experimental trace more closely than the pulse produced by the one-region model. The width of the predicted pressure pulse matches the experimental trace more closely. Figure 6-19 shows the model's predicted power and pressure traces for the CRAC experiment #20.4, which is a much slower transient than experiment #08.

6.3 SILENE

Figures 6-20 and 6-21 show a comparison between the model's peak power and pressure and the experimental results for several of the SILENE experiments. The calculated peak power as a function of maximum inverse period has a slope of 1.8, which compares closely to a slope of 1.7 for the experimental data. The maximum relative error between the calculated peak

power and the experimental data is 15%, which occurs for the slowest transient. The maximum relative error between computed peak pressure and the experimental data is 35%, which also occurs for the slowest transient modeled. Table 6-4 gives the predicted peak power and pressure results for several of the SILENE experiments.

Figures 6-22 through 6-29 give a comparison between the model's predicted power and pressure traces and the experimental traces for several of the SILENE experiments. The multi-region model's power pulses match the experimental traces quite well. The width of predicted power pulses and the delayed neutrons tails match the experiments much better than those produced by the one-region model. Also, the predicted pressure pulses match the experimental pulses more closely than those produced by the one-region model. The tails of the predicted pressure pulses decrease much more slowly, and match the shape of the experimental pressure pulses much more closely.

Table 6-1 Empirical constant F_2 and reactivity feedback coefficients α_T and ϕ_g for the reactors modeled.

	KEWB	CRAC	SILENE
F_2	1.48×10^{-4}	2.8×10^{-4}	4.05×10^{-4}
α_T (\$/C)	0.133	0.145	0.162
ϕ_g (\$/m^3)	3000	3000	2000

Table 6-2 Predicted peak power and pressure for several of the KEWB experiments.

Experiment #	Peak Power (MW)	Peak Pressure (MPa)
3039	465	0.31
3041	684	0.47
3043	897	0.62
3014	1577	1.07
3027	2034	1.36
3016	2410	1.58
3017	2902	1.87
3018	3935	2.46

Table 6-3 Predicted peak power and pressure for several of the CRAC experiments.

Experiment #	Peak Power (MW)	Peak Pressure (MPa)
61	110	0.01
22	183	0.11
62.3	234	0.22
20.4	283	0.31
08	819	1.07

Table 6-4 Predicted peak power and pressure for several of the SILENE experiments.

Experiment #	Peak Power (MW)	Peak Pressure (MPa)
S1-11	200	0.11
S5-08	393	0.29
S1-169	412	0.30
S2-12	498	0.37
S1-16	577	0.43
S2-169	606	0.45
S4-169	626	0.47
S2-173	778	0.58

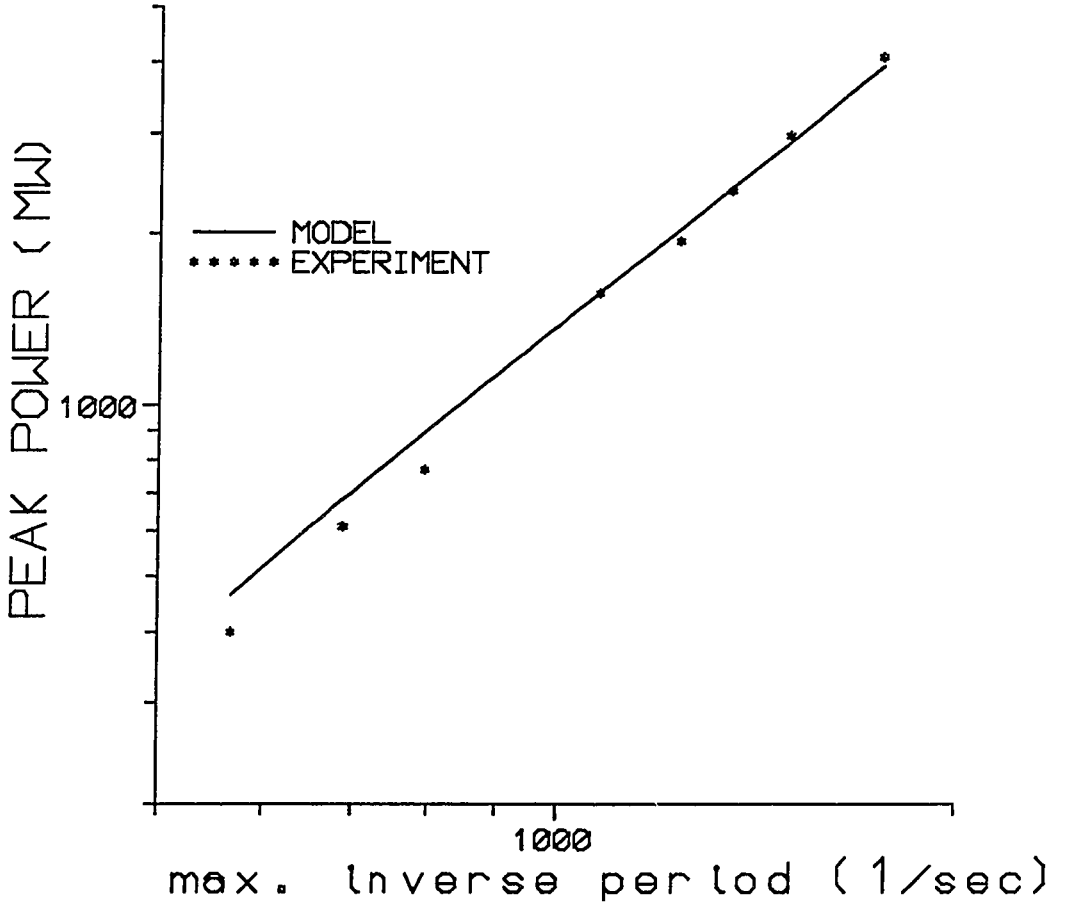

Figure 6-1 Peak power versus maximum inverse period for the KEWB-5 experiments.

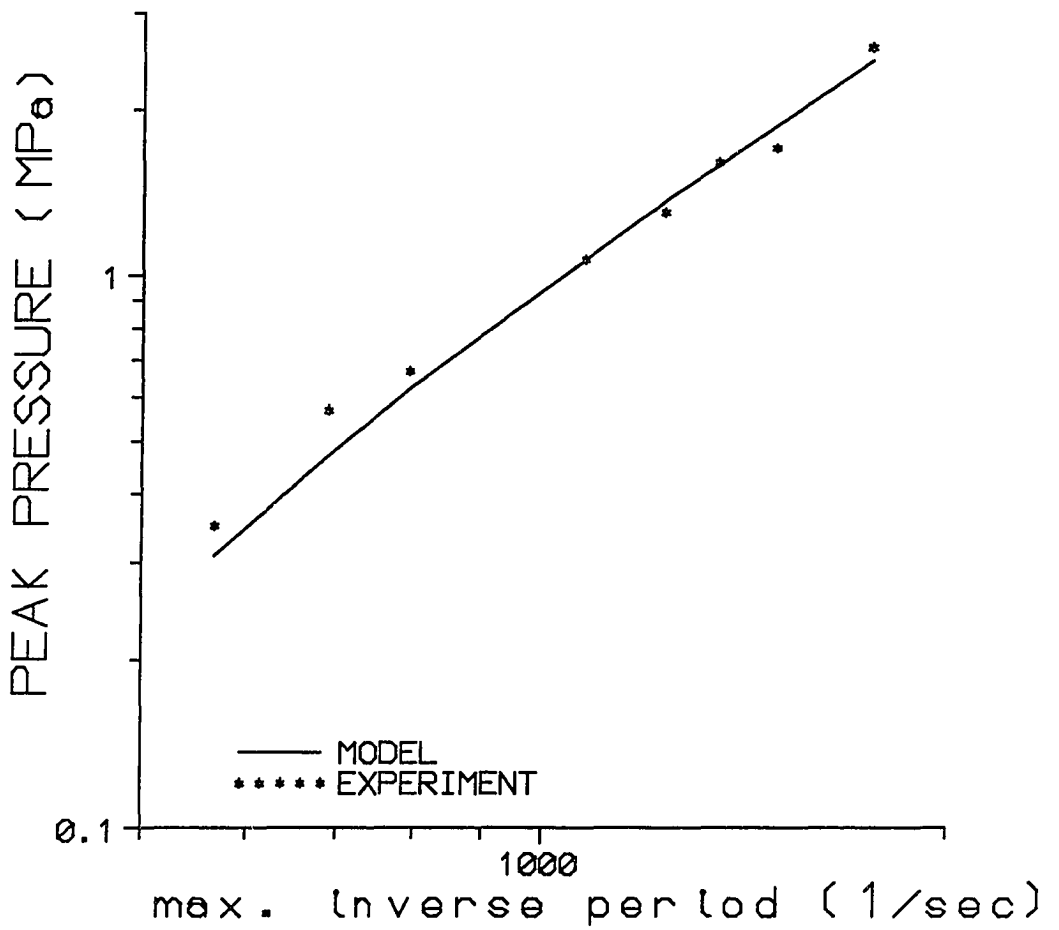

Figure 6-2 Peak pressure versus maximum inverse period for the KEWB-5 experiments.

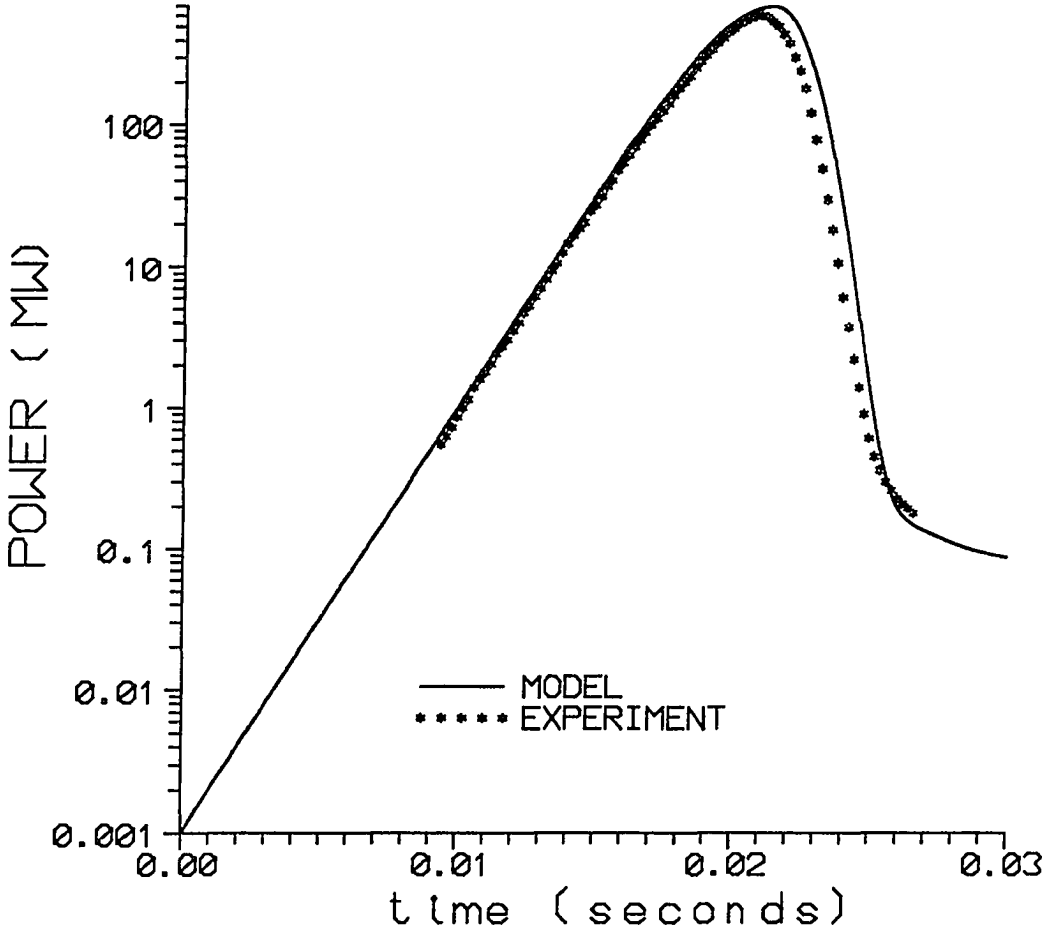

Figure 6-3 Predicted power versus time for KEWB-5 experiment #3041.

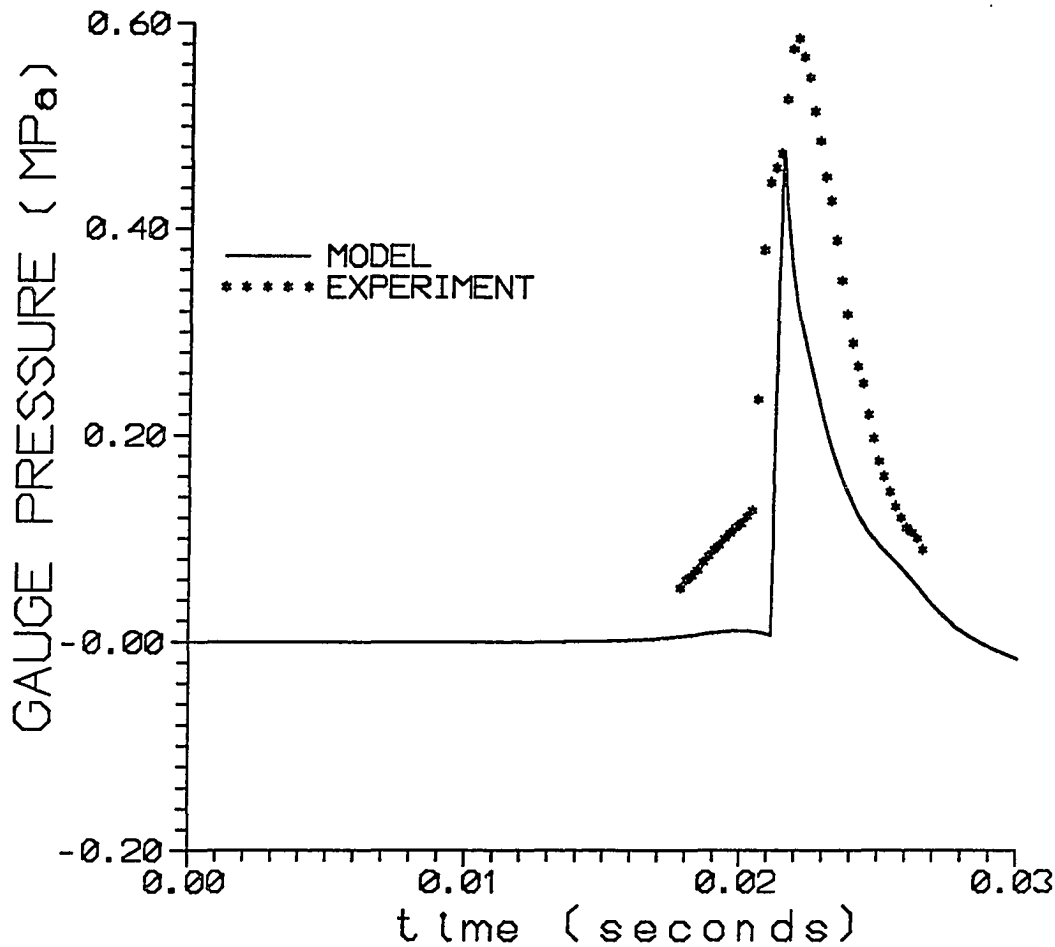

Figure 6-4 Predicted bottom center region pressure versus time for KEWB-5 experiment #3041.

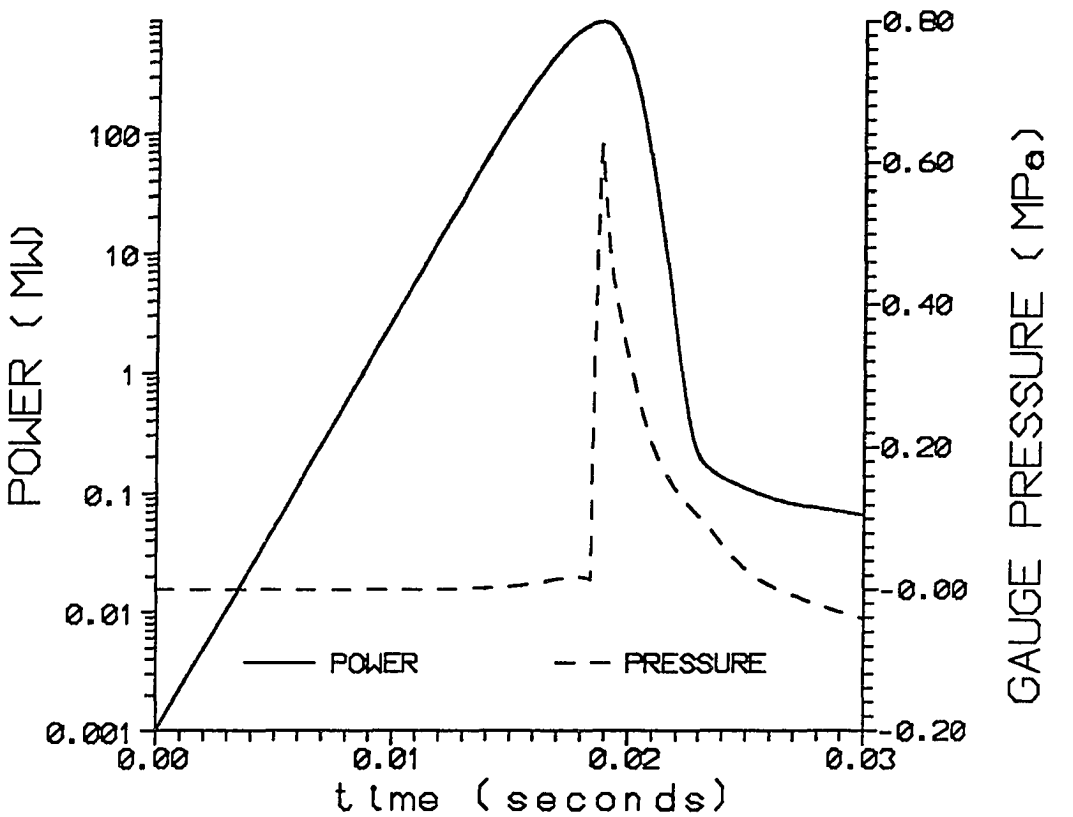

Figure 6-5 Predicted power and bottom center region pressure versus time for KEWB-5 experiment #3043.

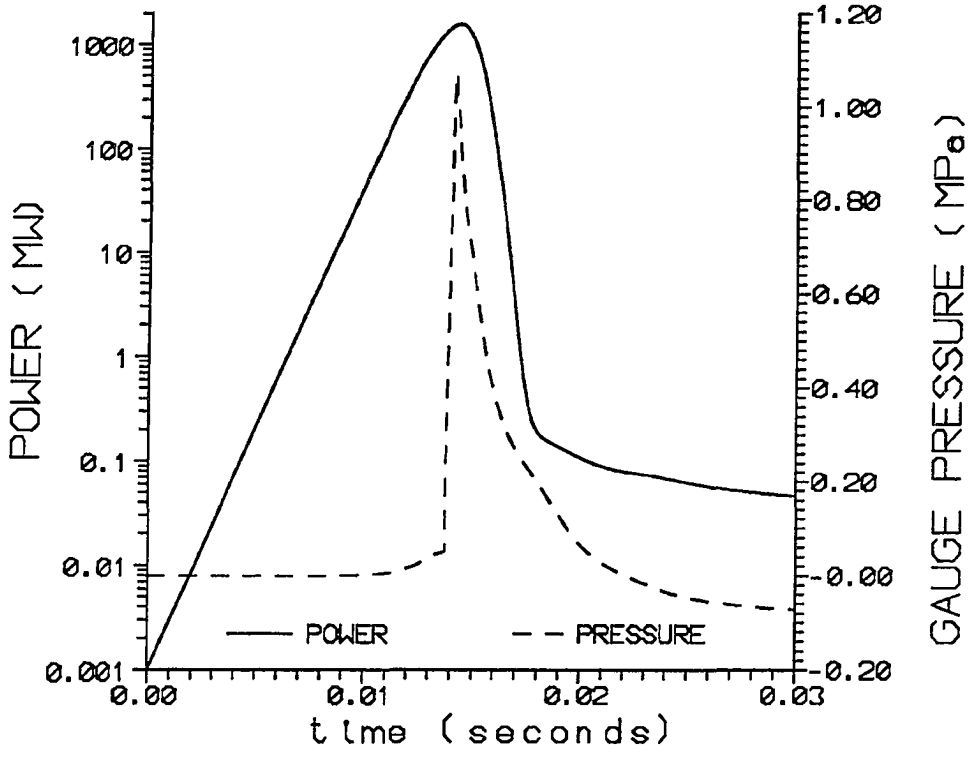

Figure 6-6 Predicted power and bottom center region pressure versus time for KEWB-5 experiment #3014.

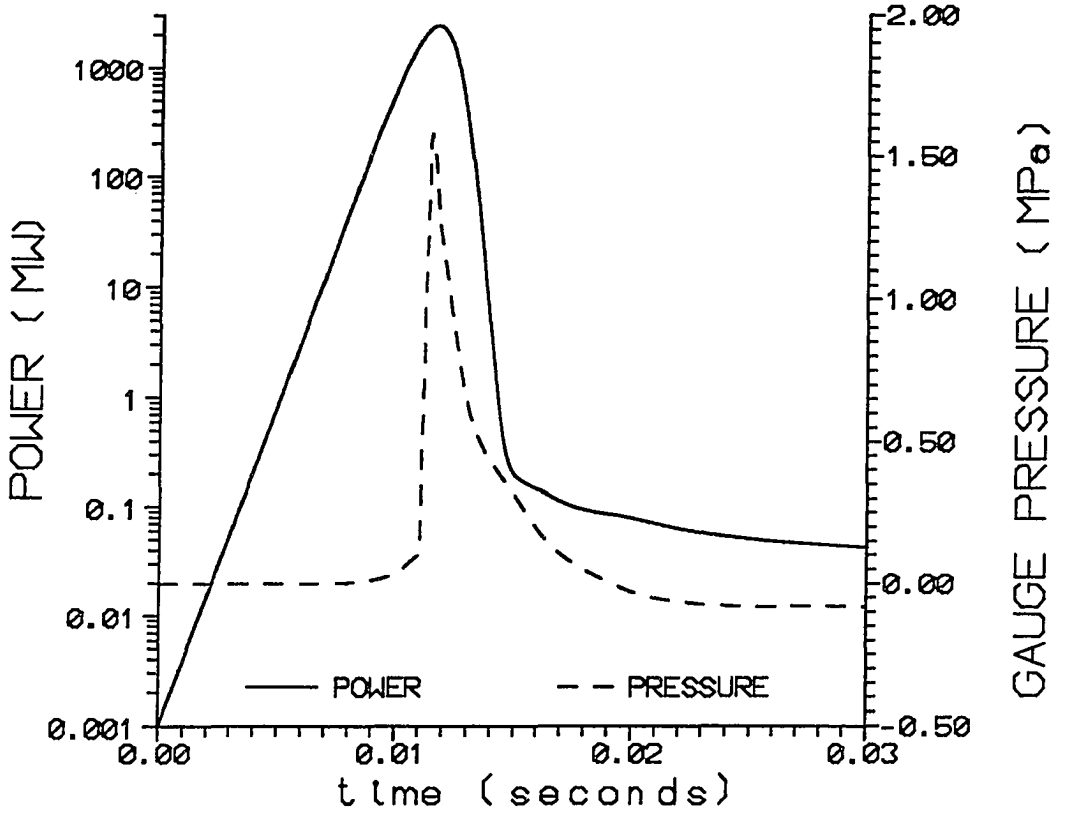

Figure 6-7 Predicted power and bottom center region pressure versus time for KEWB-5 experiment #3016.

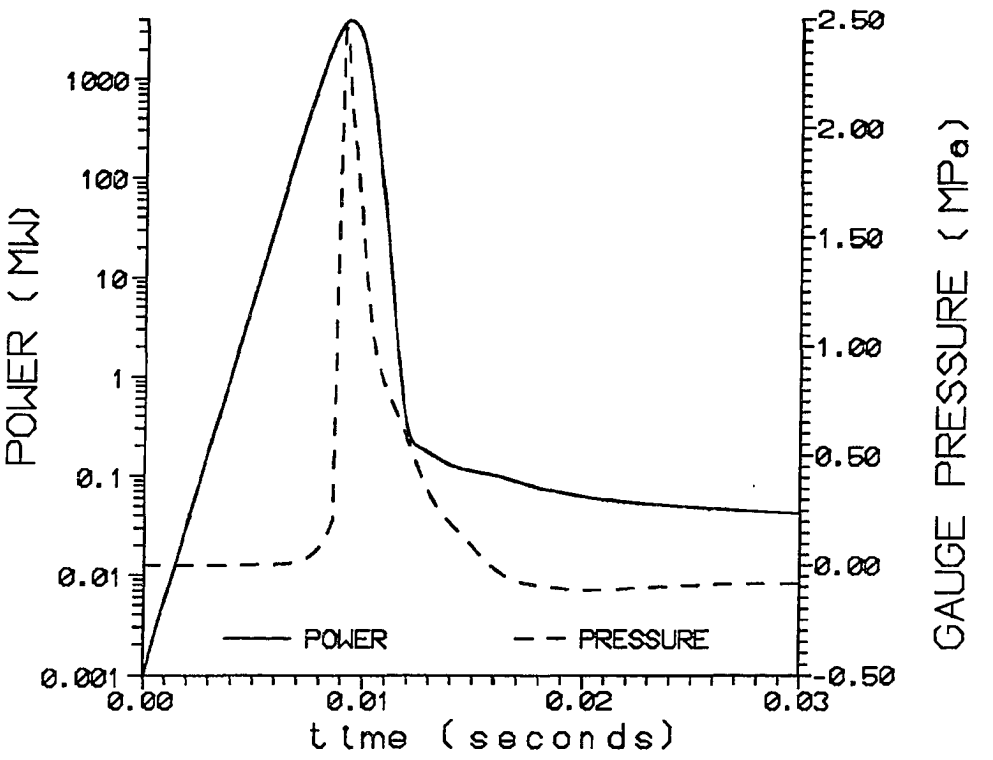

Figure 6-8 Predicted power and bottom center region pressure versus time for KEWB-5 experiment #3018.

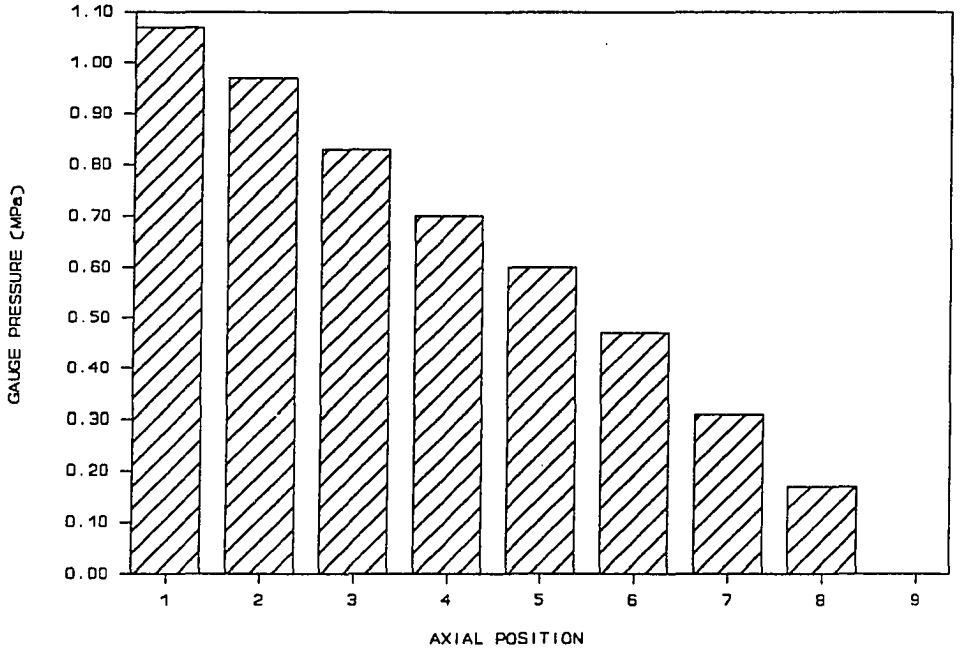

Figure 6-9 Pressure versus axial position for KEWB-5 experiment #3014 at the time of peak pressure (1-bottom center region 9-top center region).

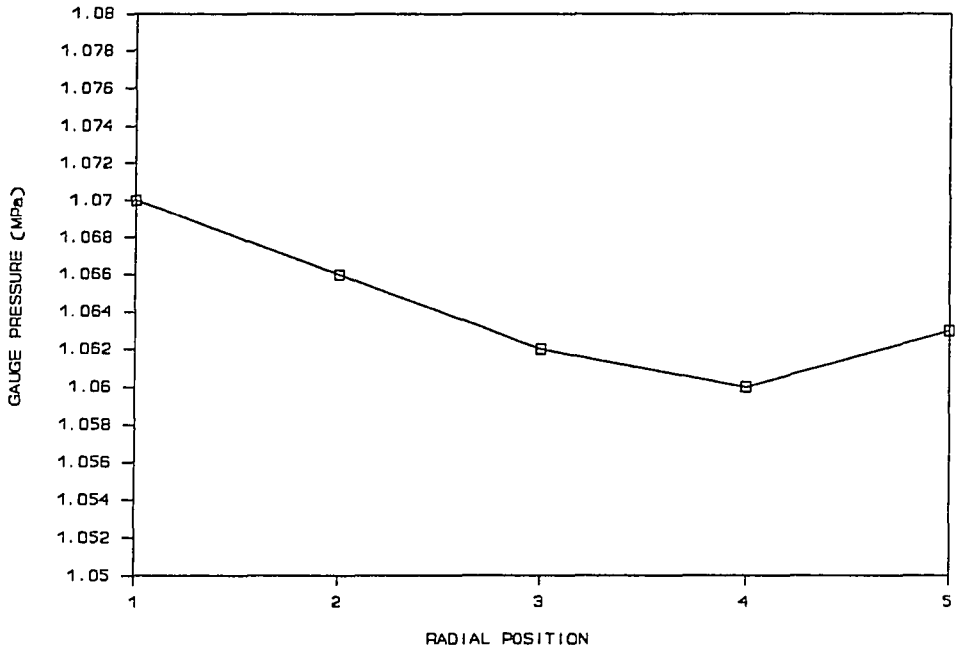

Figure 6-10 Bottom pressure versus radial position for KEWB-5 experiment #3014 at the time of peak pressure (1-center 5-outermost position).

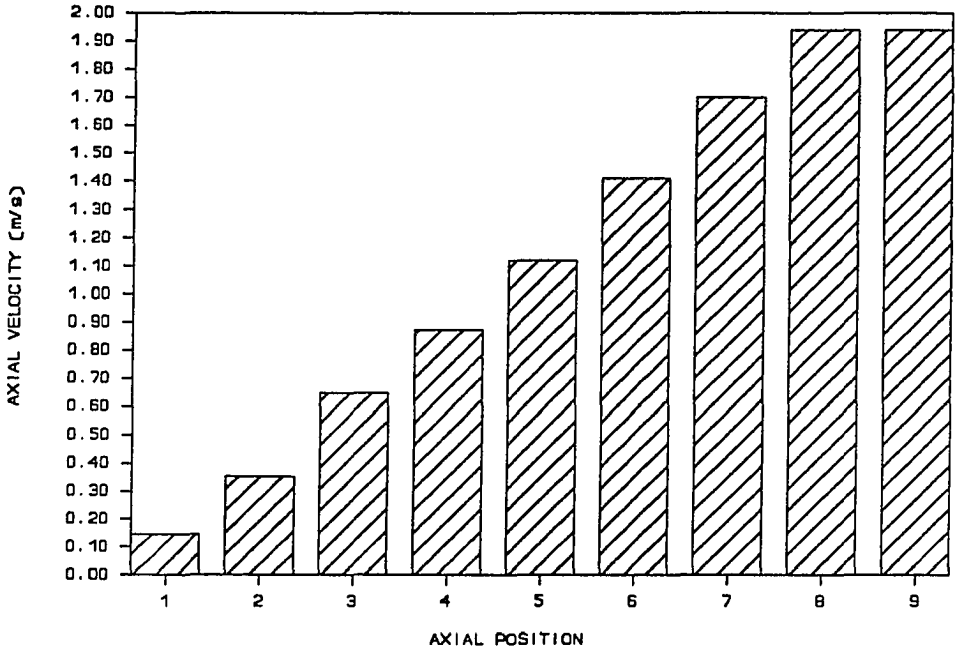

Figure 6-11 Axial velocity in the upwards direction versus axial position for KEWB-5 experiment #3014 at the time of peak pressure (1-bottom center 9-top center).

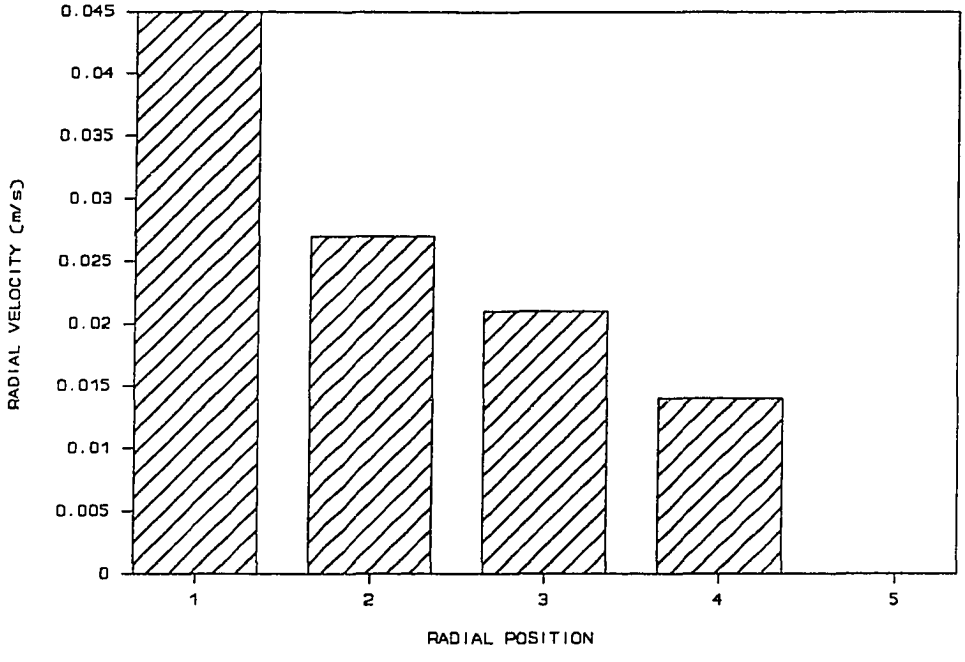

Figure 6-12 Radial velocity, in the outward direction along the bottom of the core, versus radial position for KEWB-5 experiment #3014 at the time of peak pressure (1-center 5-outermost position).

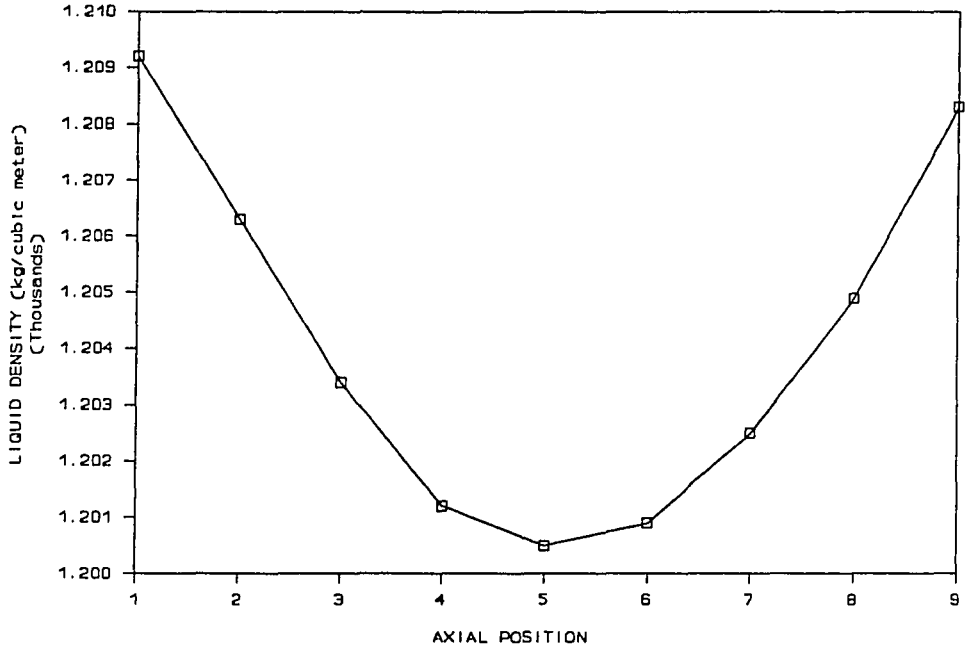

Figure 6-13 Liquid density versus axial position for KEWB-5 experiment #3014 at the time of peak pressure (1-bottom center 9-top center).

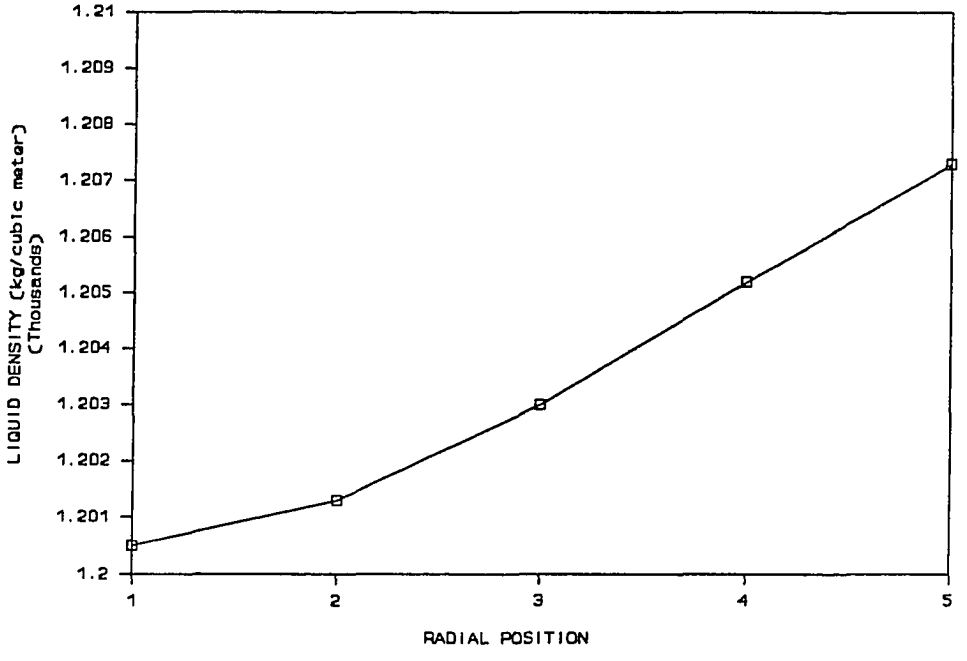

Figure 6-14 Liquid density at the center of the core versus radial position for KEWB-5 experiment #3014 at the time of peak pressure (1-center 5-outermost position).

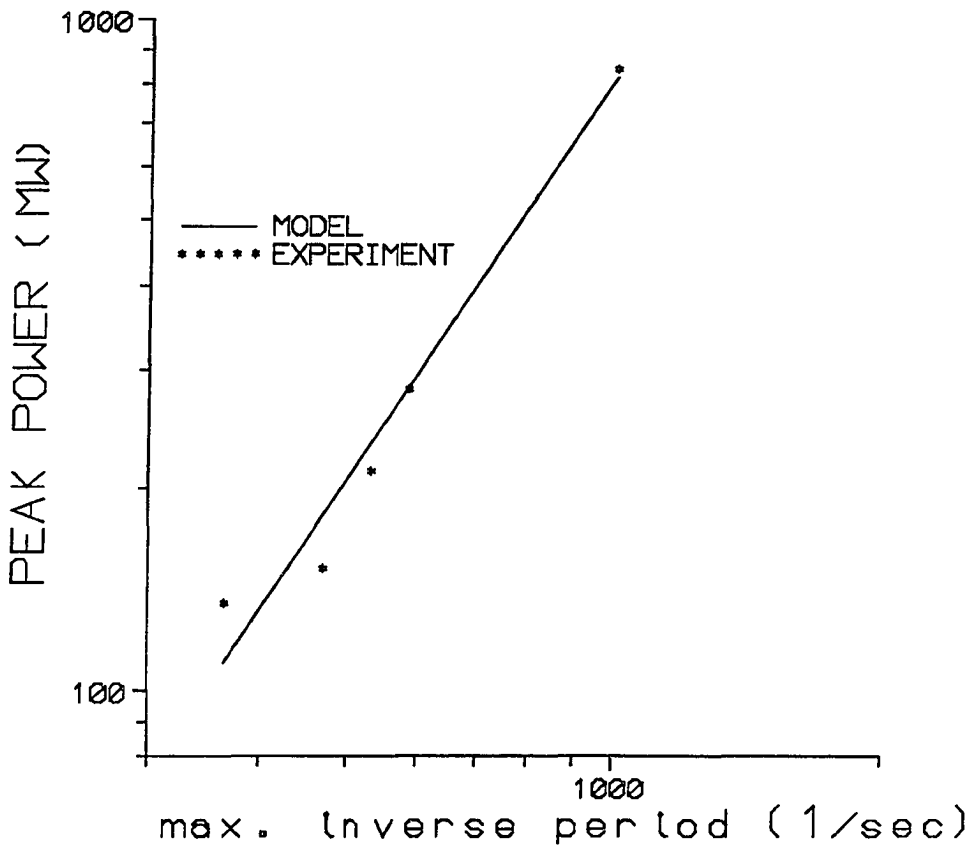

Figure 6-15 Peak power versus maximum inverse period for the CRAC experiments.

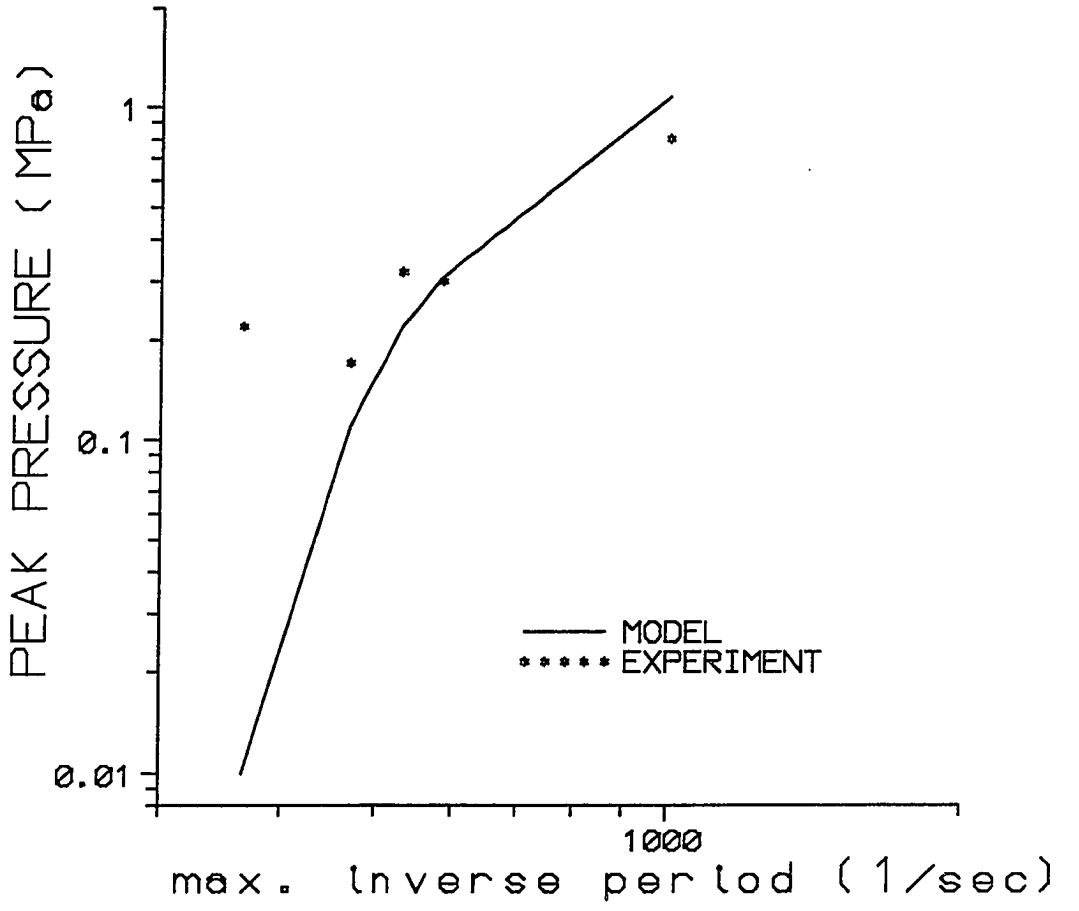

Figure 6-16 Peak pressure versus maximum inverse period for the CRAC experiments.

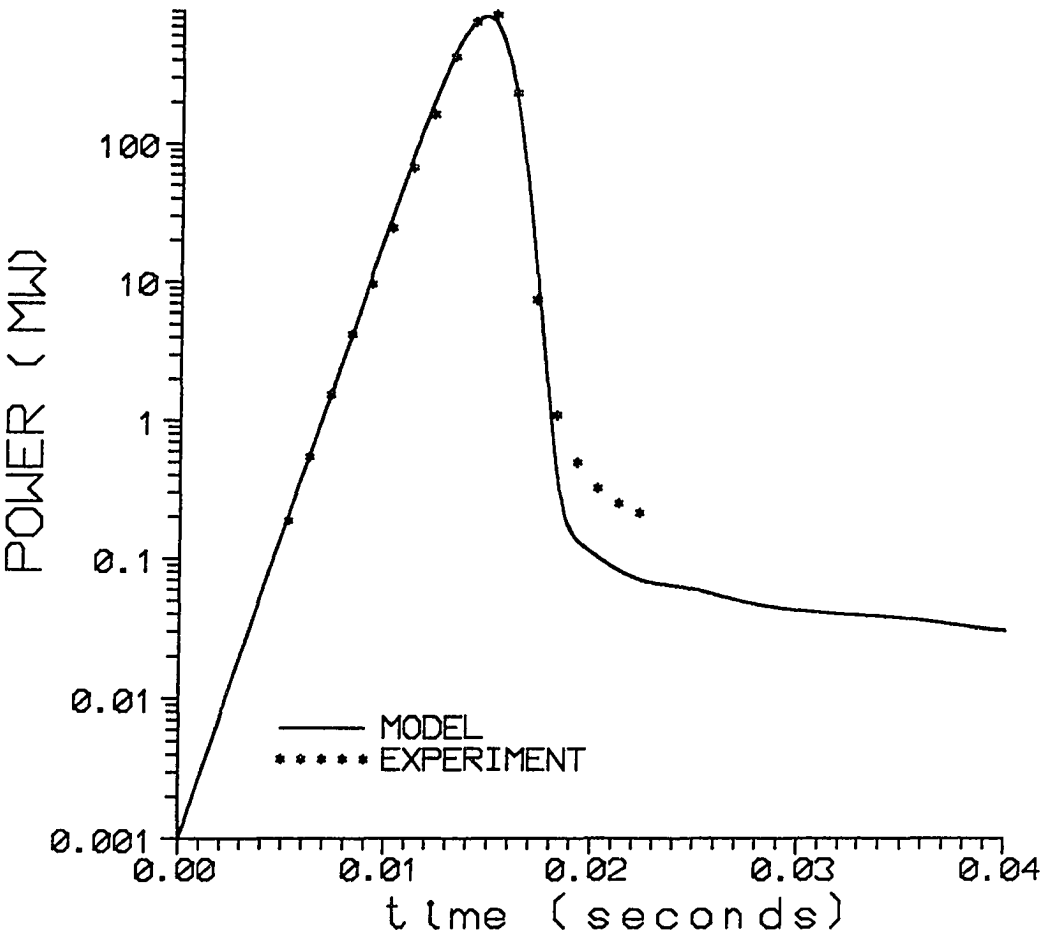

Figure 6-17 Predicted power versus time for CRAC experiment #08.

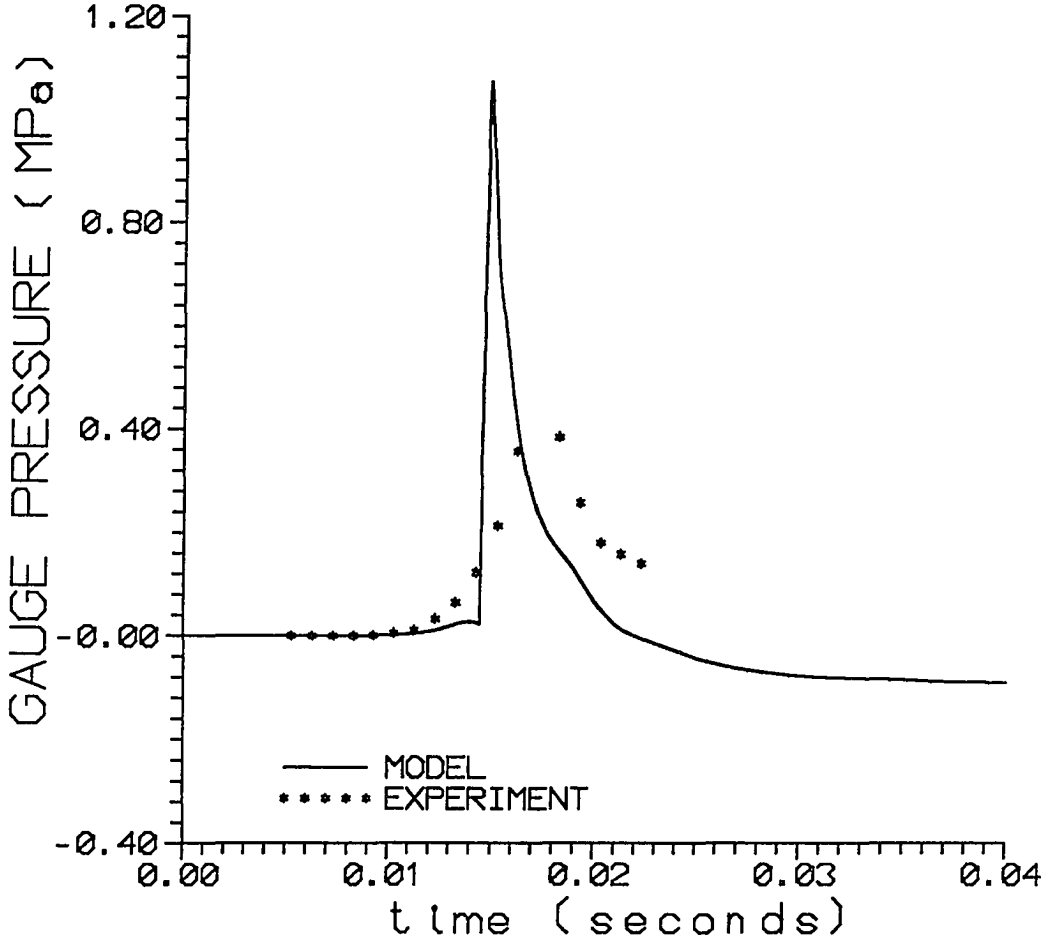

Figure 6-18 Predicted bottom center region pressure versus time for CRAC experiment #08.

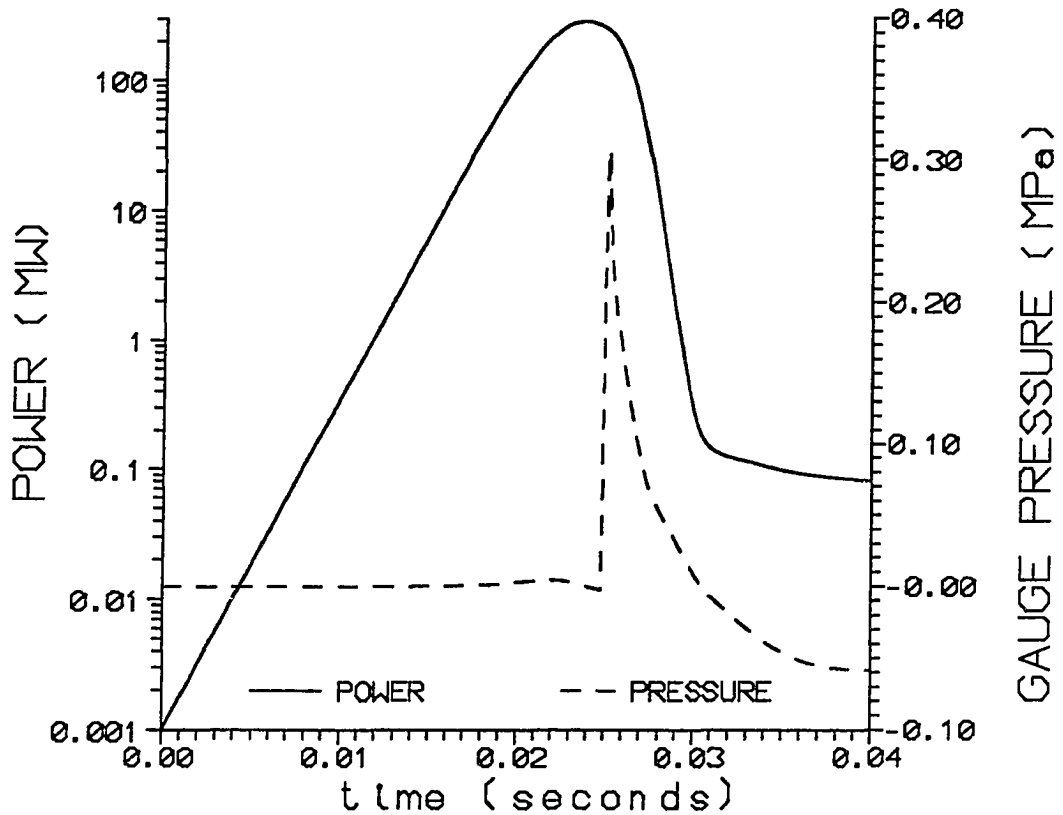

Figure 6-19 Predicted power and bottom center region pressure versus time for CRAC experiment #20.4.

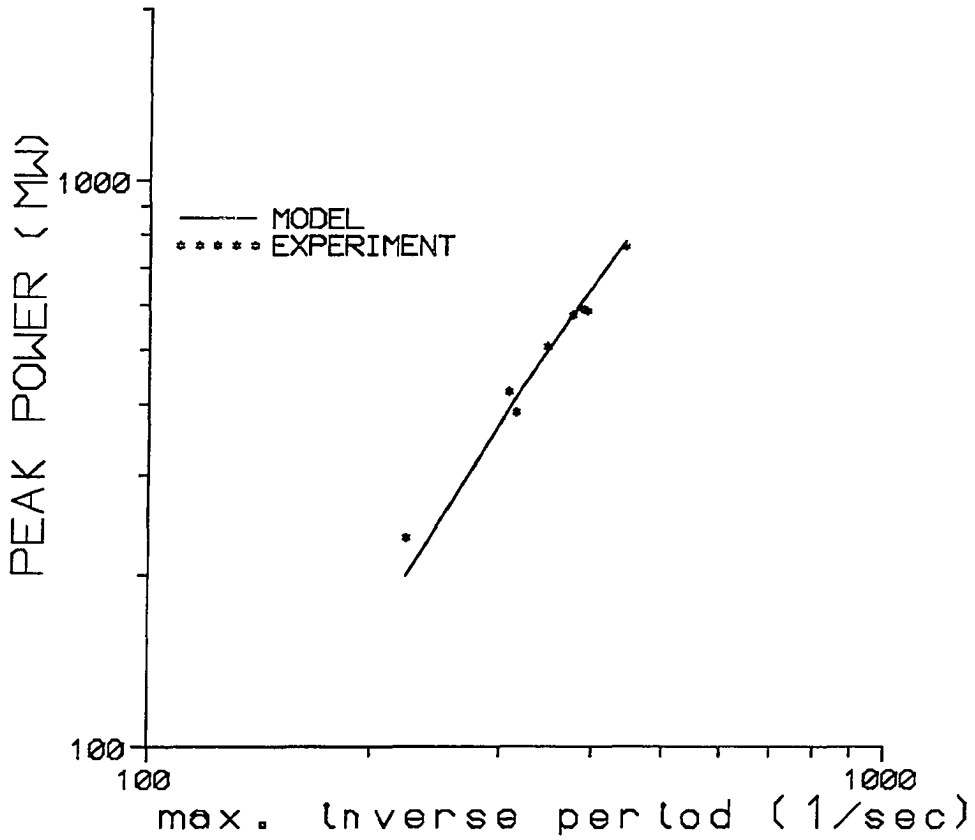

Figure 6-20 Peak power versus maximum inverse period for the SILENE experiments.

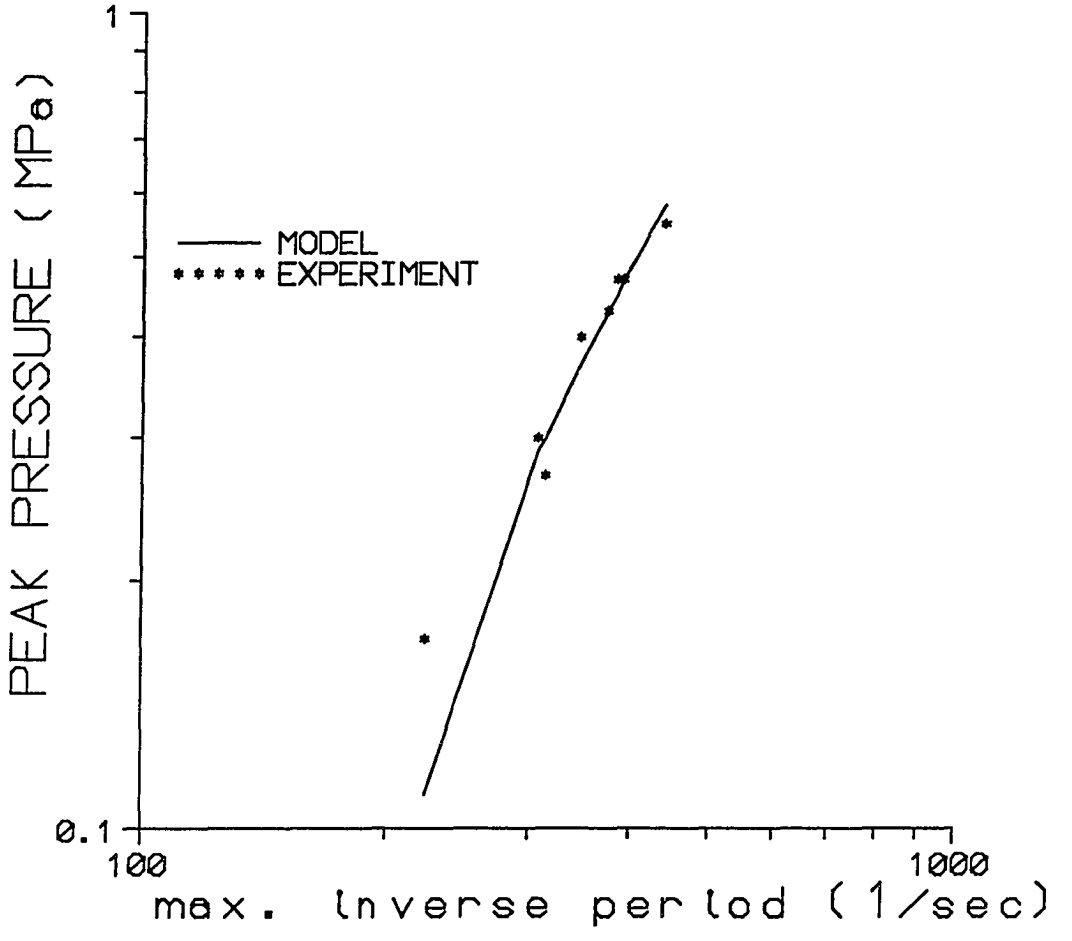

Figure 6-21 Peak pressure versus maximum inverse period for the SILENE experiments.

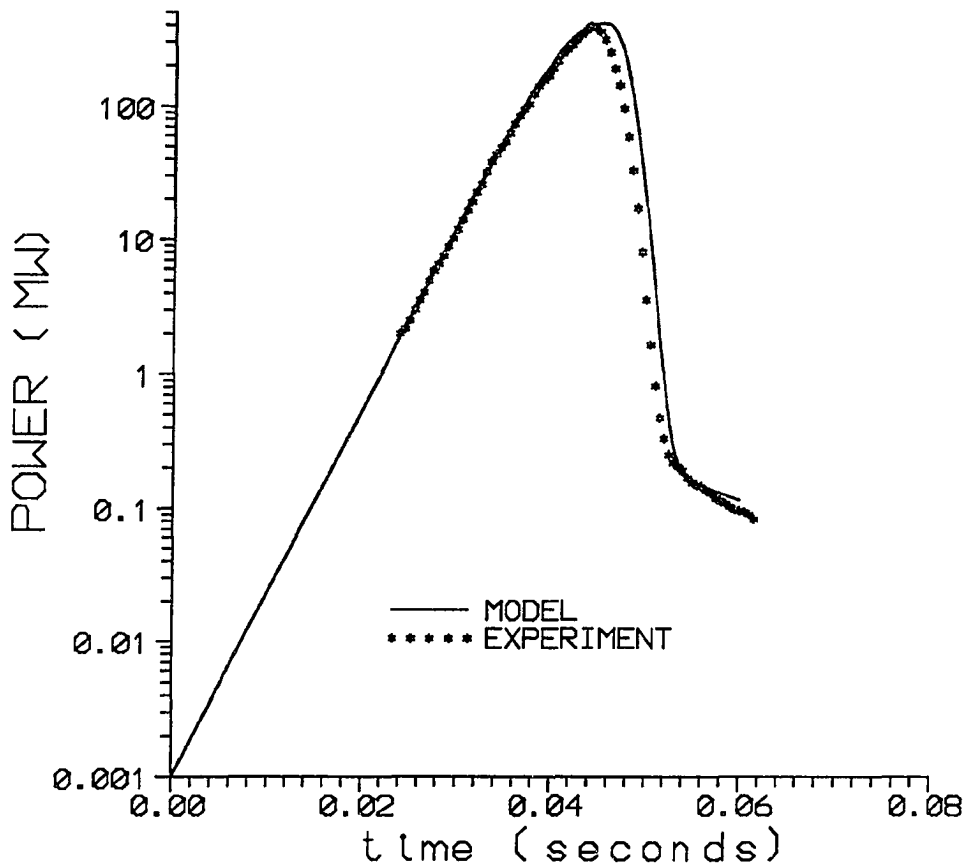

Figure 6-22 Predicted power versus time for SILENE experiment #S1-169.

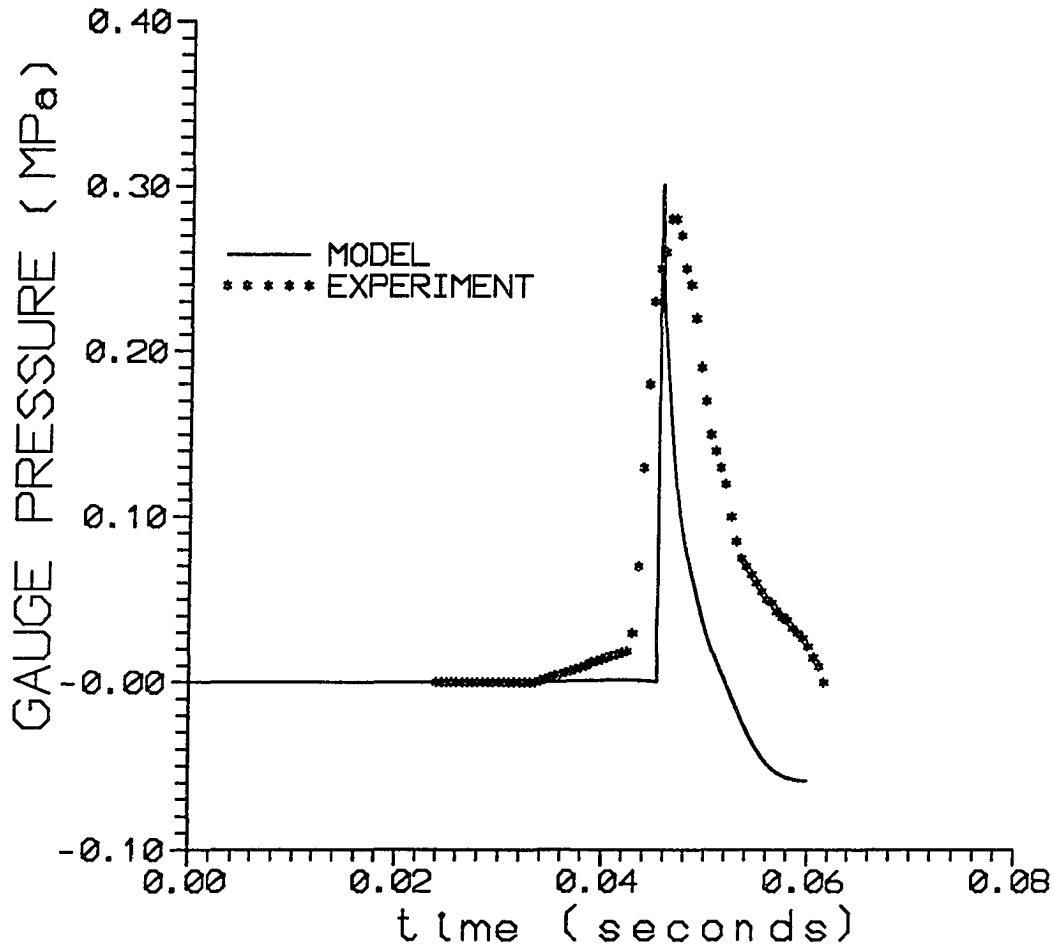

Figure 6-23 Predicted bottom center region pressure versus time for SILENE experiment #S1-169.

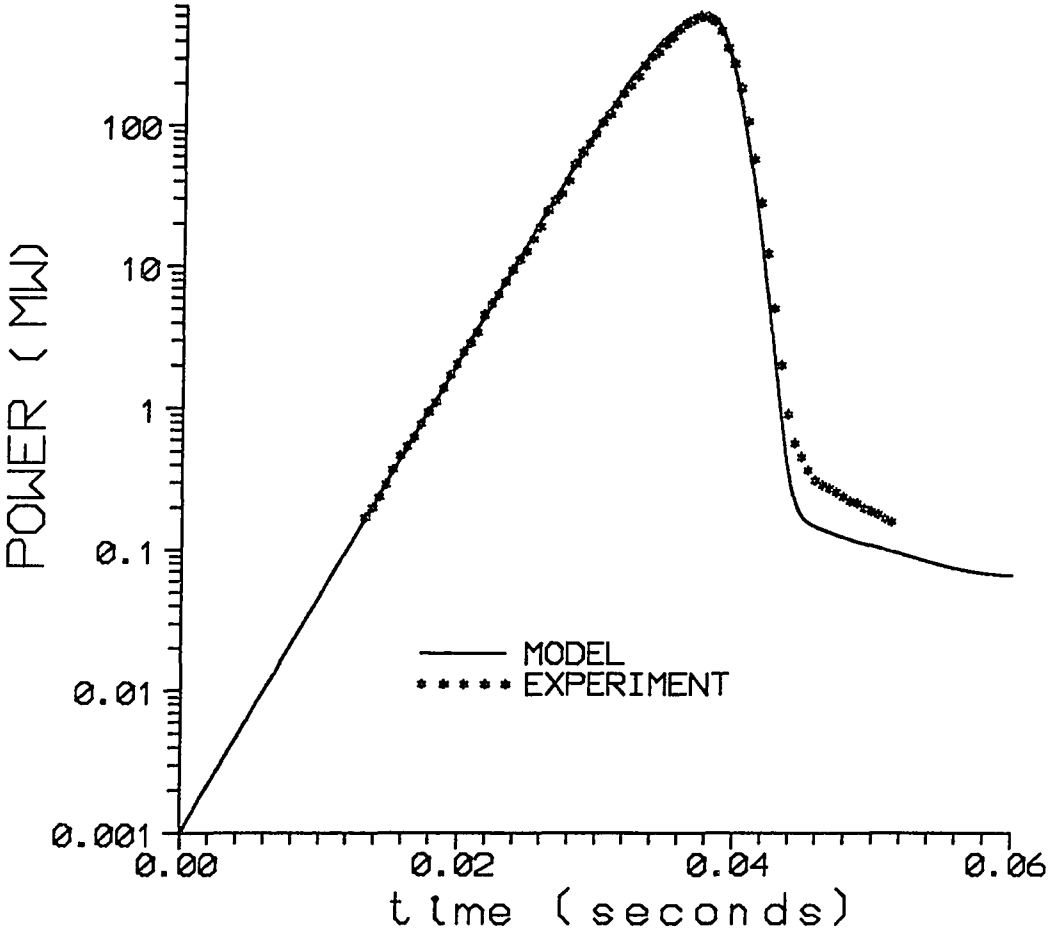

Figure 6-24 Predicted power versus time for SILENE experiment #S2-169.

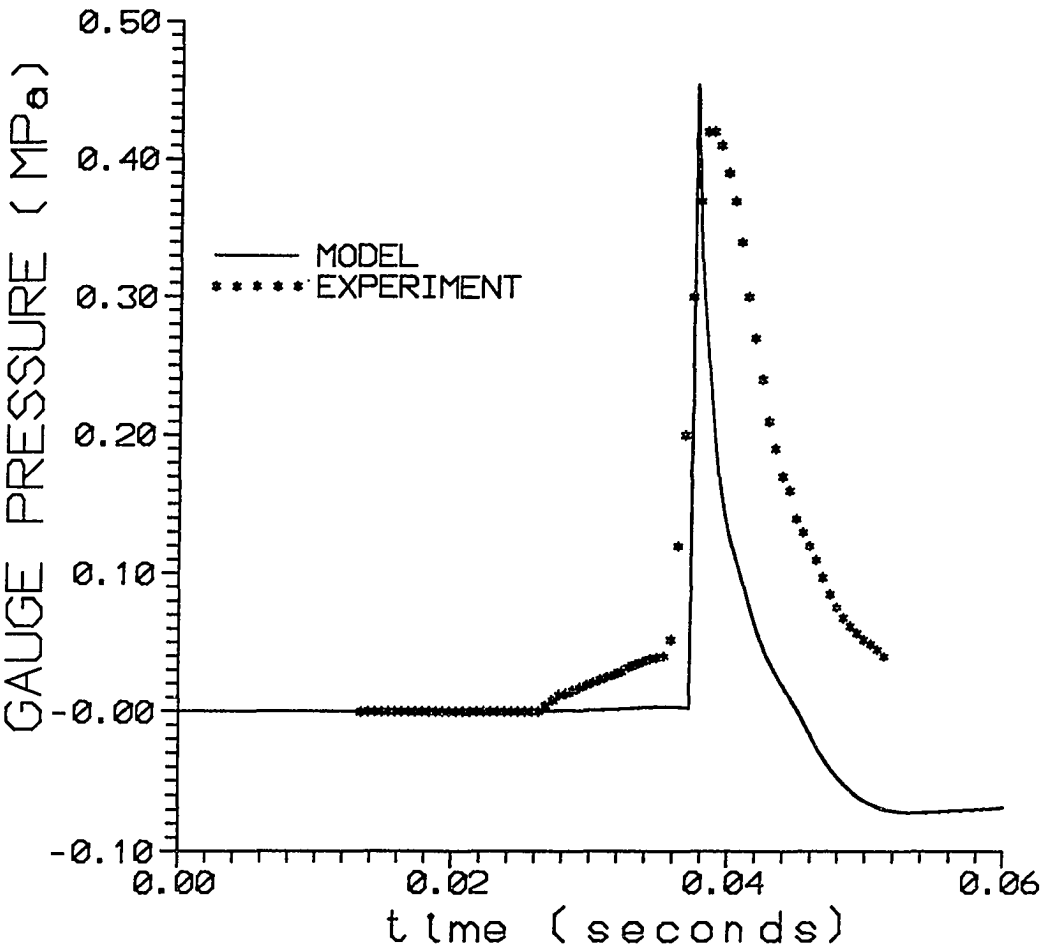

Figure 6-25 Predicted bottom center region pressure versus time for SILENE experiment #S2-169.

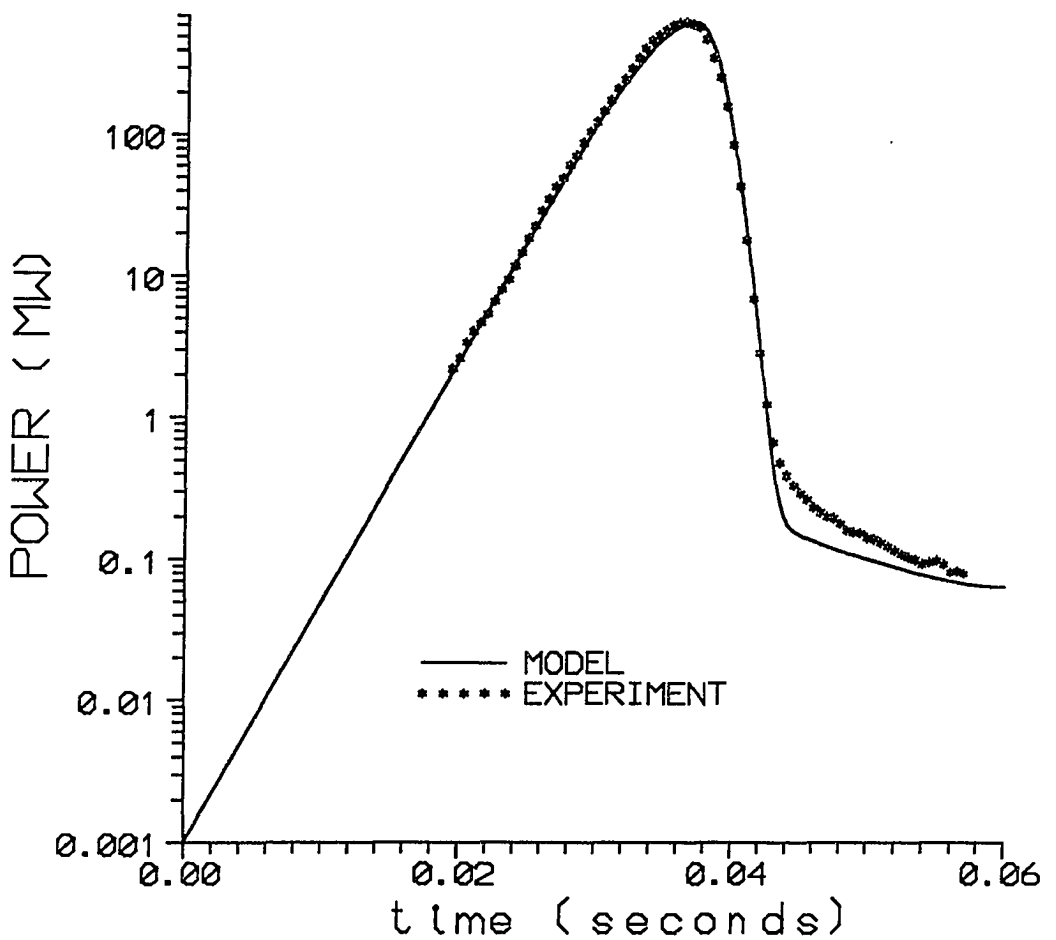

Figure 6-26 Predicted power versus time for SILENE experiment #S4-169.

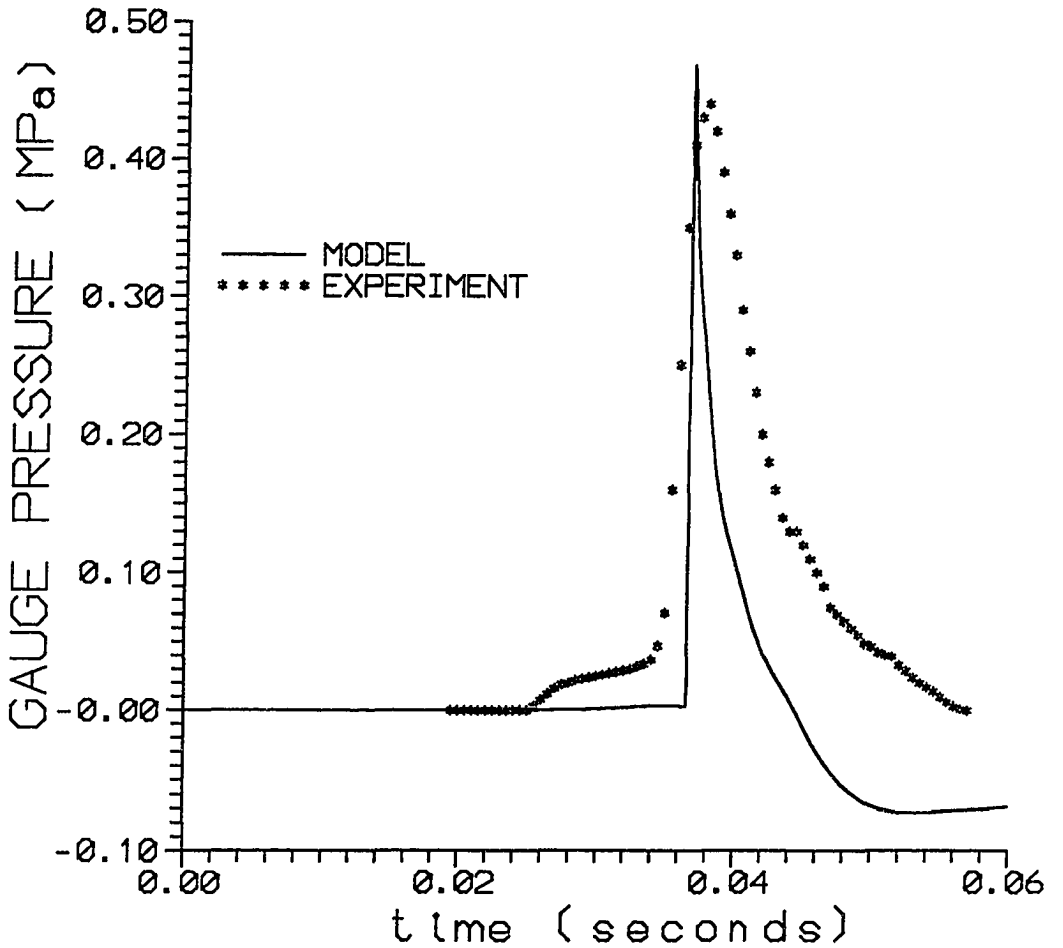

Figure 6-27 Predicted bottom center region pressure versus time for SILENE experiment #S4-169.

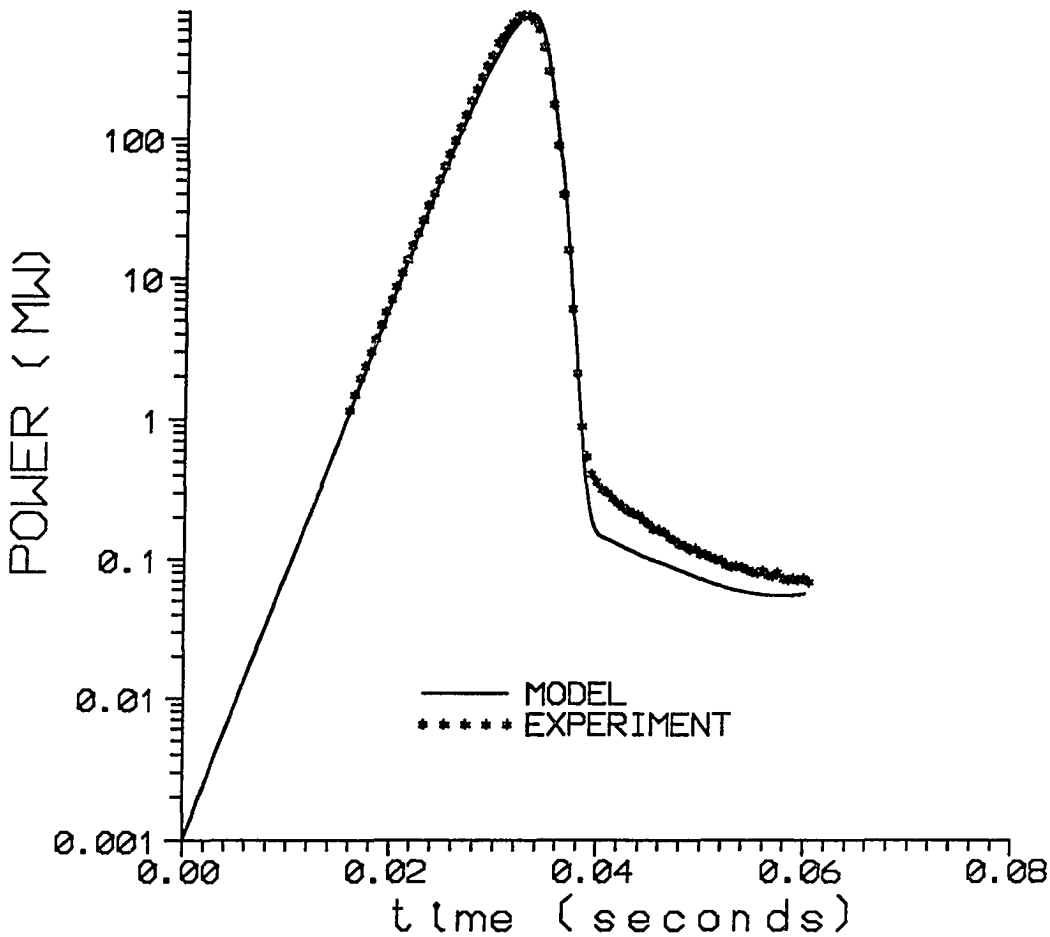

Figure 6-28 Predicted power versus time for SILENE experiment #S2-173.

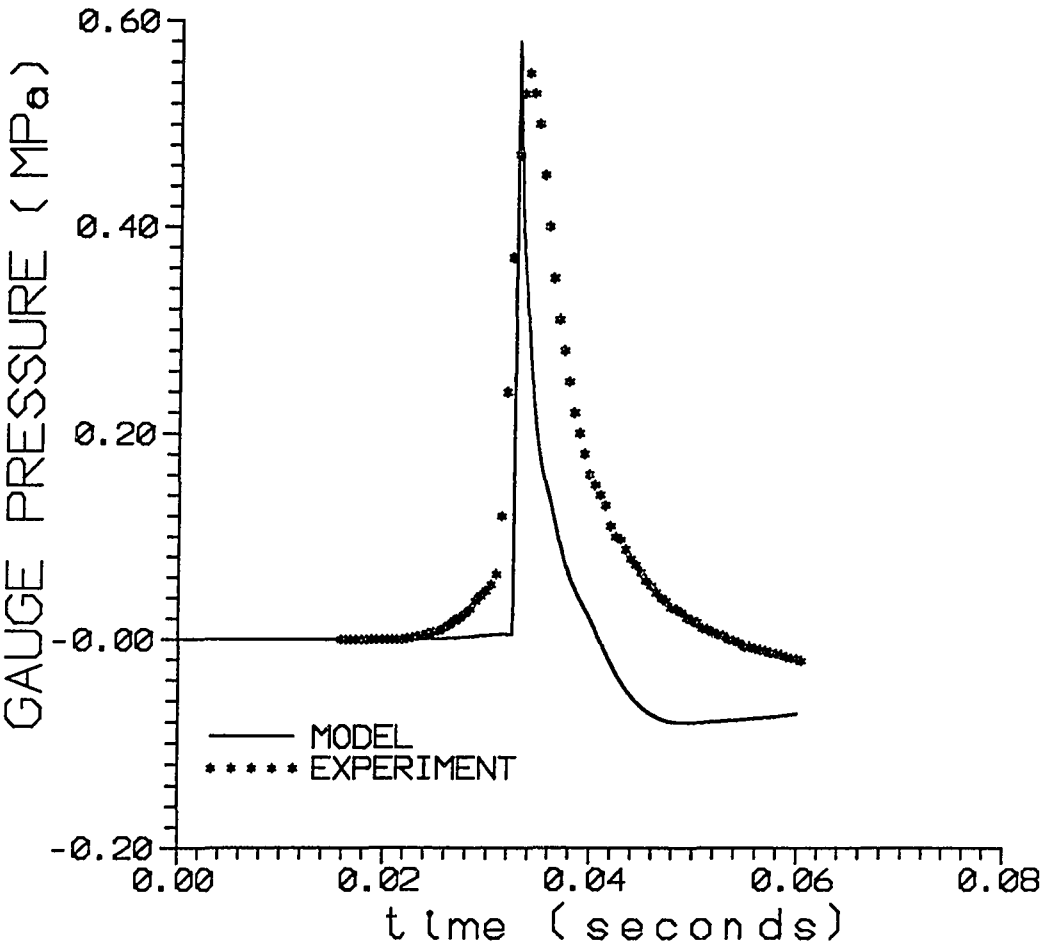

Figure 6-29 Predicted bottom center region pressure versus time for SILENE experiment #S2-173.

CHAPTER 7

SUMMARY AND CONCLUSIONS

A one-region model and a two-dimensional multi-region model have been developed to simulate fast power excursions in cylindrical homogeneous aqueous fissile solution assemblies. Both these models use a new radiolytic gas model, which has been developed to track the nucleation of large and small gas bubbles as a function of time during a power excursion. An equation of state has been developed for both models, which accounts for the important mechanisms that lead to the production and relief of inertial pressure. The two-dimensional multi-region model has been developed to better account for the spatial distribution in solution temperature, pressure, and acceleration.

The radiolytic gas production model presented in Chapter 2 was developed in order to track the rate at which radiolytic gas bubbles are produced, and thus the rate at which radiolytic gas bubble volume is added to the solution assembly. The model recognizes that small microbubbles are formed from thermal spikes, which are created by the fission fragments.

These microbubbles are formed continuously from the start of the power excursion. They contribute a small amount to the production of inertial pressure and provide enough gas bubble volume to alter the properties of the solution.

The most important feature of the radiolytic gas production model is its ability to track the formation of large gas bubbles. The model assumes that large gas bubbles are formed after the fuel solution has become saturated with dissolved gas. The dissolved gas is assumed to be a mixture of hydrogen and oxygen gas. Calculations made with the radiolytic gas production model show that neglecting either of the dissolved gas constituents can significantly underestimate the rate at which large bubbles are formed. This occurs because the rate at which large bubbles form is directly proportional to the excess gas concentration, x. Calculations made with the gas production model have also shown that only about one tenth of the excess dissolved gas available is used in the formation of large gas bubbles. This means that most of the dissolved gas will come out of solution sometime after peak pressure. It is believed that this process is similar to violent cavitation. The radiolytic gas can cause the liquid solution to "boil" and even splash upwards violently. The radiolytic gas production

model only assumes that the dissolved gas comes out of solution as a linear function of solution pressure. Future work in this area will have to consider the actual mechanism by which dissolved gas comes out of solution after the peak pressure, and the way in which it causes the liquid solution to be accelerated. It should be noted, however, that this cavitation-like process has no effect upon the production of inertial pressure or the value of the peak pressure since it is pressure relief that triggers this process. The most important conclusion resulting from tests made with earlier radiolytic gas production models is that the rate at which large bubbles are produced is inversely proportional to the solution pressure. Introduction of the pressure term into equation (2-6) has led to more accurate predictions of peak pressure for power excursions.

The equation of state developed for both the one-region and the multi-region models has demonstrated that the production of inertial pressure depends on two different physical mechanisms. The first is the "lag" in thermal expansion that the solution suffers as the power increases exponentially. The temperature of the fuel solution increases so rapidly that the entire volume of the solution cannot expand fast enough to relieve the building pressure. The second mechanism is the rapid formation and

expansion of radiolytic gas bubbles. The gas volume appears so rapidly that the liquid volume cannot expand rapidly enough to accommodate it. As a result, the liquid is compressed and inertial pressure is produced. Both these mechanisms may be seen from the pressure traces produced by the models. Initially the pressure of the solution rises due to the "lag" in thermal expansion. When the dissolved gas concentration reaches the threshold value, the slope of the pressure increases sharply. At this point both mechanisms are producing inertial pressure.

The two-dimensional multi-region model has provided new information about power excursions. The model provides axial and radial distributions of temperature, pressure, velocity, and density. The axial and radial distributions of liquid density show that the inertial pressure, due to thermal expansion lag, accelerates the fuel material away from the center of the solution assembly. This produces a redistribution of the fuel material towards the outer boundaries of the assembly. This will cause some of the fuel material to be moved from a region of high flux importance to a region of low flux importance, thus altering the reactivity of the assembly. The axial distribution of velocity show that the solution velocity increases with increasing height in the assembly. As a result the rate of pressure

relief increases with increasing height in the assembly, which is seen from the axial distribution in pressure. The radial distribution of velocity shows that some of the fuel solution is accelerated from the center regions outward toward the assembly boundary. This causes the pressure in the outermost regions, next to the wall, to be higher than some of the interior regions. This effect can be seen from the radial distribution of pressure.

Both the one-region model and the multi-region model predict the peak power and pressure for power excursion quite well. The one-region model is more accurate for slower transients, approximately $2.0 or less. The multi-region model works better for faster transients, approximately $2.0 or higher. The multi-region model produces much more accurate power and pressure traces than the one-region model. The width and the shape of the tail for both the power and pressure pulses compare more closely to the experimental traces. The improved power pulses are a result of the enhanced reactivity feedback model, while the improved pressure pulses are a result of the multi-region formulation.

The two-dimensional multi-region model has been very successful in predicting the magnitude of power and pressure pulses in homogeneous solution assemblies. The model has provided new information on the

physical mechanisms involved in the production of inertial pressure. Also, the model has provided new information on both the axial and radial distribution of several of the assemblies parameters. Future work in this area should include a study of reactivity feedback during power excursions. The reactivity changes due to temperature changes in the fuel material, redistribution of the fuel material in the assembly, and expansion of the assembly volume should be considered. Also, the multi-region model only predicts the first power and pressure pulses of a power excursion. Modeling of the reassembly of the fuel solution after the first pulse and subsequent pulses should also be considered in future work.

APPENDIX A

ONE-REGION COMPUTER CODE FOR KEWB

```
------------------------------------------------------------
--    ONE-REGION MODEL - KEWB
--       SYSTEM        V      EM      VL      A
--
--       KEWB 5      0.024    29.0   8.3E-4   0.07
--       CRAC        0.018    21.0   8.3E-4   0.07
--       SILENE      0.037    43.0   8.6E-4   0.10
--
------------------------------------------------------------
TMAX=0.040 |  NN=5001 |  scale=2000
irule 3
-- COEFFICIENTS IN BUBBLE EQUATION OF STATE
RG=6.89E-4
SIGMA=7.5E-8
DTMIN=1.0E-9 |  DTMAX=1.0E-8
-- BUBBLE PROPERTIES
RB1=5.0E-5 |  BL=0.5E-4
FF=1.450E-4*3.0E+17 |  VB=5.3E-13
A0=-23.10932
Ptmax=0.0 |  ENPMAX=0.0
A1=13.15603
A2=-8.6950906E-2
A3=3.2788806E-4
-- LIQUID ISOTHERMAL COMPRESSIBILITY
AK0=4.5E-4
-- SOLUTION PROPERTIES
EM=29.0
XT=1.20E-4
VL=8.3E-4
```

```
A=0.07
CV=3.6E-3
P0=0.1
G=2.0E-3
-- POWER GENERATION PARAMETERS
R0=3.0 | B=0.0
RS=0.0
PHI=10000.
V0=0.024
BOL=543.5
AL1=0.0124 | F1=0.033
AL2=0.0305 | F2=0.219
AL3=0.111 | F3=0.196
AL4=0.301 | F4=0.395
AL5=1.14 | F5=0.115
AL6=3.01 | F6=0.042
EN0=0.001
-- INITIAL VALUES
EN=1.
E=1.E-6
P=0.1
TEMP=20.0
V=0.024
------------------------------
display N14
drun
------------------------------
DYNAMIC
------------------------------
-- NEUTRON DYNAMICS
-- REACTIVITY FEEDBACK
RFB=PHI*(V-V0)
R=R0+B*t-RFB
-- POINT REACTOR KINETICS
SUM=F1*D1+F2*D2+F3*D3+F4*D4+F5*D5+F6*D6
ENDOT=BOL*((R-1.0)*EN+SUM-RS)
OMEGA=ENDOT/EN
```

```
d/dt EN=ENDOT
d/dt D1=AL1*(EN-D1)
d/dt D2=AL2*(EN-D2)
d/dt D3=AL3*(EN-D3)
d/dt D4=AL4*(EN-D4)
d/dt D5=AL5*(EN-D5)
d/dt D6=AL6*(EN-D6)
ENP=EN0*EN
d/dt E=ENP
-- DISSOLVED GAS PRODUCTION
XE=G*E/EM
XR=XE-XT
X=XR*swtch(XE-XT)
-- RADIOLYTIC GAS PRODUCTION MODEL
RB=5.0E-8+RB1*swtch(X)
-- MICROBUBBLE PRODUCTION
NBDOT1=ENP*3.0E+17-NB1/10.0E-6
d/dt NB1=NBDOT1
-- LARGE GAS BUBBLE PRODUCTION
NBDOT2=FF/P*X*ENP-NB2/BL
d/dt NB2=NBDOT2
-- TOTAL BUBBLE VOLUME
VGAS=NB2*VB+NB1*5.3E-22
-- VOLUME CHANGE DUE TO GAS COMPRESSION
VC=NBDOT*VB+NBDOT2*5.3E-22
-- VOID FRACTION EQUATIONS
TABS=TEMP+273.15
PA=P+2.0*SIGMA/RB
PB=P+(4.0/3.0)*SIGMA/RB
FA=X*RG*TABS
FB=FA+VL*(1.0-X)*PA
F=VGAS/V0+FA/FB*swtch(Ptmax-0.05-P)*(1-P/(Ptmax+0.01))
-- LIQUID ISOBARIC COMPRESSIBILITY
BETA0=1.0E-6*(A0+A1*TEMP+A2*TEMP*TEMP+A3*
TEMP*TEMP*TEMP)
-- MIXTURE ISOBARIC COMPRESSIBILITY
BETA=BETA0*(1.0-F)+F/TABS*PA/PB
```

```
-- MIXTURE ISOTHERMAL COMPRESSIBILITY
AK=AK0*(1.0-F)+F/PB
-- VOLUME EXPANSION
d/dt V=VDOT-VC
-- MOMENTUM EQUATION
d/dt VDOT=1.0E+6*A*A*(P-P0)/EM
-- ENERGY EQUATION
TDOT=(ENP-EN0-(BETA/AK)*TABS*VDOT)/(EM*CV)
d/dt TEMP=TDOT
-- EQUATION OF STATE
PDOT=(BETA*TDOT-(VDOT-VC)/V)/AK
d/dt P=PDOT
-- OUTPUT DISPLAY
-- GAUGE PRESSURE
PRESS=P-P0
PREX=PRESS
PKPA=1000.0*PREX
-- MAXIMUM GRAUGE PRESSURE
Ptmax=Ptmax+(P-Ptmax)*swtch(P-Ptmax)
-- MAXIMUM POWER
ENPMAX=ENPMAX+(ENP-ENPMAX)*swtch(ENP-ENPMAX)
RE=R*300
dispt ENP,PKPA,RE
```

APPENDIX B

MULTI-REGION COMPUTER CODE FOR KEWB

```
------------------------------------------------------------
--      MULTI-REGION MODEL - KEWB
--      45-REGION (5-RADIAL POINTS, 9-AXIAL POINTS)
--
--
--      SYSTEM      V       EM      VL      A
--
--      KEWB 5      0.024   29.0    8.3E-4  0.07
--      CRAC        0.018   21.0    8.3E-4  0.07
--      SILENE      0.037   43.0    8.6E-4  0.10
--
------------------------------------------------------------
TMAX=0.040 |  NN=4001 |  scale=2000
irule 3 |  DTMIN=1.0E-9 |  DTMAX=1.0E-8
-- COEFFICIENTS IN BUBBLE EQUATION OF STATE
RG=6.89E-4 |  SIGMA=7.5E-8
A0=-23.10932
A1=13.15603
A2=-8.6950906E-2
A3=3.2788806E-4
-- LIQUID ISOTHERMAL COMPRESSIBILIT
AK0=4.5E-4
-- SOLUTION PROPERTIES
EM=29.0 |  CN=1.0E+6
XT=1.20E-4 |  BL=0.50e-4
VL=8.2759E-4
A=0.07 |  RB1=5.0E-5
FF=1.480*0.4/1.0e+4
CV=3.6E-3 |  CP=CV
```

```
P0=0.1
G=2.0E-3
-- POWER GENERATION PARAMETERS
R0=3.0 | B=0.0
RS=0.0
ALPHA=0.133 | PHI2=3000
V0=0.024
BOL=543.5
AL1=0.0124 | F1=0.033
AL2=0.0305 | F2=0.219
AL3=0.111 | F3=0.196
AL4=0.301 | F4=0.395
AL5=1.14 | F5=0.115
AL6=3.01 | F6=0.042
EN0=0.001
ENPMAX=0.0
-- INITIAL VALUES
TEMP0=20.0
F=0.0
EN=1.
T0=20.0
Ptmax=0.0
-- INITIAL PRESSURE
P1=P0 | P2=P0 | P3=P0 | P4=P0 | P5=P0
P6=P0 | P7=P0 | P8=P0 | P9=P0 | P10=P0
P11=P0 | P12=P0 | P13=P0 | P14=P0 | P15=P0
P41=P0 | P51=P0 | P61=P0 | P71=P0 | P81=P0 | P91=P0
P101=P0 | P111=P0 | P121=P0 | P131=P0 | P141=P0 | P151=P0
P42=P0 | P52=P0 | P62=P0 | P72=P0 | P82=P0 | P92=P0
P102=P0 | P112=P0 | P122=P0 | P132=P0 | P142=P0 | P152=P0
P53=P0 | P63=P0 | P73=P0 | P83=P0
-- INITIAL TEMPERATURE
T41=T0 | T51=T0 | T61=T0 | T71=T0 | T81=T0 | T91=T0
T101=T0 | T111=T0 | T121=T0 | T131=T0 | T141=T0 |
T151=T0
T42=T0 | T52=T0 | T62=T0 | T72=T0 | T82=T0 | T92=T0
T102=T0 | T112=T0 | T122=T0 | T132=T0 | T142=T0 |
```

```
T152=T0
T53=T0 | T63=T0 | T73=T0 | T83=T0
T1=T0 | T2=T0 | T3=T0 | T4=T0 | T5=T0
T6=T0 | T7=T0 | T8=T0 | T9=T0 | T10=T0
T11=T0 | T12=T0 | T13=T0 | T14=T0 | T15=T0
-- RADIAL POSITIONS
r1=0.015 | r2=0.045 | r3=0.075 | r4=0.105
rc1=0.015 | rc2=0.03 | rc3=0.06 | rc4=0.09 | rc5=0.12
-- DELTA r,x
dr=0.03 | dz=0.0378 | dr1=0.015 | dr2=0.03 | dr3=0.03 |
dr4=0.045
-- INITIAL DENSITY
RHO=EM/V0 | VR=V0
RO1=RHO | RO2=RHO | RO3=RHO | RO4=RHO | RO5=RHO
RO6=RHO | RO7=RHO | RO8=RHO | RO9=RHO | RO10=RHO
RO11=RHO | RO12=RHO | RO13=RHO | RO14=RHO |
RO15=RHO
RO41=RHO | RO51=RHO | RO61=RHO | RO71=RHO |
RO81=RHO
RO91=RHO | RO101=RHO | RO111=RHO | RO121=RHO |
RO131=RHO
RO141=RHO | RO151=RHO
RO42=RHO | RO52=RHO | RO62=RHO | RO72=RHO |
RO82=RHO
RO92=RHO | RO102=RHO | RO112=RHO | RO122=RHO |
RO132=RHO
RO142=RHO | RO152=RHO
RO53=RHO | RO63=RHO | RO73=RHO | RO83=RHO
------------------------------
display N14
-- display C15
-- disconnect 1
-- connect 'fig.dat' as output 1
drun
-- disconnect 1
------------------------------
DYNAMIC
```

```
-----------------------------
-- NEUTRON DYNAMICS
-- REACTIVITY FEEDBAC
RFB=PHI*(T4-TEMP0)+PHI2*F*V0
R=R0+B*t-RFB
-- POINT KINETICS EQUATIONS
SUM=F1*D1+F2*D2+F3*D3+F4*D4+F5*D5+F6*D6
ENDOT=BOL*((R-1.0)*EN+SUM-RS)
OMEGA=ENDOT/EN
d/dt EN=ENDOT
d/dt D1=AL1*(EN-D1)
d/dt D2=AL2*(EN-D2)
d/dt D3=AL3*(EN-D3)
d/dt D4=AL4*(EN-D4)
d/dt D5=AL5*(EN-D5)
d/dt D6=AL6*(EN-D6)
ENP=EN0*EN
B1=1 | B2=0.95 | B3=0.77 | B4=0.5 | B5=0.17
S1=1 | S2=0.94 | S3=0.78 | S4=0.55 | S5=0.29
-- POWER DENSITY DISTRIBUTION
ENP1=ENP/V0*B5*S1 | EN01=EN0/V0*B5*S1
ENP2=ENP/V0*B5*S2 | EN02=EN0/V0*B5*S2
ENP3=ENP/V0*B5*S3 | EN03=EN0/V0*B5*S3
ENP4=ENP/V0*B4*S1 | EN04=EN0/V0*B4*S1
ENP5=ENP/V0*B4*S2 | EN05=EN0/V0*B4*S2
ENP6=ENP/V0*B4*S3 | EN06=EN0/V0*B4*S3
ENP7=ENP/V0*B3*S1 | EN07=EN0/V0*B3*S1
ENP8=ENP/V0*B3*S2 | EN08=EN0/V0*B3*S2
ENP9=ENP/V0*B3*S3 | EN09=EN0/V0*B3*S3
ENP10=ENP/V0*B2*S1 | EN010=EN0/V0*B2*S1
ENP11=ENP/V0*B2*S2 | EN011=EN0/V0*B2*S2
ENP12=ENP/V0*B2*S3 | EN012=EN0/V0*B2*S3
ENP13=ENP/V0*B1*S1 | EN013=EN0/V0*B1*S1
ENP14=ENP/V0*B1*S2 | EN014=EN0/V0*B1*S2
ENP15=ENP/V0*B1*S3 | EN015=EN0/V0*B1*S3
ENP41=ENP10 | EN041=EN010
ENP51=ENP11 | EN051=EN011
```

```
ENP61=ENP12 | EN061=EN012
ENP71=ENP7 | EN071=EN07
ENP81=ENP8 | EN081=EN08
ENP91=ENP9 | EN091=EN09
ENP101=ENP4 | EN0101=EN04
ENP111=ENP5 | EN0111=EN05
ENP121=ENP6 | EN0121=EN06
ENP131=ENP1 | EN0131=EN01
ENP141=ENP2 | EN0141=EN02
ENP151=ENP3 | EN0151=EN03
ENP42=ENP/V0*B4*S4 | EN042=EN0/V0*B4*S4
ENP52=ENP/V0*B4*S5 | EN052=EN0/V0*B4*S5
ENP62=ENP/V0*B3*S4 | EN062=EN0/V0*B3*S4
ENP72=ENP/V0*B3*S5 | EN072=EN0/V0*B3*S5
ENP82=ENP/V0*B2*S4 | EN082=EN0/V0*B2*S4
ENP92=ENP/V0*B2*S5 | EN092=EN0/V0*B2*S5
ENP102=ENP/V0*B1*S4 | EN0102=EN0/V0*B1*S4
ENP112=ENP/V0*B1*S5 | EN0112=EN0/V0*B1*S5
ENP122=ENP82 | EN0122=EN082
ENP132=ENP92 | EN0132=EN092
ENP142=ENP62 | EN0142=EN062
ENP152=ENP72 | EN0152=EN072
ENP53=ENP42 | EN053=EN042
ENP63=ENP52 | EN063=EN052
ENP73=ENP/V0*B5*S4 | EN073=EN0/V0*B5*S4
ENP83=ENP/V0*B5*S5 | EN083=EN0/V0*B5*S5
d/dt E=ENP13
ENPMAX=ENPMAX+(ENP-ENPMAX)*swtch(ENP-ENPMAX)
-- DISSOLVED GAS PRODUCTION
XE=G*E/RO13
XR=XE-XT
X=XR*swtch(XE-XT)
-- VOID FRACTION AFTER PEAK PRESSURE
RB=5.0e-8+RB1*swtch(X)
PG=P13+2*SIGMA/RB
FC1=X*RG*(T13+273)
FC2=(1-X)/RO13
```

```
FZ=FC1/(PG*FC2+FC1)*(1-P131/(Ptmax+0.01))
-- LARGE GAS BUBBLE PRODUCTION
NBDOT2=X/P13*FF*ENP*3.560e+16*swtch(X)-NB2/BL
-- MICROBUBBLE PRODUCTION
NBDOT1=0.4*ENP*3.56E+16-NB1/1.0E-5
d/dt NB2=NBDOT2
d/dt NB1=NBDOT1
-- DENSITY CHANGED DUE TO COMPRESSION
DC=(NBDOT2*5.236e-13+NBDOT1*5.25E-22)*EM/V0/V0
-- TOTAL BUBBLE VOLUME
VGASB=NB2*5.236e-13+NB1*5.25E-22
-- VOID FRACTION
F=VGASB/V0+FZ*swtch(Ptmax-0.05-P131)
KC1=P13+4/3*SIGMA/RB
-- MEDIUM COMPRESSIBILITY
KM=(1-F)*AK0+F/KC1
-- LIQUID ISOBARIC COMPRESSIBILITY
BET01=1.0E-6*(A0+A1*T1+A2*T1*T1+A3*T1*T1*T1)
BET02=1.0E-6*(A0+A1*T2+A2*T2*T2+A3*T2*T2*T2)
BET04=1.0E-6*(A0+A1*T4+A2*T4*T4+A3*T4*T4*T4)
BET05=1.0E-6*(A0+A1*T5+A2*T5*T5+A3*T5*T5*T5)
BET03=1.0E-6*(A0+A1*T3+A2*T3*T3+A3*T3*T3*T3)
BET06=1.0E-6*(A0+A1*T6+A2*T6*T6+A3*T6*T6*T6)
BET07=1.0E-6*(A0+A1*T7+A2*T7*T7+A3*T7*T7*T7)
BET08=1.0E-6*(A0+A1*T8+A2*T8*T8+A3*T8*T8*T8)
BET09=1.0E-6*(A0+A1*T9+A2*T9*T9+A3*T9*T9*T9)
BET010=1.0E-6*(A0+A1*T10+A2*T10*T10+A3*T10*T10*T10)
BET011=1.0E-6*(A0+A1*T11+A2*T11*T11+A3*T11*T11*T11)
BET012=1.0E-6*(A0+A1*T12+A2*T12*T12+A3*T12*T12*T12)
BET013=1.0E-6*(A0+A1*T13+A2*T13*T13+A3*T13*T13*T13)
BET014=1.0E-6*(A0+A1*T14+A2*T14*T14+A3*T14*T14*T14)
BET015=1.0E-6*(A0+A1*T15+A2*T15*T15+A3*T15*T15*T15)
--
ROB=(P13+2*SIGMA/RB)/RG/T13
-- REGION 4 (RADIAL POSITION-1,AXIAL POSITION-8)
d/dt E4=ENP4
XE4=G*E4/RO4
```

```
XR4=XE4-XT
X4=XR4*swtch(XE4-XT)
DC4=DC
FV4=0.0
K4=KM
-- ISOBARIC COMPRESSIBILITY
BETA4=(1-FV4)*BET04+FV4/(T4+273)
-- AXIAL VELOCITY
d/dt U4Z=1/RO4*CN*(P4-P1)/dz
-- RADIAL VELOCITY
d/dt U4R=1/RO4*CN*(P4-P5)/dr
d/dt VR=U4R*A
-- CONTINUITY EQUATION
RDOT4=DC4-RO4*(U4Z-U7Z)/dz-RO4/rc1*(U4R*r1)/dr1
d/dt RO4=RDOT4
-- ENERGY EQUATION
TDOT4=(ENP4-EN04)/RO4/CP
d/dt T4=TDOT4
-- EQUATION OF STATE
PDOT4=((BETA4*TDOT4+RDOT4/RO4)/K4)*swtch(P4)
d/dt P4=PDOT4
-- REGION 5 (2,8)
d/dt E5=ENP5
XE5=G*E5/RO5
XR5=XE5-XT
X5=XR5*swtch(XE5-XT)
DC5=DC
FV5=0.0
K5=KM
BETA5=(1-FV5)*BET05+FV5/(T5+273)
d/dt U5Z=1/RO5*CN*(P5-P2)/dz
d/dt U5R=1/RO5*CN*(P5-P6)/dr
RDOT5=DC5-RO5*(U5Z-U8Z)/dz-RO5/rc2*(U5R*r2-U4R*r1)/dr
d/dt RO5=RDOT5
TDOT5=(ENP5-EN05)/RO5/CP
d/dt T5=TDOT5
PDOT5=(BETA5/K5*TDOT5+RDOT5/RO5/K5)*swtch(P5)
```

```
d/dt P5=PDOT5
-- REGION 6 (3,8)
d/dt E6=ENP6
XE6=G*E6/RO6
XR6=XE6-XT
X6=XR6*swtch(XE6-XT)
DC6=DC
FV6=0.0
K6=KM
BETA6=(1-FV6)*BET06+FV6/(T6+273)
d/dt U6Z=1/RO6*CN*(P6-P3)/dz
d/dt U6R=1/RO6*CN*(P6-P42)/dr
RDOT6=DC6-RO6*(U6Z-U9Z)/dz-RO6/rc3*(U6R*r3-U5R*r2)/dr2
d/dt RO6=RDOT6
TDOT6=(ENP6-EN06)/RO6/CP
d/dt T6=TDOT6
PDOT6=(BETA6/K6*TDOT6+RDOT6/K6/RO6)*swtch(P6)
d/dt P6=PDOT6
-- REGION 7 (1,7)
d/dt E7=ENP7
XE7=G*E7/RO7
XR7=XE7-XT
X7=XR7*swtch(XE7-XT)
DC7=DC
FV7=0.0
K7=KM
BETA7=(1-FV7)*BET07+FV7/(T7+273)
d/dt U7Z=1/RO7*CN*(P7-P4)/dz
d/dt U7R=1/RO7*CN*(P7-P8)/dr
RDOT7=DC7-RO7*(U7Z-U10Z)/dz-RO7/rc1*U7R*r1/dr1
d/dt RO7=RDOT7
TDOT7=(ENP7-EN07)/RO7/CP
d/dt T7=TDOT7
PDOT7=(BETA7/K7*TDOT7+RDOT7/K7/RO7)*swtch(P7)
d/dt P7=PDOT7
-- REGION 8 (2,7)
d/dt E8=ENP8
```

```
XE8=G*E8/RO8
XR8=XE8-XT
X8=XR8*swtch(XE8-XT)
DC8=DC
FV8=0.0
K8=KM
BETA8=(1-FV8)*BET08+FV8/(T8+273)
d/dt U8Z=1/RO8*CN*(P8-P5)/dz
d/dt U8R=1/RO8*CN*(P8-P9)/dr
RDOT8=DC8-RO8*(U8Z-U11Z)/dz-RO8/rc2*(U8R*r2-U7R*r1)/dr
d/dt RO8=RDOT8
TDOT8=(ENP8-EN08)/RO8/CP
d/dt T8=TDOT8
PDOT8=(BETA8/K8*TDOT8+RDOT8/K8/RO8)*swtch(P8)
d/dt P8=PDOT8
-- REGION 9 (3,7)
d/dt E9=ENP9
XE9=G*E9/RO9
XR9=XE9-XT
X9=XR9*swtch(XE9-XT)
DC9=DC
FV9=0.0
K9=KM
BETA9=(1-FV9)*BET09+FV9/(T9+273)
d/dt U9Z=1/RO9*CN*(P9-P6)/dz
d/dt U9R=1/RO9*CN*(P9-P62)/dr
RDOT9=DC9-RO9*(U9Z-U12Z)/dz-RO9/rc3*(U9R*r3-U8R*r2)/dr2
d/dt RO9=RDOT9
TDOT9=(ENP9-EN09)/RO9/CP
d/dt T9=TDOT9
PDOT9=(BETA9/K9*TDOT9+RDOT9/K9/RO9)
d/dt P9=PDOT9
-- REGION 10 (1,6)
d/dt E10=ENP10
XE10=G*E10/RO10
XR10=XE10-XT
X10=XR10*swtch(XR10-XT)
```

```
DC10=DC
FV10=0.0
K10=KM
BETA10=(1-FV10)*BET010+FV10/(T10+273)
d/dt U10Z=1/RO10*CN*(P10-P7)/dz
d/dt U10R=1/RO10*CN*(P10-P11)/dr
RDOT10=DC10-RO10*(U10Z-U13Z)/dz-RO10/rc1*(U10R*r1)/dr1
d/dt RO10=RDOT10
TDOT10=(ENP10-EN010)/RO10/CP
d/dt T10=TDOT10
PDOT10=(BETA10/K10*TDOT10+RDOT10/K10/RO10)
d/dt P10=PDOT10
-- REGION 11 (2,6)
d/dt E11=ENP11
XE11=G*E11/RO11
XR11=XE11-XT
X11=XR11*swtch(XE11-XT)
DC11=DC
FV11=0.0
K11=KM
BETA11=(1-FV11)*BET011+FV11/(T11+273)
d/dt U11Z=1/RO11*CN*(P11-P8)/dz
d/dt U11R=1/RO11*CN*(P11-P12)/dr
RDOT11=DC11-RO11*(U11Z-U14Z)/dz-
RO11/rc2*(U11R*r2-U10R*r1)/dr
d/dt RO11=RDOT11
TDOT11=(ENP11-EN011)/RO11/CP
d/dt T11=TDOT11
PDOT11=(BETA11/K11*TDOT11+RDOT11/K11/RO11)
d/dt P11=PDOT11
-- REGION 12 (3,6)
d/dt E12=ENP12
XE12=G*E12/RO12
XR12=XE12-XT
X12=XR12*swtch(XE12-XT)
DC12=DC
FV12=0.0
```

```
K12=KM
BETA12=(1-FV12)*BET012+FV12/(T12+273)
d/dt U12Z=1/RO12*CN*(P12-P9)/dz
d/dt U12R=1/RO12*CN*(P12-P82)/dr
RDOT12=DC12-
RO12*(U12Z-U15Z)/dz-RO12/rc3*(U12R*r3-U11R*r1)/dr2
d/dt RO12=RDOT12
TDOT12=(ENP12-EN012)/RO12/CP
d/dt T12=TDOT12
PDOT12=(BETA12/K12*TDOT12+RDOT12/RO12/K12)
d/dt P12=PDOT12
-- REGION 13 (1,5)
d/dt E13=ENP13
XE13=G*E13/RO13
XR13=XE13-XT
X13=XR13*swtch(XE13-XT)
DC13=DC
FV13=0.0
K13=KM
BETA13=(1-FV13)*BET013+FV13/(T13+273)
d/dt U13Z=1/RO13*CN*(P13-P10)/dz
d/dt U13R=1/RO13*CN*(P13-P14)/dr
RDOT13=DC13-RO13*(U13Z-U41Z)/dz-RO13/rc1*U13R
d/dt RO13=RDOT13
TDOT13=(ENP13-EN013)/RO13/CP
d/dt T13=TDOT13
PDOT13=(BETA13/K13*TDOT13+RDOT13/RO13/K13)
d/dt P13=PDOT13
-- REGION 14 (2,5)
d/dt E14=ENP14
XE14=G*E14/RO14
XR14=XE14-XT
X14=XR14*swtch(XE14-XT)
DC14=DC
FV14=0.0
K14=KM
BETA14=(1-FV14)*BET014+FV14/(T14+273)
```

```
d/dt U14Z=1/RO14*CN*(P14-P11)/dz
d/dt U14R=1/RO14*CN*(P14-P15)/dr
RDOT14=DC14-RO14*(U14Z-U51Z)/dz-
RO14/rc2*(U14R*r2-U13R*r1)/dr
d/dt RO14=RDOT14
TDOT14=(ENP14-EN014)/RO14/CP
d/dt T14=TDOT14
PDOT14=BETA14/K14*TDOT14+RDOT14/RO14/K14
d/dt P14=PDOT14
-- REGION 15 (3,5)
d/dt E15=ENP15
XE15=G*E15/RO15
XR15=XE15-XT
X15=XR15*swtch(XE15-XT)
DC15=DC
FV15=0.0
K15=KM
BETA15=(1-FV15)*BET015+FV15/(T15+273)
d/dt U15Z=1/RO15*CN*(P15-P12)/dz
d/dt U15R=1/RO15*CN*(P15-P102)/dr
RDOT15=DC15-RO15*(U15Z-U61Z)/dz-
RO15/rc3*(U15R*r3-U14R*r2)/dr2
d/dt RO15=RDOT15
TDOT15=(ENP15-EN015)/RO15/CP
d/dt T15=TDOT15
PDOT15=BETA15/K15*TDOT15+RDOT15/RO15/K15
d/dt P15=PDOT15
-- BET01=1.0E-6*(A0+A1*T1+A2*T1*T1+A3*T1*T1*T1)
-- BET02=1.0E-6*(A0+A1*T2+A2*T2*T2+A3*T2*T2*T2)
BET041=1.0E-6*(A0+A1*T41+A2*T41*T41+A3*T41*T41*T41)
BET051=1.0E-6*(A0+A1*T51+A2*T51*T51+A3*T51*T51*T51)
-- BET03=1.0E-6*(A0+A1*T3+A2*T3*T3+A3*T3*T3*T3)
BET061=1.0E-6*(A0+A1*T61+A2*T61*T61+A3*T61*T61*T61)
BET071=1.0E-6*(A0+A1*T71+A2*T71*T71+A3*T71*T71*T71)
BET081=1.0E-6*(A0+A1*T81+A2*T81*T81+A3*T81*T81*T81)
BET091=1.0E-6*(A0+A1*T91+A2*T91*T91+A3*T91*T91*T91)
BET0101=1.0E-6*(A0+A1*T101+A2*
```

```
T101*T101+A3*T101*T101*T101)
BET0111=1.0E-6*(A0+A1*
T111+A2*T111*T111+A3*T111*T111*T111)
BET0121=1.0E-6*(A0+A1*T121+A2*
T121*T121+A3*T121*T121*T121)
BET0131=1.0E-6*(A0+A1*T131+A2*
T131*T131+A3*T131*T131*T131)
BET0141=1.0E-6*(A0+A1*T141+A2*
T141*T141+A3*T141*T141*T141)
BET0151=1.0E-6*(A0+A1*T151+A2*T151*
T151+A3*T151*T151*T151)
--
-- REGION 41 (1,4)
DC41=DC
FV41=0.0
K41=KM
BETA41=(1-FV41)*BET041+FV41/(T41+273)
d/dt U41Z=1/RO41*CN*(P41-P13)/dz
d/dt U41R=1/RO41*CN*(P41-P51)/dr
RDOT41=DC41-RO41*(U41Z-U71Z)/dz-RO41/rc1*(U41R*r1)/dr1
d/dt RO41=RDOT41
TDOT41=(ENP41-EN041)/RO41/CP
d/dt T41=TDOT41
PDOT41=((BETA41*TDOT41+RDOT41/RO41)/K41)*swtch(P41)
d/dt P41=PDOT41
-- REGION 51 (2,4)
DC51=DC
FV51=0.0
K51=KM
BETA51=(1-FV51)*BET051+FV51/(T51+273)
d/dt U51Z=1/RO51*CN*(P51-P14)/dz
d/dt U51R=1/RO51*CN*(P51-P61)/dr
RDOT51=DC51-RO51*(U51Z-U81Z)/dz-
RO51/rc2*(U51R*r2-U41R*r1)/dr
d/dt RO51=RDOT51
TDOT51=(ENP51-EN051)/RO51/CP
d/dt T51=TDOT51
```

```
PDOT51=(BETA51/K51*TDOT51+
RDOT51/RO51/K51)*swtch(P51)
d/dt P51=PDOT51
-- REGION 61 (3,4)
DC61=DC
FV61=0.0
K61=KM
BETA61=(1-FV61)*BET061+FV61/(T61+273)
d/dt U61Z=1/RO61*CN*(P61-P15)/dz
d/dt U61R=1/RO61*CN*(P61-P122)/dr
RDOT61=DC61-RO61*(U61Z-U91Z)/dz-
RO61/rc3*(U61R*r3-U51R*r2)/dr2
d/dt RO61=RDOT61
TDOT61=(ENP61-EN061)/RO61/CP
d/dt T61=TDOT61
PDOT61=(BETA61/K61*TDOT61+
RDOT61/K61/RO61)*swtch(P61)
d/dt P61=PDOT61
-- REGION 71 (1,3)
DC71=DC
FV71=0.0
K71=KM
BETA71=(1-FV71)*BET071+FV71/(T71+273)
d/dt U71Z=1/RO71*CN*(P71-P41)/dz
d/dt U71R=1/RO71*CN*(P71-P81)/dr
RDOT71=DC71-RO71*(U71Z-U101Z)/dz-RO71/rc1*U71R*r1/dr1
d/dt RO71=RDOT71
TDOT71=(ENP71-EN071)/RO71/CP
d/dt T71=TDOT71
PDOT71=(BETA71/K71*TDOT71+
RDOT71/K71/RO71)*swtch(P71)
d/dt P71=PDOT71
-- REGION 81 (2,3)
DC81=DC
FV81=0.0
K81=KM
BETA81=(1-FV81)*BET081+FV81/(T81+273)
```

```
d/dt U81Z=1/RO81*CN*(P81-P51)/dz
d/dt U81R=1/RO81*CN*(P81-P91)/dr
RDOT81=DC81-RO81*(U81Z-U111Z)/dz-
RO81/rc2*(U81R*r2-U71R*r1)/dr
d/dt RO81=RDOT81
TDOT81=(ENP81-EN081)/RO81/CP
d/dt T81=TDOT81
PDOT81=(BETA81/K81*TDOT81+
RDOT81/K81/RO81)*swtch(P81)
d/dt P81=PDOT81
-- REGION 91 (3,3)
DC91=DC
FV91=0.0
K91=KM
BETA91=(1-FV91)*BET091+FV91/(T91+273)
d/dt U91Z=1/RO91*CN*(P91-P61)/dz
d/dt U91R=1/RO91*CN*(P91-P142)/dr
RDOT91=DC91-RO91*(U91Z-U121Z)/dz-
RO91/rc3*(U91R*r3-U81R*r2)/dr2
d/dt RO91=RDOT91
TDOT91=(ENP91-EN091)/RO91/CP
d/dt T91=TDOT91
PDOT91=(BETA91/K91*TDOT91+RDOT91/K91/RO91)
d/dt P91=PDOT91
-- REGION 101 (1,2)
DC101=DC
FV101=0.0
K101=KM
BETA101=(1-FV101)*BET0101+FV101/(T101+273)
d/dt U101Z=1/RO101*CN*(P101-P71)/dz
d/dt U101R=1/RO101*CN*(P101-P111)/dr
RDT101=DC101-RO101*(U101Z-U131Z)/dz-
RO101/rc1*(U101R*r1)/dr1
d/dt RO101=RDT101
TDT101=(ENP101-EN0101)/RO101/CP
d/dt T101=TDT101
PDT101=(BETA101/K101*TDT101+RDT101/K101/RO101)
```

```
d/dt P101=PDT101
-- REGION 111 (2,2)
DC111=DC
FV111=0.0
K111=KM
BETA111=(1-FV111)*BET0111+FV111/(T111+273)
d/dt U111Z=1/RO111*CN*(P111-P81)/dz
d/dt U111R=1/RO111*CN*(P111-P121)/dr
RDT111=DC111-RO111*(U111Z-U141Z)/dz-
RO111/rc2*(U111R*r2-U101R*r1)/dr
d/dt RO111=RDT111
TDT111=(ENP111-EN0111)/RO111/CP
d/dt T111=TDT111
PDT111=(BETA111/K111*TDT111+RDT111/K111/RO111)
d/dt P111=PDT111
-- REGION 121 (3,2)
DC121=DC
FV121=0.0
K121=KM
BETA121=(1-FV121)*BET0121+FV121/(T121+273)
d/dt U121Z=1/RO121*CN*(P121-P91)/dz
d/dt U121R=1/RO121*CN*(P121-P53)/dr
RDT121=DC121-RO121*(U121Z-
U151Z)/dz-RO121/rc3*(U121R*r3-U111R*r1)/dr2
d/dt RO121=RDT121
TDT121=(ENP121-EN0121)/RO121/CP
d/dt T121=TDT121
PDT121=(BETA121/K121*TDT121+RDT121/RO121/K121)
d/dt P121=PDT121
-- REGION 131 (1,1)
d/dt E131=ENP131
XE131=G*E131/RO131
XR131=XE131-XT
X131=XR131*swtch(XE131-XT)
DC131=DC
FV131=0.0
K131=KM
```

```
BETA131=(1-FV131)*BET0131+FV131/(T131+273)
d/dt U131Z=1/RO131*CN*(P131-P101)/dz
d/dt U131R=1/RO131*CN*(P131-P141)/dr
RDT131=DC131-RO131*(U131Z)/dz-RO131/rc1*U131R
d/dt RO131=RDT131
TDT131=(ENP131-EN0131)/RO131/CP
d/dt T131=TDT131
PDT131=(BETA131/K131*TDT131+RDT131/RO131/K131)
d/dt P131=PDT131
-- REGION 141 (2,1)
d/dt E141=ENP141
XE141=G*E141/RO141
XR141=XE141-XT
X141=XR141*swtch(XE141-XT)
DC141=DC
FV141=0.0
K141=KM
BETA141=(1-FV141)*BET0141+FV141/(T141+273)
d/dt U141Z=1/RO141*CN*(P141-P111)/dz
d/dt U141R=1/RO141*CN*(P141-P151)/dr
RDT141=DC141-RO141*(U141Z)/dz-
RO141/rc2*(U141R*r2-U131R*r1)/dr
d/dt RO141=RDT141
TDT141=(ENP141-EN0141)/RO141/CP
d/dt T141=TDT141
PDT141=BETA141/K141*TDT141+RDT141/RO141/K141
d/dt P141=PDT141
-- REGION 151 (3,1)
d/dt E151=ENP151
XE151=G*E151/RO151
XR151=XE151-XT
X151=XR151*swtch(XE151-XT)
DC151=DC
FV151=0.0
K151=KM
BETA151=(1-FV151)*BET0151+FV151/(T151+273)
d/dt U151Z=1/RO151*CN*(P151-P121)/dz
```

```
d/dt U151R=1/RO151*CN*(P151-P73)/dr
RDT151=DC151-RO151*(U151Z)/dz-
RO151/rc3*(U151R*r3-U141R*r2)/dr2
d/dt RO151=RDT151
TDT151=(ENP151-EN0151)/RO151/CP
d/dt T151=TDT151
PDT151=BETA151/K151*TDT151+RDT151/RO151/K151
d/dt P151=PDT151
-- BET01=1.0E-6*(A0+A1*T1+A2*T1*T1+A3*T1*T1*T1)
-- BET02=1.0E-6*(A0+A1*T2+A2*T2*T2+A3*T2*T2*T2)
BET042=1.0E-6*(A0+A1*T42+A2*T42*T42+A3*T42*T42*T42)
BET052=1.0E-6*(A0+A1*T52+A2*T52*T52+A3*T52*T52*T52)
-- BET03=1.0E-6*(A0+A1*T3+A2*T3*T3+A3*T3*T3*T3)
BET062=1.0E-6*(A0+A1*T62+A2*T62*T62+A3*T62*T62*T62)
BET072=1.0E-6*(A0+A1*T72+A2*T72*T72+A3*T72*T72*T72)
BET082=1.0E-6*(A0+A1*T82+A2*T82*T82+A3*T82*T82*T82)
BET092=1.0E-6*(A0+A1*T92+A2*T92*T92+A3*T92*T92*T92)
BET0102=1.0E-6*(A0+A1*T102+A2*
T102*T102+A3*T102*T102*T102)
BET0112=1.0E-6*(A0+A1*T112+A2*
T112*T112+A3*T112*T112*T112)
BET0122=1.0E-6*(A0+A1*T122+A2*T122*
T122+A3*T122*T122*T122)
BET0132=1.0E-6*(A0+A1*T132+A2*
T132*T132+A3*T132*T132*T132)
BET0142=1.0E-6*(A0+A1*T142+A2*
T142*T142+A3*T142*T142*T142)
BET0152=1.0E-6*(A0+A1*T152+A2*
T152*T152+A3*T152*T152*T152)
--
-- REGION 42 (4,8)
d/dt E42=ENP42
XE42=G*E42/RO42
XR42=XE42-XT
X42=XR42*swtch(XE42-XT)
DC42=DC
FV42=0.0
```

```
K42=KM
BETA42=(1-FV42)*BET042+FV42/(T42+273)
d/dt U42Z=1/RO42*CN*(P42-P0)/dz
d/dt U42R=1/RO42*CN*(P42-P52)/dr
RDOT42=DC42-RO42*(U42Z-U62Z)/dz-
RO42/rc4*(U42R*r4-U6R*r3)/dr3
d/dt RO42=RDOT42
TDOT42=(ENP42-EN042)/RO42/CP
d/dt T42=TDOT42
PDOT42=((BETA42*TDOT42+RDOT42/RO42)/K42)*swtch(P42)
d/dt P42=PDOT42
-- REGION 52 (5,8)
d/dt E52=ENP52
XE52=G*E52/RO52
XR52=XE52-XT
X52=XR52*swtch(XE52-XT)
DC52=DC
FV52=0.0
K52=KM
BETA52=(1-FV52)*BET052+FV52/(T52+273)
d/dt U52Z=1/RO52*CN*(P52-P0)/dz
-- d/dt U5R=1/RO5*CN*(P5-P6)/dr
RDOT52=DC52-RO52*(U52Z-U72Z)/dz-RO52/rc5*(-U42R*r4)/dr4
d/dt RO52=RDOT52
TDOT52=(ENP52-EN052)/RO52/CP
d/dt T52=TDOT52
PDOT52=(BETA52/K52*TDOT52+
RDOT52/RO52/K52)*swtch(P52)
d/dt P52=PDOT52
-- REGION 62 (4,7)
d/dt E62=ENP62
XE62=G*E62/RO62
XR62=XE62-XT
X62=XR62*swtch(XE62-XT)
DC62=DC
FV62=0.0
K62=KM
```

```
BETA62=(1-FV62)*BET062+FV62/(T62+273)
d/dt U62Z=1/RO62*CN*(P62-P42)/dz
d/dt U62R=1/RO62*CN*(P62-P72)/dr
RDOT62=DC62-RO62*(U62Z-U82Z)/dz-
RO62/rc4*(U62R*r4-U9R*r3)/dr3
d/dt RO62=RDOT62
TDOT62=(ENP62-EN062)/RO62/CP
d/dt T62=TDOT62
PDOT62=(BETA62/K62*TDOT62+
RDOT62/K62/RO62)*swtch(P62)
d/dt P62=PDOT62
-- REGION 72 (5,7)
d/dt E72=ENP72
XE72=G*E72/RO72
XR72=XE72-XT
X72=XR72*swtch(XE72-XT)
DC72=DC
FV72=0.0
K72=KM
BETA72=(1-FV72)*BET072+FV72/(T72+273)
d/dt U72Z=1/RO72*CN*(P72-P52)/dz
-- d/dt U7R=1/RO7*CN*(P7-P8)/dr
RDOT72=DC72-RO72*(U72Z-U92Z)/dz-RO72/rc5*(-U62R*r4)/dr3
d/dt RO72=RDOT72
TDOT72=(ENP72-EN072)/RO72/CP
d/dt T72=TDOT72
PDOT72=(BETA72/K72*TDOT72+
RDOT72/K72/RO72)*swtch(P72)
d/dt P72=PDOT72
-- REGION 82 (4,6)
d/dt E82=ENP82
XE82=G*E82/RO82
XR82=XE82-XT
X82=XR82*swtch(XE82-XT)
DC82=DC
FV82=0.0
K82=KM
```

```
BETA82=(1-FV82)*BET082+FV82/(T82+273)
d/dt U82Z=1/RO82*CN*(P82-P62)/dz
d/dt U82R=1/RO82*CN*(P82-P92)/dr
RDOT82=DC82-RO82*(U82Z-U102Z)/dz-
RO82/rc4*(U82R*r4-U12R*r3)/dr3
d/dt RO82=RDOT82
TDOT82=(ENP82-EN082)/RO82/CP
d/dt T82=TDOT82
PDOT82=(BETA82/K82*TDOT82+
RDOT82/K82/RO82)*swtch(P82)
d/dt P82=PDOT82
-- REGION 92 (5,6)
d/dt E92=ENP92
XE92=G*E92/RO92
XR92=XE92-XT
X92=XR92*swtch(XE92-XT)
DC92=DC
FV92=0.0
K92=KM
BETA92=(1-FV92)*BET092+FV92/(T92+273)
d/dt U92Z=1/RO92*CN*(P92-P72)/dz
RDOT92=DC92-RO92*(U92Z-U112Z)/dz-RO92/rc5*(-U82R*r4)/dr4
d/dt RO92=RDOT92
TDOT92=(ENP92-EN092)/RO92/CP
d/dt T92=TDOT92
PDOT92=(BETA92/K92*TDOT92+RDOT92/K92/RO92)
d/dt P92=PDOT92
-- REGION 102(4,5)
d/dt E102=ENP102
XE102=G*E102/RO102
XR102=XE102-XT
X102=XR102*swtch(XE102-XT)
DC102=DC
FV102=0.0
K102=KM
BETA102=(1-FV102)*BET0102+FV102/(T102+273)
d/dt U102Z=1/RO102*CN*(P102-P82)/dz
```

```
d/dt U102R=1/RO102*CN*(P102-P112)/dr
RDT102=DC102-RO102*(U102Z-U122Z)/dz-
RO102/rc4*(U102R*r4-U15R*r3)/dr3
d/dt RO102=RDT102
TDT102=(ENP102-EN0102)/RO102/CP
d/dt T102=TDT102
PDT102=(BETA102/K102*TDT102+RDT102/K102/RO102)
d/dt P102=PDT102
-- REGION 112 (5,5)
d/dt E112=ENP112
XE112=G*E112/RO112
XR112=XE112-XT
X112=XR112*swtch(XE112-XT)
DC112=DC
FV112=0.0
K112=KM
BETA112=(1-FV112)*BET0112+FV112/(T112+273)
d/dt U112Z=1/RO112*CN*(P112-P92)/dz
-- d/dt U11R=1/RO11*CN*(P11-P12)/dr
RDT112=DC112-RO112*(U112Z-U132Z)/dz-
RO112/rc5*(-U102R*r4)/dr4
d/dt RO112=RDT112
TDT112=(ENP112-EN0112)/RO112/CP
d/dt T112=TDT112
PDT112=(BETA112/K112*TDT112+RDT112/K112/RO112)
d/dt P112=PDT112
-- REGION 122 (4,4)
DC122=DC
FV122=0.0
K122=(1-FV122)*AK0+FV122/P122
BETA122=(1-FV122)*BET0122+FV122/(T122+273)
d/dt U122Z=1/RO122*CN*(P122-P102)/dz
d/dt U122R=1/RO122*CN*(P122-P132)/dr
RDT122=DC122-RO122*(U122Z-U142Z)/dz-
RO122/rc4*(U122R*r4-U61R*r3)/dr3
d/dt RO122=RDT122
TDT122=(ENP122-EN0122)/RO122/CP
```

```
d/dt T122=TDT122
PDT122=(BETA122/K122*TDT122+RDT122/RO122/K122)
d/dt P122=PDT122
-- REGION 132 (5,4)
DC132=DC
FV132=0.0
K132=KM
BETA132=(1-FV132)*BET0132+FV132/(T132+273)
d/dt U132Z=1/RO132*CN*(P132-P112)/dz
-- d/dt U13R=1/RO13*CN*(P13-P14)/dr
RDT132=DC132-RO132*(U132Z-U152Z)/dz-
RO132/rc5*(-U122R*r4)/dr4
d/dt RO132=RDT132
TDT132=(ENP132-EN0132)/RO132/CP
d/dt T132=TDT132
PDT132=(BETA132/K132*TDT132+RDT132/RO132/K132)
d/dt P132=PDT132
-- REGION 142 (4,3)
DC142=DC
FV142=0.0
K142=KM
BETA142=(1-FV142)*BET0142+FV142/(T142+273)
d/dt U142Z=1/RO142*CN*(P142-P122)/dz
d/dt U142R=1/RO142*CN*(P142-P152)/dr
RDT142=DC142-RO142*(U142Z-U53Z)/dz-
RO142/rc4*(U142R*r4-U91R*r3)/dr3
d/dt RO142=RDT142
TDT142=(ENP142-EN0142)/RO142/CP
d/dt T142=TDT142
PDT142=BETA142/K142*TDT142+RDT142/RO142/K142
d/dt P142=PDT142
-- REGION 152 (5,3)
DC152=DC
FV152=0.0
K152=KM
BETA152=(1-FV152)*BET0152+FV152/(T152+273)
d/dt U152Z=1/RO152*CN*(P152-P132)/dz
```

```
RDT152=DC152-RO152*(U152Z-U63Z)/dz-
RO152/rc5*(-U142R*r4)/dr4
d/dt RO152=RDT152
TDT152=(ENP152-EN0152)/RO152/CP
d/dt T152=TDT152
PDT152=BETA152/K152*TDT152+RDT152/RO152/K152
d/dt P152=PDT152
BET053=1.0E-6*(A0+A1*T53+A2*T53*T53+A3*T53*T53*T53)
BET063=1.0E-6*(A0+A1*T63+A2*T63*T63+A3*T63*T63*T63)
BET073=1.0E-6*(A0+A1*T73+A2*T73*T73+A3*T73*T73*T73)
BET083=1.0E-6*(A0+A1*T83+A2*T83*T83+A3*T83*T83*T83)
--
-- REGION 53 (4,2)
DC53=DC
FV53=0.0
K53=KM
BETA53=(1-FV53)*BET053+FV53/(T53+273)
d/dt U53Z=1/RO53*CN*(P53-P142)/dz
d/dt U53R=1/RO53*CN*(P53-P63)/dr
RDOT53=DC53-RO53*(U53Z-U73Z)/dz-
RO53/rc4*(U53R*r4-U121R*r3)/dr3
d/dt RO53=RDOT53
TDOT53=(ENP53-EN053)/RO53/CP
d/dt T53=TDOT53
PDOT53=(BETA53/K53*TDOT53+
RDOT53/RO53/K53)*swtch(P53)
d/dt P53=PDOT53
-- REGION 63 (5,2)
DC63=DC
FV63=0.0
K63=KM
BETA63=(1-FV63)*BET063+FV63/(T63+273)
d/dt U63Z=1/RO63*CN*(P63-P152)/dz
RDOT63=DC63-RO63*(U63Z-U83Z)/dz-RO63/rc5*(-U53R*r4)/dr4
d/dt RO63=RDOT63
TDOT63=(ENP63-EN063)/RO63/CP
d/dt T63=TDOT63
```

```
PDOT63=(BETA63/K63*TDOT63+
RDOT63/K63/RO63)*swtch(P63)
d/dt P63=PDOT63
-- REGION 73 (4,1)
d/dt E73=ENP73
XE73=G*E73/RO73
XR73=XE73-XT
X73=XR73*swtch(XE73-XT)
DC73=DC
FV73=0.0
K73=KM
BETA73=(1-FV73)*BET073+FV73/(T73+273)
d/dt U73Z=1/RO73*CN*(P73-P53)/dz
d/dt U73R=1/RO73*CN*(P73-P83)/dr
RDOT73=DC73-RO73*(U73Z)/dz-
RO73/rc4*(U73R*r4-U151R*r3)/dr3
d/dt RO73=RDOT73
TDOT73=(ENP73-EN073)/RO73/CP
d/dt T73=TDOT73
PDOT73=(BETA73/K73*TDOT73+
RDOT73/K73/RO73)*swtch(P73)
d/dt P73=PDOT73
-- REGION 83 (5,1)
d/dt E83=ENP83
XE83=G*E83/RO83
XR83=XE83-XT
X83=XR83*swtch(XE83-XT)
DC83=DC
FV83=0.0
K83=KM
BETA83=(1-FV83)*BET083+FV83/(T83+273)
d/dt U83Z=1/RO83*CN*(P83-P63)/dz
-- d/dt U8R=1/RO8*CN*(P8-P9)/dr
RDOT83=DC83-RO83*(U83Z)/dz-RO83/rc5*(-U73R*r4)/dr4
d/dt RO83=RDOT83
TDOT83=(ENP83-EN083)/RO83/CP
d/dt T83=TDOT83
```

```
PDOT83=(BETA83/K83*TDOT83+
RDOT83/K83/RO83)*swtch(P83)
d/dt P83=PDOT83
-- DISPLAY
-- PEAK PRESSURE
Ptmax=Ptmax+(P131-Ptmax)*swtch(P131-Ptmax)
PREX=P131-P0
PKPA=1000.0*PREX
-- REACTIVITY
RE=300*R
dispt ENP,PKPA,RE
```

REFERENCES

Barbry, F., "Note de Synthese Concernant les Observations Effectuees sur la Formation de gaz de Radiolyse et de Leurs Consequences", C.E.A. Report SEESNC No. 115 (1973).

Barbry, F., "Principaux Resultats Experimentaux Obtenus Lors de la Premiere Annee de Fonctionnement", C.E.A. Report SEESNC No. 125 (1975).

Barbry, F., and R. Medioni, "SILENE, An Experimental Irradiation Reactor", Fourth Symposium on Neutron Dosimetry Commission of the European Communities (June 1981).

Barbry, F., "Fuel Solution Criticality Accident Studies with the SILENE Reactor: Phenomenology, Consequences and Simulated Intervention", International Seminar on Criticality Studies Programs and Needs (September 1983).

Barbry, F., "Review of Pressure Wave Measurement Experiments in the SILENE Reactor", C.E.A. Technical Note SRSC No. 87.96 (1987).

Bickley, A., D. J. Mather, and P. M. Shaw, "The Code CRITEX to Simulate Transient Criticality in Fissile Solutions", UKAEA-UK, Trans. Amer. Nucl. Soc. 55, pp. 406, (1987).

Dunenfeld, M. S., "Kinetic Experiments on Water Boilers - "A" Core Report - Part 2, Analysis of Results", NAA-SR-5416, Atomics International (1962).

Dunenfeld, M.S. and R. K. Stitt, "Summary Review of the Kinetics Experiments on Water Boilers", NAA-SR-7087, Atomics International (1963).

Hetrick, D. L., *Dynamics of Nuclear Reactors*, Chicago: University of Chicago Press (1971).

Hetrick, D. L. and A. B. Smith, "Nuclear Excursions in Aqueous Solutions of Fissile Material", Trans. Amer. Nucl. Soc. 55, pp. 407-408 (1987).

Kimpland, R. H., "A New Multiregion Computer Model for Predicting Nuclear Excursions in Aqueous Homogeneous Solution Assemblies", Trans. Amer. Nucl. Soc. 65, pp. 246-247 (1992).

Korn, G. A., *Interactive Dynamic System Simulation*, McGraw-Hill, Inc. (1989).

Kornreich, D. E., "Reactivity Feedback Mechanisms in Aqueous Fissile Solutions", Masters Thesis, University of Arizona (1992).

Kornreich, D. E., Private Communication (1993).

Lécorché, P. and R. L. Seale, "A Review of the Experiments Performed to Determine the Radiological Consequences of a Criticality Accident", Y-CDC-12, Oak Ridge National Laboratory (1973).

Malenfant, R. E, H. M. Forehand, and J. J. Koelling, "SHEBA: A Solution Critical Assembly", Trans. Amer. Nucl. Soc. 35, pp. 279-280 (1980).

Mather, D. J., CHAMPAGNE - A Computer Code Modelling the Growth of a Bubble in a Super-Saturated Solution, Unpublished (1988).

Norman, A. and P. Spiegler, "Radiation Nucleation of Bubbles in Water", Nuclear Science and Engineering: 16, pp. 213-217 (1963).

Paxton, H. C., "Significance of Accidental Excursions", Nuclear Safety 1975, D. L. Hetrick, ed., Published by ANS (1975).

Peterson, D. M., W. R. Stratton and T. P. McLaughlin, "PAD: A One-Dimensional, Coupled Neutronic-Thermodynamic-Hydrodynamic Computer Code", LA-6540-MS. Los Alamos Laboratory (1976).

Pribyl, D. J., "Nuclear Excursions in Criticality Accidents With Fissile Solutions", Masters Thesis, University of Arizona (1989).

Reynolds, W. C. and H. C. Perkins, *Engineering Thermodynamics*, McGraw-Hill Book Company (1977).

Seitz, F., "On the Theory of the Bubble Chamber", The Physics of Fluids Vol. 1, No. 1 (1957).

Sizov, A. N., V. F. Kolesov, and G. G. Solovev, "Dynamics of Homogeneous Water Pulsed Reactors", Voprosy atmnoi nauki i tekhniki. Seriia: Impul'snye reaktory i prostye kriticheskie sborki, issue 1, pp. 22-31 (1985).

Smith, A. B., "Nuclear Excursions in Aqueous Solutions of Fissile Materials", Masters Thesis, University of Arizona (1989).

Spiegler, P., C. F. Bumpus, Jr. and A. Norman, "Production of Void and Pressure by Fission Track Nucleation of Radiolytic Gas Bubbles During Power Bursts in a Solution Reactor", NAA-SR-7086. Atomics International (1962).